Thesis

The Use of Natural Heat as a Tracer to Quantify Groundwater Surface Water Interactions: Maules Creek, New South Wales, Australia

Submitted by

Gabriel Rau

20th March 2008

UNIVERSITY OF NEW SOUTH WALES
School of Civil & Environmental Engineering
Water Research Laboratory

Universität Stuttgart
Germany

Diplomarbeit

The Use of Natural Heat as a Tracer to Quantify Groundwater Surface Water Interactions: Maules Creek, New South Wales, Australia

Submitted by

Gabriel Rau
Matrikelnummer 2076951

20th March 2008

Supervision

Dr. Martin Andersen
Prof. Ian Acworth

University of New South Wales
School of Civil and
Environmental Engineering
Water Research Laboratory

King Street, Manly Vale
2093 Sydney, NSW
AUSTRALIA

Examination

Prof. Dr.-Ing. Rainer Helmig

Universität Stuttgart
Department of Hydromechanics
and Modeling of Hydrosystems

Pfaffenwaldring 61
70569 Stuttgart
GERMANY

Author's Statement

I hereby certify that I have prepared this Thesis independently, and that only those sources, aids and advisors that are duly noted herein have been used and/or consulted.

Date ____________________________ Signature ________________________________

Abstract

Water management in New South Wales (Australia) does not currently consider the connection between groundwater and surface water. Using water resources impacts on interactions between both sources, which are important factors contributing to unique ecological niches in the aquatic environment. The basic connectivity was described and an outline of the significance was given. Connecting flows must be estimated in order to adequately manage water balances. These are difficult to quantify especially when the traditional Darcy method is used. Natural heat promises to be an excellent alternative as it can be used to trace water movement through the shallow surface water sediment. Publications are reviewed and the theory for the two most suitable methods is extracted and explained: temperature forward modelling and the use of temperature fluctuations. Furthermore, multi-level temperature arrays and water level measurements were designed and jointly deployed in three different surface water pools in the Maules Creek sub-catchment. Results are inspected, processed and compared to the level measurements. Spectral analysis reveals the presence of atmospheric tides which causes significant level fluctuations. This demonstrates that these ponds are windows to the groundwater table. Both heat methods produces accurate vertical velocities for the location Elfin Crossing which are between -0.2 and -0.7 m/d, indicating that there is streambed water loss to the subsurface. Additionally, recorded water levels decreased consistently during the same time period. The other locations illustrate similar but biased results caused by restricted boundary conditions to the heat transport theory such as one-dimensionality. A numerical model verifies that heat dispersion is a significant mechanism to be considered and that horizontal flow impacts on the result of both methods. Thus, horizontal flow can be detected but quantification remains difficult because solutions diverge. It is suggested that advective flow driven by gradients in the alluvial aquifer is responsible for level decline.

Acknowledgements

Writing this thesis as an exchange student in Australia was a very interesting and enriching experience. However, this task involved a lot of preparation and work, therefore it could not have been achieved without the support of many people.

My sincere thanks goes to

- Professor Ian Acworth for giving me the chance to write my thesis at the Water Research Laboratory (WRL) in Australia by welcoming me into the groundwater team and funding my work
- Dr. Martin Andersen for award winning excellency in thesis supervision, including never ending time to listen to my outcries, offering suggestions and good will whenever I was stuck with anything, scuba diving and shelly beach BBQ sessions
- Prof. Dr.-Ing. Rainer Helmig from Universität Stuttgart for trusting me and agreeing to my desire of writing my thesis in the antipodal paradise
- Anna Greve for helping me with the German invasion of Australia, sharing her office with me and for always distracting me with nice little chats but also serious discussions about life and the world
- Andrew McCallum for exactly the same as Anna but also for the preparation he did before I arrived, for never wearing a kilt and for native “Aussie” language support
- The whole WRL staff for being friendly, helpful and extremely relaxed
- Kristie Ussher and her parents simply for being the best, housing next to the beach, endless supply of fruits and sweets, mental support and handling my strong scientific enthusiasm and dedication
- All the members of my family in Germany for accepting the fact that I am too far away all the time (if only the airfare was cheaper!)

Contents

List of Figures

List of Tables

1. Introduction

1.1. Background

Water is vital to all living creatures on earth and therefore it should be regarded as one of our most precious resources. Fresh water demand follows the global trend of constant increase in populations and economic development. In order to ensure a continuous water supply, new management strategies and sources have to be investigated and accessed. This requires profound knowledge about the natural hydrological processes, as overexploitation impacts on the environment.

Like many other countries usually located in the world's arid climate zones, Australia is much affected by decreasing rainfall and increasing droughts possibly due to large scale climatic cycles (Fawcett, 2007). These drought conditions severely impact on agriculture by increasing the need for irrigation to ensure ongoing production. Unfortunately, drought conditions limit the Australian export capacity significantly according to the Annual Trade Report 2006 (ADFAT, 2006), since agricultural goods are a valuable part of Australia's international export trade. Australian water statistics from the National Water Commission reveal some interesting facts (ABS, 2006): an astonishing number of 65% of the total Australian fresh water consumption was used for agricultural purposes, compared to households using 11% in the year 2004-2005. The distinction between sources of distributed water points out, that 96% of the total volume is received from surface water sources, whilst only 4% is extracted from the ground. Recycled water was mainly used for irrigational purposes. Water reuse is increasing in the last years, but unfortunately the rate is still only 4% of the total water volume sup-plied in 2004-2005. This is a very small amount for a country with such huge irrigation need in order to ensure ongoing agricultural production, export and economical benefit.

However, most crops in Australia are watered by flood irrigation. This means that water is transported in open channels from groundwater pumps to the field, sometimes travelling quite far. It feeds irrigation pipes which release it to the slightly sloped field plain where it runs along especially constructed ditches. Due to lack of rainfall during drought conditions there are increasingly high demands. Thus, growth of many crops such as e.g. cotton requires large amounts of water. Additionally, irrigation methods cause severe water loss through evaporation in high sunshine areas. This results in increasing consumption and risks overexploitation of water resources. Hence, surface water levels are dropping for the long term and much effort is being put into research towards an improved water resource management for Australia's agriculture industry.

Groundwater offers one of the most reliable sources of fresh water especially for water supply. In contrast to surface water, it is stored beneath the surface, fairly protected from most atmospheric or anthropogenic influences such as loss through evaporation or contamination by pollutants. However, groundwater reservoirs are connected to the hydrological cycle and play an important role in sustaining river ecology by providing e.g. baseflow. Even today, water management in Australia still disregards the high connectivity between both sources and manages them separately. In order to ensure sustainability, the amount of groundwater extraction must be less than its natural recharge. Unfortunately, recharge is still one of the big unknowns in water balance calculations because there are many possibilities of interaction. Finding and allocating water flows from and to aquifers is quite a challenge but necessary and strongly depends on the hydrogeological conditions.

Managing water resources requires deep knowledge about complex subsurface water flow processes as well as hydrologic mechanisms. To investigate the boundary between surface water and groundwater, this thesis will focus on quantification of the water fluxes across this boundary. In particular, the use of natural heat as a tracer to estimate water movement between river ponds and groundwater is investigated in detail. Results will help towards a better understanding of water connectivity in Maules Creek and methods may be used to further improve water management.

1.2. Motivation

The use of heat as a tracer has been chosen for a detailed investigation because it promises to offer the ability to correctly quantify surface water groundwater exchange velocities. It is based on a different physical approach than the Darcy method. This requires the hydraulic conductivity value which combines liquid and solid properties and can only be estimated. In the past, such exchange rates have mainly been calculated from Darcy's law but these results deliver rough estimations only. In fact, level gradients do not necessarily provide a good indication of water flow unless the distribution of subsurface properties is accurately known. Thus, determination and use of appropriate properties imposes a challenge on investigators.

Surface water bodies are subject to diurnal temperature change. Moreover, water carries heat as it flows and it features well known thermal properties which can be used to study its movement. The study of heat propagation may help towards improved exchange flow quantifications. Theoretical methods have been developed but little work has been done to deploy and test these methods under realistic conditions in the field. However, research on connectivity is important because it may improve the management of water budgets, thus helping agriculture as well as protecting the environment. The two most important quantification methods found in literature are explained, temperature logging devices are constructed, applied to the field and the outcome is evaluated and discussed in this thesis.

2. Connectivity between surface and groundwater

2.1. Groundwater movement

Groundwater is water which fills the void between grains in the subsurface. However, this expression can only be used for the saturated zone. Groundwater levels constantly vary caused by natural or artificial influences such as gradient flow, extraction or infiltration of water volume. For reasons of water management and balance calculations, it may be important to consider that groundwater divides may spatially and temporally differ significantly from surface water divides. This can cause infiltrated water to be carried into different management zones or even catchment areas.

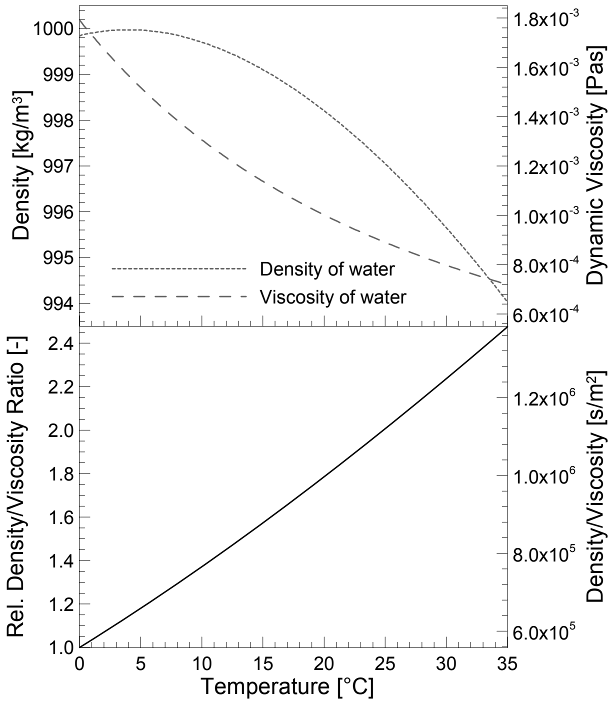

Figure 1: Plot of water density and viscosity for a typical surface water temperature range (NIST, 2008). The relative density viscosity ratio is based on the ratio value at zero degrees.

For velocity calculations in porous media the hydraulic conductivity is generally used. Its value depends on both, physical properties of the solid matrix as well as the fluid. The relevant matrix properties include grain shape, size and porosity and they are combined and given with the intrinsic conductivity value. The water's properties are its dynamic viscosity and density, both mainly a function of temperature but also feature a minor pressure dependency. Since this investigation focuses only on shallow surface waters, pressure influences on parameters are assumed negligible. However, a temperature increase of 25°C can significantly change the hydraulic conductivity to double in value (Constantz, 1994), leading to twice the exchange of water in constant level gradient conditions (see Figure 1). For the simplified description of water flow, all relevant physical properties can be combined and expressed as hydraulic conductivity defined as (Muskat, 1937)

[1] $$k_f = k \cdot g \cdot \frac{\rho_f}{\mu} \quad \text{[m/s]},$$

where k is the intrinsic permeability [m^2] containing the properties of the solids, ρ_w is water density [kg/m^3], g is the gravitational constant [~ 9.81 m/s^2] and μ represents the dynamic viscosity of water [Pas].

As mentioned above, the water table fluctuates over time and space, forming a subsurface landscape. Due to pressure equalisation, water usually flows from higher levels to lower levels along the level gradient. Darcy assumed that the change in groundwater viscosity and density resulting from temperature variation is negligibly small. Therefore, his mathematical formulation is fairly simple using a linear proportionality constant to calculate water velocity in porous media

[2] $$\vec{v}_f = -\vec{\vec{k}}_f \cdot \nabla h \quad \text{[m/s]},$$

with the hydraulic conductivity of the porous media k_f [m/s] and the water level gradient h [m/m]. This may be given as the spatial change of water level or the differentiation of a continuous function describing water levels.

The subsurface hydraulic conductivity varies greatly, but generally only its spatial distribution is considered. Temporal changes such as clogging are slow and often neglected in flow calculations. Hydraulic conductivity also depends on rock properties which generally feature inhomogeneous and isotropic distribution throughout the subsurface. For the purpose of flow modelling, it is practical to combine properties of subsurface layers with similar conductivities e.g. the streambed and consider it as one unit. Hence, models and calculations are simplified. Despite our knowledge, it would be helpful but it is very difficult to extract a multi-dimensional image containing exact distribution of soil properties. For the purpose of approximation samples can be taken from the study site and tested for conductivity within laboratory environments producing good results (Yeh, 2000). This does not, however, fully represent the undisturbed value because mixing of sample influences the natural layers and conditions. In addition small samples only poorly represent large scale environments as they would not adequately contain heterogeneities. However, there are in-situ methods which determine hydraulic conductivity estimates. Various types of slug tests can be carried out and evaluated quite easily in different field conditions (e.g. Domenico, 1990). Conductivity values obtained by these methods can be used with different groundwater models, helping to assess quantity and direction of subsurface water flow if water levels are known. However, a water level gradient is only the driving force and its existence does not necessarily proof active flow. Thus the Darcy method can deliver erroneous results.

2.2. Connectivity between surface and groundwater

When looking at the large spatial and temporal scale all water in the hydrologic cycle is connected. Description at this scale is generally difficult because it involves different mathematical model approaches for surface water and groundwater flow as well as phase change due to evaporation etc. Scientific scenarios therefore generally look at smaller scales offering the assumption of a distinct system unit with defined boundary conditions which helps to simplify the rather complex description. The focus on such systems has the disadvantage of ignoring effects propagating beyond system boundaries, caused by events such as intensive water extraction. As an example, this has been done for the water resource management in New South Wales which currently neglects connectivity between surface and groundwater (Sinclair, 2006). These impacts can have destructive consequences for our environment, thus an outline about its importance will be given.

In contrast to surface water, groundwater is generally hard to describe because it is hidden in the subsurface. Especially modelling of larger scale systems requires many detailed parameters mostly varying throughout space but some also in time. Until today, the spatial variation of physical soil properties can only be sparsely estimated even when using high technology surveying methods to support traditional borehole investigations. Much work is still to be done to improve existing and develop new techniques in the area of groundwater physics. However, a good view of the variability of interfaces between surface water and groundwater bodies can be obtained by imagining groundwater levels to form a distinct subsurface landscape. Wherever this water level surface area interferes with the landscape surface area there is a connecting boundary between surface and groundwater. This means that whenever water levels are higher than the ground surface water bodies occur with the solid surface representing its interface. Certainly, groundwater levels are much more variable in time and space than the solid landscape because it is mostly liquid. Also, water level fluctuations are caused by e.g. subsurface gradient flow, water recharge or discharge, consumption by plants and organisms, transpiration or evaporation. The spatial water level distribution is influenced by subsurface soil properties, whereas temporal fluctuations of the water table are generally induced by numerous ways of water flow.

2.3. Surface streams

Rivers, streams and creeks are probably the most complex surface water bodies in terms of possible connectivity with groundwater. Their geological body usually consists of alluvial sands, gravels, cobbles but can also be bedrock or clay. Inorganic and organic sediments can be degraded from the originating source e.g. dead plants, aquatic life or sand and deposited along the flow path according to the flow velocity. Depending on the frequency and volume of water flow, river beds are usually of complex stratigraphical and geometrical structure. This is caused by slow but constant degradation and deposition of materials which influence the geomorphology e.g. change the shape of the active channel. As a result, the active channel can be moved transversally over long time periods (Huggenberger et al., 1998). Hence, all properties of deposited material vary greatly usually forming layers which are permeable to water flow. This creates a highly organised and complex alluvial structure, always depending on the dynamics of erosion and sedimentation. The distribution of the riparian zone is also influenced by discharge, composition and amount of transported sediments and the dynamic character of the river (Huggenberger et al. 1998). As a result, the near environment of an active stream channel is often a wetland with extensive growth of flora relying on a dependable source of water.

Because of these complex geological and morphological structures, interactions between streams and the surrounding subsurface are difficult to describe. However, there are four general cases as illustrated in Figure 2 (Winter et al., 1998). Illustration (a) shows a neutral reach, where surface water and groundwater is at the same level. This case is exceptional and often just a temporary condition between changing flow levels. Picture (b) illustrates the possible conditions of a disconnected surface stream. The groundwater level next to these surface water bodies is characterised to be below the active channel bed. In this case, stream flow is usually limited to wet periods caused by rain or dam water release. Flowing water may penetrate the matrix and percolate until it reaches the groundwater table. In this case pumping from a nearby well does not affect surface water levels (Winter et al., 1998). During dry periods with no upstream water flow source, levels drop and flow finally stops. In some cases, water may be trapped by impermeable layers leaving stagnant pools which often disappear due to slow leakage, animal consumption or evapotranspiration. This type of interaction represents a rather complicated case for modelling as it can temporarily involve the necessity to incorporate multiple phases such as solids, water, vapour and air (gas) in the model equations.

Figure 2 (c) illustrates characteristic levels as necessary for the exchange processes of losing streams. Groundwater heads in the immediate vicinity are usually above the channel bed, and stream water level is above the one of groundwater. The existing level gradient forces water to infiltrate the subsurface. The volume of water penetrating the soil body strongly depends on the hydraulic conductivity of the streambed sediments (Huggenberger et al., 1998). Contrary to this, Figure 2 (d) exemplifies a gaining reach where surrounding subsurface water levels are higher than the stream forcing water to discharge from the ground into the stream channel. This mechanism is known to provide baseflow sustaining flow events. However, flow can also disappear into the subsurface leaving a series of pools and rifles. This can be observed particularly in permeable sediments and flow velocities are usually very slow and may be invisible to the eye.

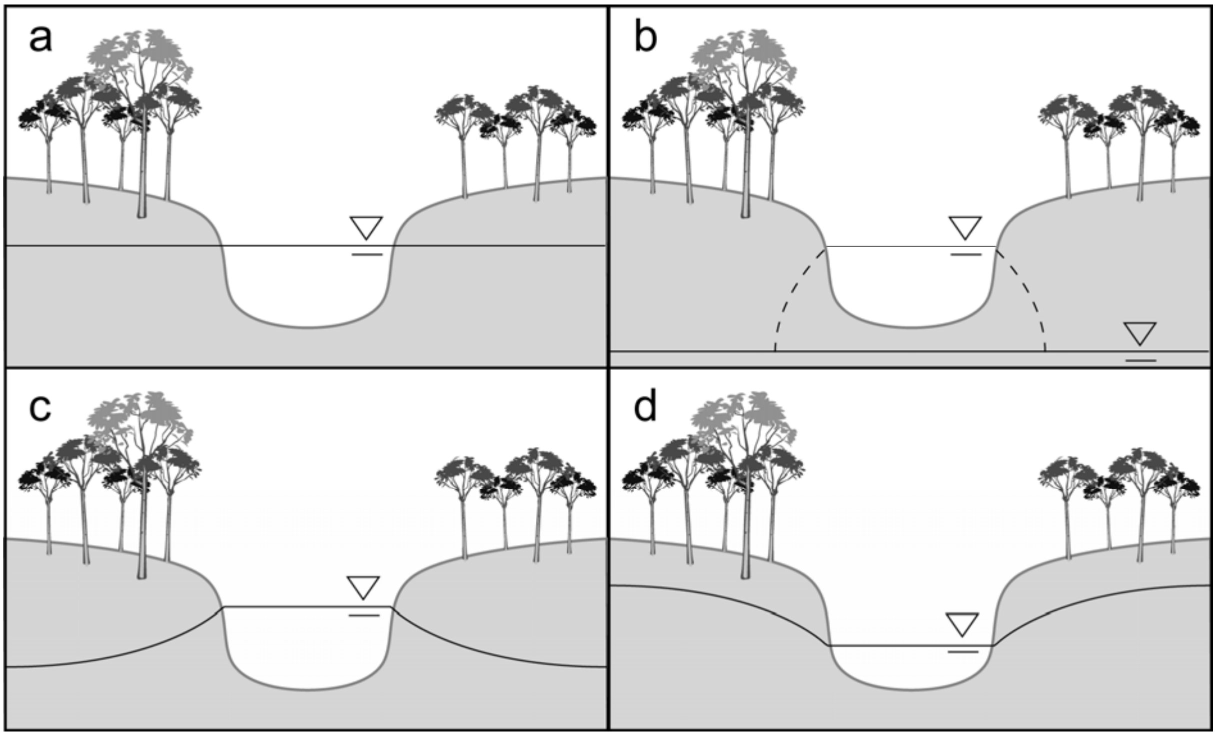

Figure 2: Generalised illustration of the interaction between surface and groundwater showing (a) neutral reach, (b) disconnected reach, (c) losing reach and (d) gaining reach.

The above described scenarios of interaction can occur on different sections of the same river depending on geologic setup and climatic conditions (Winter et al., 1998). Hence, water levels in most streams vary greatly over time depending on surface rainfall and characteristics of the catchment area. Furthermore, all above explained mechanisms may happen to the same part of the river but changing over time. This greatly complicates the description of exchange. As a conclusion, the general interaction between shallow surface water and groundwater can be characterised as highly coupled hydraulic system with numerous different influences to be considered.

2.4. Bank storage

During and after high rainfall events, surface water within a catchment area is quickly aggregated in streams and rivers causing water levels to rise very fast. If the surrounding groundwater levels are in between baseflow levels and flood levels, there is a temporary reversal in water flow direction (see Figure 3). Depending on the flood volume, duration, streambed hydraulic conductivity and porosity of the surrounding sediments, significant amounts of water can penetrate the riparian aquifer. After the recharge the level gradient reverses due to decreasing flow level which forces water out of the river bank back into the stream. Riparian water storage can act as a natural buffer maintaining stream flow between rapid flow events caused by e.g. rainfall (Sophocleous, 2002) or dam releases upstream. Especially during floods when water levels quickly rise above the river bank large areas are covered and widespread infiltration contributes to recharge of groundwater. There is delayed release and discharge to the stream because of increased travel paths through the soil environment which can take up to years (Winter et al., 1998). A large part of baseflow can be the result of bank storage. Furthermore, this mechanism is an important factor maintaining stream flow and stream ecology during periods without precipitation.

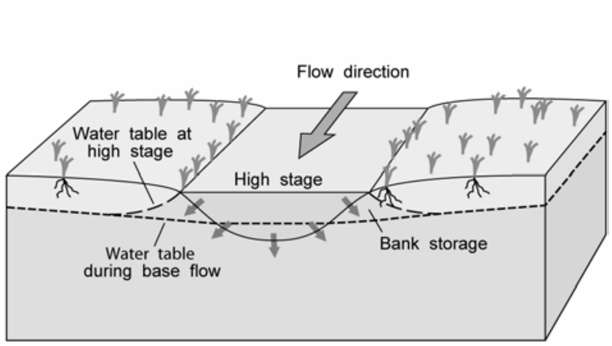

Figure 3: Illustration of bank storage due to high surface water levels (Winter et al., 1998).

2.5. Lakes, ponds and wetlands

Lakes and ponds usually occur in depressions of landscape surface such as billabongs[1]. Similar to streams, there are several ways to interact with the surrounding groundwater. Ac-

[1] Billabong [billa: creek, bong: dead]: expression used by indigenous Australians to describe stagnant water in a depression within the alluvial environment, also referred to as oxbow lake or dead end.

cording to Winter et al. (1998), three different types of interactions occur: distinct inflow or outflow through an entire bed section or both, variable seepage gain and loss within the same section. However, evaporation loss is generally high because of large surface areas of the water body. Most stagnant surface waters tend to accumulate organic matter over time resulting from algae or plant growth, die back and biochemical degradation. This may clog the sediments and is known as colmation[2]. On the long term this process can strongly limit groundwater exchange flows by decreasing the sediment conductivity (Brunke et al., 1997).

In some cases surface water may be trapped and prevented from percolation. This may be the case if layers of less permeable clays occur in the subsurface underneath or when silty or organic sediments have accumulated on the bottom. Level changes do not directly affect groundwater since the water body is disconnected. In this case, the water level increases with rainfall during wet, and decreases due to evaporation as well as transpiration during dry and sunny periods.

Wetlands are generally present when groundwater reaches the landscape surface and feature exchange mechanisms which are similar to lakes. In contrast to streams and lakes, wetlands can also occur on inclinations. This is caused by groundwater levels intersecting with the landscape surface (Winter et al., 1998). Capillary rise may increase this effect. The roots of plant species requiring moist conditions can easily reach the water table. As a result, growth of vegetation is green and lush. In some cases, artesian discharge is possible which can initiate stream flow (spring) if substantial. This may occur in karstic environments especially in case of secondary porosity (cracks) dominantly creating preferential flow paths.

2.6. Ecological significance of exchange flows

The significance of interaction between surface water and groundwater has only recently been discovered as a subject of interest because it impacts on water quality and quantity and as a result affects stream health (Woessner, 2000). Both water sources are highly connected with many possible ways of exchange and temporally as well as spatially varying conditions. These depend on many factors such as climate, hydrology, landform and geology (Winter et al., 1998). Flow through these boundaries has a significant influence on the physical, chemical and biological properties of water. In order to optimise groundwater management, these

[2] colmation: derived from German “die Kolmation” translatable as auto-clogging

variable and ever changing pathways of penetration and flow must be studied to help protect the environment.

2.7. Hyporheic zone

During exchange processes, water passes through the transition zone between riparian environments and active stream channels. Understanding these flows is not only vital for groundwater management, but they also impact on the sensitive ecology of aquatic or benthic life within the hyporheic zone as well as in the stream. The hyporheic zone is part of the streambed and is defined as the region of mixing between surface water and subsurface water (Sophocleous, 2002). It is found to play an important role on the surrounding hydrochemistry, hydrobiology and therefore also hydroecology in small and large scales (Brunke et al., 1997).

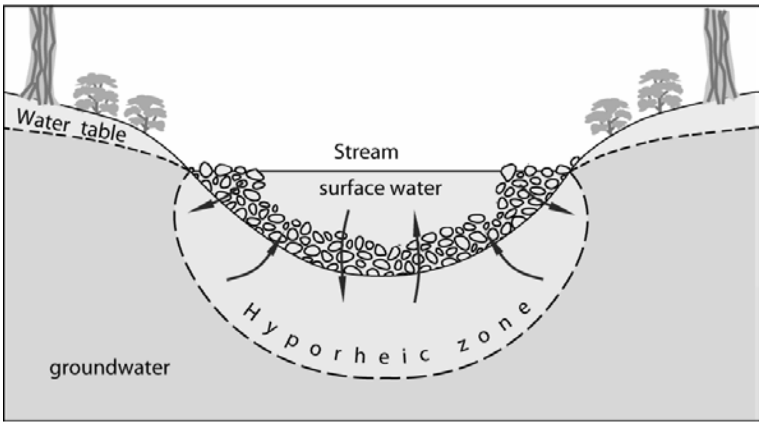

Figure 4: The hyporheic zone (Winter et al., 1998).

Especially nutrient dynamics of the open stream channel is controlled by recharge or discharge through this area (Findlay, 1995). Several physical and biochemical mechanisms such as filtration, absorption, adsorption, retention and decay can influence the water quality enormously. Many chemical processes which occur in this zone are described in Dahm (1998) and evidence for these can be obtained by measuring depth profiles of parameters such as pH, electric conductivity (EC) and dissolved oxygen (DO) etc.

According to Ryan et al. (2006) heterogeneity, bathymetry and groundwater flow are the three major factors affecting solute transport in the sediments. Also, hyporheic processes such as water exchange, invertebrate activity gas production and geochemical reactions can change the hydraulic conductivity (Song et al., 2007) causing spatial and temporal change of streambed properties along a river. As a conclusion, methods for exchange flow quantification in combination with further chemical and biological investigations can support the understanding of complex aquatic and benthic processes as well as biologic life in the hyporheic biotope.

2.8. Riparian environment

The environment between aquatic and terrestrial ecosystems is defined as the riparian zone (Gregory et al., 1991). It contains high stature vegetation and is flooded only occasionally, therefore also referred to as floodplain forest (Dahm et al., 1998). However, it is hydrologically linked to the stream water by underground flow paths. There has even been evidence of surface water bypassing a meander neck by moving only underground (Peterson et al., 2006), contributing to the water supply of the riparian ecosystem. The ever changing water levels cause fluctuations in saturated and unsaturated zones offering diverse conditions. This creates many unique biotopes each hosting numerous different species (Huggenberger et al., 1998). Therefore, riparian zones are ecological regions hosting tremendous biodiversity in flora and fauna.

Water flow from active stream channels into the riparian environment in aggrading river systems depends on the sediments consisting mainly of sands, gravels and cobbles (Huggenberger et al., 1998). The cycling of nutrients within this system is largely depending on the interaction between surface and groundwater, providing the basis for biological life. Therefore, changes in the height of the water table strongly influence the nutrient dynamics (Dahm, 1998). As an example, extraction of groundwater near surface streams can cause the groundwater table to drop until it is below the baseflow level of the stream. In this case, bank storage is prevented and this part of the river can turn into a losing reach, potentially drying out. The impact of extraction can be long term and influence the stream flow even in the next pumping season (Chen et al., 2001). Long term overexploitation can additionally cause drainage of adjacent riparian aquifers until the water level is below the streambed. As a result of this mismanagement, water levels drop and wetlands as well as riparian environments are dewatered causing reduction in biodiversity within surrounding biotopes. Understanding of water interaction and storage mechanisms helps to protect these important habitats.

2.9. Groundwater storage, recharge and discharge

Surface water and groundwater have been used for water storage, extraction and supply for a long time. Especially the storage of water in the ground plays a major role for water supply because areas with high demand, high evaporation and low rainfall can profit from such practices. However, even modern water management in Australia ignores connectivity (e.g. Braaten et al., 2002; Sinclair, 2006) and mostly considers both sources as if they were separate units. This conception can lead to severe impacts on the environment, as withdrawal of surface water can deplete groundwater or extraction from groundwater can lower surface water levels (Winter et al., 1998).

Managing groundwater resources postulates that variables such as recharge and discharge flows are known. These water fluxes, however, can have natural or artificial causes like e.g. gradient flow caused by seasonal changes in precipitation, well pumping, leakage from adjacent geological formations or simply by interacting with surface water levels. Depending on the landscape topography, surface water like rain, rivers, streams and lakes form the main sources of recharge and discharge for groundwater bodies. Some basic mechanisms connecting both distinct sources like e.g. event flow, baseflow, subsurface storm flow, overland flow, interflow and return flow are explained by Sophocleous (2002). All these different water flows are very difficult to quantify but can significantly influence water balance calculations. Several studies have been done to estimate groundwater recharge from stream flow using stream flow records (e.g. Chen, 2003), remotely sensed thermographic profiles (Loheide et al., 2006) and multi reservoir modelling (Pulido-Velazquez et al., 2005). They can contribute to a better understanding of the linkage between surface water and groundwater.

3. The use of heat as a tracer

Temperature changes occur naturally within the environment indicating heat flow. It is impossible to quantify heat flow directly because it is a process variable. However, this can be done by measuring temperature changes of the observed system, and multiplying it with the physical properties of the material. Hence, temperature represents a measurable indicator (state variable) for heat and allows its quantification by applying a balance equation. The general heat equation is as follows

[3] $$Q = m \cdot c_p \cdot \nabla T \quad [J]$$

with q being heat [J], m is the mass of the system [kg], c_p representing the specific heat capacity [J/kgK] (isobaric system) and ∇T the temperature gradient [K]. It quantifies the amount of heat required to raise the temperature of a certain mass of a specific material to a certain degree. Hence, by measuring the temperature heat can be calculated assuming that physical properties are known. Heat capacity may be considered as a function of temperature, but in this case the dependency is negligibly small because of the little range of temperatures which are to be studied (between 0 °C and 35 °C).

Heat only propagates from higher to lower temperatures constantly trying to equalise its system distribution. The major driving force for temperature change and therefore heat flow on the earth's surface is solar radiation. Throughout the sun's daily course incidental radiation is interfered by numerous factors such as season or climate (angle), atmospheric influences (cloud cover, shadows) etc. As light is absorbed at the surface, temperature changes and the natural temperature gradient drives heat flow. In case of surface water warming, heat propagates deeper into the streambed with a certain flow rate which depends on physical properties of the subsurface matrix e.g. heat conductivity, specific heat capacity and water flow velocity. Heat conductivity determines the velocity of a thermal front whilst specific heat capacity quantifies the amount of heat which can be stored within a certain volume. Depending on both these values and on the duration of surface warming, the penetration depth of a temperature fluctuation having a certain period can be estimated.

Another source of heat is the earth's core zone of hot melted material. Three distinct geothermal systems are named by Domenico (1990) as (a) hydrothermal convection, (b) hot igneous rocks and (c) conductive dominated. Furthermore, it has been known for many years that there is a thermal gradient (temperature rise with depth) when drilling deep into the subsurface. This is also confirmed by the fact that groundwater temperatures are usually between 1 and 2°C higher than local mean annual surface temperatures due to geothermal heat flow. Depending on the geological depth profile of the location, the geothermal gradient usually varies between 2 and 30 °C per km depth (Domenico, 1990). Researchers have used the thermal perturbation to investigate vertical subsurface water flow. Apart from heterogeneities in the subsurface matrix, this is considered to be the main factor of disturbance to the thermal gradient (Sass et al., 1971). However, geothermal heat is not the primary focus of this thesis.

3.1. Literature review

Early research work has been done in the 1960's by several authors such as Suzuki (1960), Stallman (1965) and Bredehoeft (1965) with the result that naturally occur-ring heat flow can be used as a tracer for studying groundwater movement and exchange flow. Based on these publications, there is a series of research papers appearing much later in the 1980's modifying, applying and improving the early work to specific cases within various cases of the aquatic environment. Just recently, all this work has been extended further and methods have been developed for the simple deployment of quantification of water motion using modern computing techniques. The following sections review literature for the most important work about heat being used as a tracer to assess exchange flow situations in rivers and channels. Furthermore, methods are extracted which describe the mathematical formulations of the different physical heat and fluid transport phenomena and required for the detection and quantification of flow direction and magnitude.

3.1.1. Methods using temperature values

3.1.1.1. Qualitative methods

A number of researchers have published methods utilising natural heat as a tracer to identify water exchange. The interactivity has been of interest because it is required to (a) develop water budgets, (b) identify nutrient transport and (c) help towards calculation of thermal conditions in small water bodies. In particular, temperature time series measurements were taken in the water and sediments of a creek and the thermal signature was used to detect possible water pathways. The study proved successful as a screening tool only but did not offer the possibility of flow quantification (Silliman et al., 1993).

In a different study, Constantz et al. (1994) demonstrate that the diurnal change in stream temperature is responsible for a change in hydraulic conductivity which therefore enhances stream loss. On the basis of flow and temperature measurements in a losing system they found out that the loss was much more significant than evapo-transpiration. In a similar approach, Constantz et al. (2001) used temperature measurements to detect stream flow frequency and duration in ephemeral channels. He deployed a series of temperature probes along the channel and concluded that the spatial and temporal pattern of flow can be detected. The suggested improvement was to apply a pair of probes at different depths because abrupt changes in surface measurements could also indicate other conditions than water flow.

Alexander (2003) simultaneously measured air, stream and hyporheic water temperatures in a small stream. The study was able to successfully interpret if water was discharging or recharging through the streambed or whether flow was parallel. However, they also concluded that discharging water does not necessarily indicate flow of groundwater but could be stream water which had previously entered the streambed. A very recent study uses remotely sensed thermographic profiles to identify the spatial distribution of groundwater discharge (Loheide et al., 2006). Also, the effects of baseflow and hyporheic exchange were quantified using different conceptual models. However, all these investigations highlight the complexity and variability of interaction. This suggests that more research is necessary to better understand the exchange boundary.

3.1.1.2. Numerical methods

Temperature data has also been used in numerical heat flow models serving several purposes. Ronan et al. (1998) setup a variably saturated model to simulate flow beneath an ephemeral stream and to investigate infiltration rates. The results show that once the model is calibrated it can be used to estimate the infiltration rate based on temperature records in the magnitude of calibration. Moreover, Constantz et al. (2002) performed a study using a numerical model to investigate stream loss and percolation rate in a similar environment. Simulated streambed temperatures were fitted to field records by varying hydraulic and thermal parameters. The primary disadvantage was found to be the fact that single point temperature measurements do not reflect the multi-dimensionality of water flow.

Bravo et al. (2002) suggested that temperature is a powerful additional parameter which can help converging synthetic models with field data. They modelled a wetland and calibrated it with water levels and temperatures to calculate hydraulic conductivity and flux. For a similar purpose Su et al. (2004) created a model to calculate hydraulic conductivities in an alluvial system. Temperature and heads in wells adjacent to a river channel were used for the calibration. Again, conductivities were estimated matching the observed to synthetically created temperature records. All these investigations highlight that there is much more in simple temperature measurements than just a water quality parameter. Hence, a comprehensive summary about the use of heat as groundwater tracer was published with the conclusion that the full potential has not yet been recognised (Anderson, 2005).

Author	**Method**	**Purpose**	**Notes / Results**
Keery et al., 2007	Analytical	GW-SW exchange	Method development neglecting thermal dispersion
Hatch et al., 2005	Analytical	GW-SW exchange	Method development including thermal dispersion
Silliman et al., 1995	Analytical	GW-SW exchange	Method development neglecting dispersion and application, downward flow detection of 0.03 cm/d
Becker et al., 2004	Analytical	GW-SW exchange	Method application neglecting dispersion, upward flow detection of 0.03 cm/h and 0.05 cm/h
Su et al., 2004	Numerical VS2DH	Estimation of hydraulic conductivity	Inclusion of variably saturated zone, estimation by fitting observed to calculated temperatures, detection of streambed clogging
Constantz et al., 2002	Numerical VS2DH	Stream loss investigation	Ephemeral stream (variably saturated), fitting of observed to simulated, reasonable estimates
Constantz et al., 2003	Numerical VS2DH/T	Comparison of heat and bromide	Modelling of solute and heat transport, fitting of observed to simulated, results were comparable

Table 1 summarises all published methods using heat as a tool.

3.1.2. Heat transport theory

3.1.2.1. Heat conduction

Using heat as a tracer for fluid movement can be justified by looking at the physical similarity of the processes: higher gradients cause more water velocity and heat propagation. The mathematical formulation of the Fourier heat flow equation is

[4] $$\vec{q} = -\vec{\vec{\kappa}} \cdot \nabla T \quad [\mathrm{W/m^2}]$$

with q representing the vector of heat flow [W/m^2], κ being the heat conductivity tensor [W/mK] and ∇T representing the temperature gradient [K]. In comparison, Darcy's law describing groundwater motion is

$$[5] \qquad \vec{v} = -\vec{\vec{k}}_f \cdot \nabla h \qquad \text{[m/s]}$$

with parameters see equation [2] (page 5). Both equations have a similar structure but use different parameters and units (Anderson, 2005).

However, looking at a representative volume of a soil sample, it appears that the heat conductivity value has to be adjusted in order to apply the formulation to the physical conditions of porous media and fluid. Considering fully saturated conditions with water filling the total space between randomly distributed soil grains, the bulk conductivity can be expressed as the volume rated geometric mean of solid and water conductivity, thus leading to

$$[6] \qquad \kappa_0 = \kappa_f^n \cdot \kappa_s^{(1-n)} \qquad \text{[W/mK]}$$

with κ_0 being effective conductivity, n representing the soil porosity [-] (explanation see 3.1.2.2) and κ_f and κ_s standing for fluid and solid thermal conductivity [W/mK], respectively (Woodside et al., 1961). The physical assumption is that both, fluid and solids have the same temperature. However, this applies to immobile fluids only as movement would cause microscopic dispersal of heat. The macroscopic result of the increased heat transfer due to this process is usually included in the conductive part of the heat transport equation and will be explained later. The effective heat conductivity equation for porous media can be expressed as

$$[7] \qquad \vec{q}_e = -\kappa_0 \cdot \nabla T \qquad \text{[W/m}^2\text{]}$$

where κ_0 is reduced to a scalar value. This is because simplifications such as averaging of distributed values apply. Therefore heat conduction is isotropic which means it is described as being independent from spatial direction of heat flow. However, this may not be true in a layered environment.

3.1.2.2. Heat convection

There is also an important mechanism where heat is carried by a moving fluid. This process is called heat convection, sometimes also referred to as advection. However, there are two different types: forced convection and free convection. Motion as a result of forced convection is driven by external forces for fluid movement such as pressure gradients and free convection is caused by fluid motion due to its density difference. However, Darcy's law is only applicable in case of forced convection and this thesis will focus on this case in all further discussions.

For this reason we can neglect buoyancy and consider forced convection only in the next description of heat flow

[8] $$\vec{q} = n_e \cdot \rho_f \cdot c_f \cdot T \cdot \vec{v} \quad [\mathrm{W/m^2}]$$

where ρ_w is fluid density [kg/m^3], c_w is the fluid heat capacity [J/kgK], n_e is the effective porosity [-] and v is the velocity vector of the fluid [m/s] (modified from Domenico, 1990). This equation describes heat transported by water movement, induced by a pressure gradient. The fluid only carries heat through a fraction of the total bulk volume. Because we assume saturated conditions, this fraction is represented by the effective porosity value.

In order to determine flow processes and to describe fluid movement in the streambed (porous media), soil matrix properties are required. In this case only macroscopic (volume averaged) properties are considered. The total porosity of a porous medium is defined as the ratio of total void volume to the total volume of the soil sample

[9] $$n = \frac{V_v}{V_t} \quad [-]$$

This value is important for the consideration of heat flow, as it is needed to define the bulk values of conductivity and heat capacity discussed earlier. For the actual convective heat flow process, however, the value of the effective porosity is required. This is the ratio between the total void volume participating in fluid flow (V_f) and the total volume of the soil sample V_t, or the Darcy velocity v_f divided by the specific discharge of a conservative tracer v_t

[10] $$n_e = \frac{V_f}{V_t} \equiv \frac{v_f}{v_t} \leq n \quad [-]$$

Effective porosity is distinguished from total porosity because in some cases not all water within the bulk volume takes part in the actual flow process. This influences the amount of heat convectively transported with water. It may differ from the total porosity which should be used for heat conduction because all pore water conducts heat, no matter if being immobile (e.g. occupying dead end pores) or not. None of the heat transfer models which are used in this thesis specifically mention the difference. This may be caused by the fact that the effective porosity is very difficult to quantify. It can only be estimated by using conservative tracers, preferably in-situ. In the case of distinction between both values, much bigger analytical effort would be involved prior to simple temperature investigations, hence defeat the purpose.

On the other hand, values for total and effective porosity differ only in some case. The reasons for that can be

- secondary porosity such as cracks dominating the rock structure
- materials consisting of differently shaped grains with random contact
- partly consolidated soil grains which are highly compacted.

The effective porosity value is also required for more accurate calculations of volumetric water flow from fluid velocity using the area of discharge.

The likeliness of effective and total porosity values diverging is higher for smaller grain sizes. In fact, Yeh et al. (2000) carried out a study to calculate hydraulic conductivity and effective porosity of clays using a solute transport model, low level gradients and conservative tracers. The results suggested that total porosity can be as high as approx. 0.8 in comparison to the effective porosity being only 0.05. For field applications in low flow environments the individual properties can be considered by taking samples from the investigated soil and testing it according to this method, featuring an accuracy of 5.5% (Yeh et al., 2000).

3.1.2.3. Convection versus conduction

A thermal front within the water saturated system can travel by both, convection and conduction. In order to distinguish between those two mechanisms, the dimensionless Peclet number can be used. It describes the relative magnitude of heat movement by convective and conductive heat transport (Anderson, 2005). Its formulation is given as

$$[11] \quad Pe = \frac{\rho_w \cdot c_w \cdot n \cdot v_f \cdot L}{\kappa_e} \quad [-]$$

where L represents a characteristic length of the system studied. The selection of L depends on the purpose of the investigation. According to Silliman et al. (1995), the distance between two thermistors is inappropriate as it would lead to the Peclet number being a function of depth of measurement rather than the system. For the case first mentioned, the Peclet number is able to characterise the main cause of the heat travel between two thermistors. If Pe >> 1 heat propagation is convection dominated whilst if Pe << 1 it is dominated by conduction. For the second case, the mean grain diameter is considered to be an appropriate length value representing the system. Figure 5 shows the difference between the paths of heat conduction (grey arrows) which travels throughout the entire medium, and heat convection (black arrow), which is caused by fluid flowing only in the voids between grains. Note that if heat convection is faster than conduction both mechanisms are superimposed which will cause heat conduction along the flow path. This may mix heat dispersion and conduction considerably.

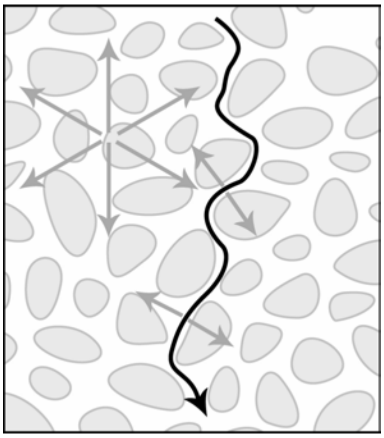

Figure 5: Illustration of the travel path of heat by conduction (grey) and convection (black).

3.1.2.4. Heat transport equation

A comprehensive mathematical description of the physical processes related to heat transport in porous media can be determined by applying a heat balance. Equations [7] and [8] are combined and a term is added which describes the gain or loss of heat caused by any change of temperature within the investigated volume. Applying the condition of total heat conservation within that volume, the equation

$$[12] \quad -\nabla \cdot \vec{q} = \rho \cdot c \cdot \frac{\partial T}{\partial t}$$

states that net loss of heat must be the same as the rate of temperature change. This equation implies the continuity condition which is necessary when using heat as a conservative tracer. It contains the effective volumetric heat capacity which combines both, the physical properties of water as well as the solid matrix per unit volume

[13] $$\rho \cdot c = n \cdot \rho_f \cdot c_f + (1-n) \cdot \rho_s \cdot c_s$$

with ρ and c being bulk density [kg/m^3] and heat capacity [J/kgK], respectively.

Further replacement of equation terms with previously mentioned formulations leads to the general formulation of the differential conductive convective heat transport equation

[14] $$\frac{\kappa_e}{\rho \cdot c} \cdot \nabla^2 T - \frac{\rho_f \cdot c_f}{\rho \cdot c} \cdot \nabla \cdot (T \cdot \vec{v}) = \frac{\partial T}{\partial t}$$

as firstly stated by Stallman (in the year 1960, according to Bredehoeft, 1965). The first term represents heat conduction (see equation [7]), the second term is responsible for heat convection (see equation [8]) and the right term describes temperature change with time. Density and heat capacity of the water and surrounding solids as well as heat conductivity is assumed to be independent from temperature change. This equation is valid for transient fluid flow in isotropic, homogeneous and fully saturated single fluid conditions.

For field applications, however, this statement can be simplified to a one-dimensional formulation only, making it more manageable to find simple analytical solutions to boundary conditions

[15] $$\frac{\kappa_e}{\rho \cdot c} \cdot \frac{\partial^2 T}{\partial z^2} - v_z \cdot \frac{\rho_f \cdot c_f}{\rho \cdot c} \cdot \frac{\partial T}{\partial z} = \frac{\partial T}{\partial t}$$

According to Stallman (1965) this equation can only be used when the following conditions are satisfied

- fluid flow is parallel, steady and uniform along the z axis
- heat properties of the fluid and the medium are homogeneous, isotropic and constant in time
- all components of heat flow occur only along the z axis
- temperature of the interstices and adjacent solids is equal at all times

Given the fact that all measured parameters such as temperature or depth depend on measurement accuracy, and properties like heat conductivity are estimated, there are a number of impacts to calculations. Furthermore, the above mentioned restrictions are rarely given in the field and will cause additional uncertainties. Therefore, a sensitivity analysis will be performed to investigate errors due to reasons like parameter estimates or violated boundary conditions.

However, the first term of the above equation contains the effective thermal diffusivity which is analogous to the one used for solute transport. Considering additional hydrothermal dispersion, the term has to be supplemented according to Anderson (2005) with

$$[16] \quad \frac{\kappa_e}{\rho \cdot c} = \frac{\kappa_0}{\rho \cdot c} + \beta \cdot |\vec{v}| = \frac{\kappa_f^n \cdot \kappa_s^{(1-n)}}{\rho \cdot c} + \beta \cdot |\vec{v}|$$

The equation does now additionally contain β [m], the thermal dispersion coefficient combined with the modulus of seepage velocity v_f [m/s]. In literature, opinions are diverging whether to neglect dispersivity and include its effect into the thermal diffusivity or to account for it separately (Anderson, 2005). The first approach would only be valid for really small seepage velocities when the value of the second term in equation [16] can be neglected. However, heat dispersivity is thought to be the same process as chemical dispersion, which is widely used in the areas of solute transport. Unlike a chemical substance heat dispersion also contributes to further heat conduction as it is capable of also propagating through the solid material (refer to chapter 3.1.2.3 on page 20). This outlines the major physical difference between both processes which are mathematically described in the same way. Hence, dispersivity considerations are quite important for the correct interpretation of heat propagation and the corresponding result of flux calculation (Hatch et al., 2006).

3.1.2.5. Temperature forward modelling

As mentioned above, heat always tries to equilibrate within a more closely observed area of an aquatic system. Therefore, temporal change of boundary temperatures may be useful for studying its propagation. This condition is given by change in temperature due to daily, seasonal and annual fluctuations in solar radiation occurring on the earth's surface. Certainly, this also affects the temperature of shallow surface water bodies such as rivers, streams and ponds. These periodic fluctuations of temperature in surface water are transferred into the subsurface mostly by water saturated or semi-saturated sediment heat conduction but especially by fluid convection through streambed sediments. Heat propagation can be measured in form of temperature changes and used for both, the simple detection of water movement direction as well as detailed investigation and quantification of water exchange flows (Constantz et al., 2003).

Silliman et al. (1995) derived a solution for predicting the temperature within a certain depth of the sediments given a temperature time series on the bottom of the water column just above the sediments. Based on the differential conduction convection equation [15] (see page 22), the following boundary conditions are considered

[17] $T(0,t) = T_w(t)$ and $\lim\limits_{z\to\infty} T(z,t) = T_A$

In this case, T_w is the temperature at the base of the water column [°C] (upper temperature) and T_A is the ambient groundwater temperature at a depth where it is unaffected by fluctuations.

A solution is searched for calculating the corresponding time series in a certain depth of the sediment. The upper boundary condition is given as a series of temperatures discretely measured over time rather than a continuous temperature function. The differential equation is of linear nature and therefore a superposition of solutions can be developed. Hence, the propagation from one point to another is easily calculated by summing the relative response which depends on depth z and on the time t. The solution scheme leads to the following set of equations (Silliman et al., 1995)

[18] $T_s^n(z,t) = T_0(z) + \sum_{i=1}^{n} \Delta T_s^{i,i-1}(z,\tau)$ with $\tau = t - t_i$

and T_s representing the n-th temperature [°C] value of the desired time series calculated at time t_n [s] and depth z [m]. Every single entry n of the second time series is calculated as the summation of all i relative temperature changes prior to time t_n and the impact at depth z and time weighted with its propagation effect. This influence can be quantified using equation

[19] $$\Delta T_s^{i,i-1}(z,\tau) = \frac{\Delta T_w^{i,i-1}}{2} \cdot \left[erfc\left(\frac{z - C\cdot\tau}{2\cdot\sqrt{D\cdot\tau}} \right) + \exp\left(\frac{C\cdot z}{D} \right) \cdot erfc\left(\frac{z + C\cdot\tau}{2\cdot\sqrt{D\cdot\tau}} \right) \right]$$

where ΔT_s is the temperature change within the sediments and ΔT_w the one in the water column. The values of C and D are given as

[20] $C = \frac{\rho_w \cdot c_w}{\rho \cdot c} \cdot n \cdot v_z$ and $D = \frac{\kappa_e}{\rho \cdot c}$

with ρ_w and ρ being density [kg/m^3] and c_w and c being specific heat capacity [J/kgK] of the water and the saturated sediments, respectively. The effective thermal diffusivity of the sediment is given with κ_e [W/mK]. Hydrothermal dispersion was not considered in the original model but was added in this study by using κ_e instead of κ_0 (see equation [16] on page 23 for further details).

Since all temperatures are expressed as summations of temperature changes and are therefore of relative nature, the pseudo initial condition T_0 is used to regain absolute values. According to Silliman et al. (1995), the value of this initial condition has a considerable effect on a certain number of the first calculated solutions. This effect can be minimised by selecting an appropriate initial temperature value which should match the real value at the initial time and desired depth.

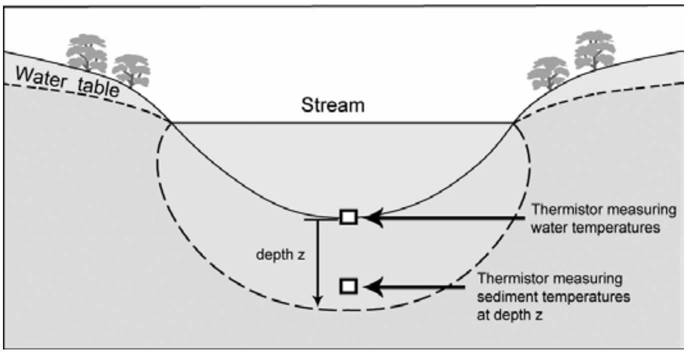

Figure 6: Illustration of two discrete measurement points in the streambed as required for forward modelling.

The above explained solution of the heat equation is only valid within the following initial condition

[21] $T_s^i(z,0) = 0$ and boundaries $\Delta T_s^{i,i-1}(0,\tau) = \Delta T_w^{i,i-1}$ and $\lim_{z\to\infty} T_s^{i,i-1}(z,\tau) = 0$

An important fact is also mentioned in the publication. It is the condition that the solution itself only satisfies the differential heat equation in the case of $T_0 = T_A$.

Silliman et al. (1995) developed and used this particular forward calculation method to estimate the vertical water flux from the best fit of observed and calculated sediment temperatures, based on the water column time series. They state that the solution is sensitive and usable for water fluxes which are greater than 7.2×10^{-3} m/d but downwards only due to the nature of the boundary conditions. However, Becker et al. (2004) illustrate that the same method can be applied to derive both, upward (negative) and downward (positive) flux directions. Restrictions are, once again, only vertical water flux and the initial condition, because its influence is never completely zero but decreases with time.

As an example, Figure 7 shows the temperature response to a sudden increase of 1°C of surface water temperature in 0.15 m depth of the sediment. It is calculated by the forward modelling approach. The depth response clearly depends on water seepage velocity as well as the direction of flow. Physical properties of the sediment are indicated in table 4 (page 73).

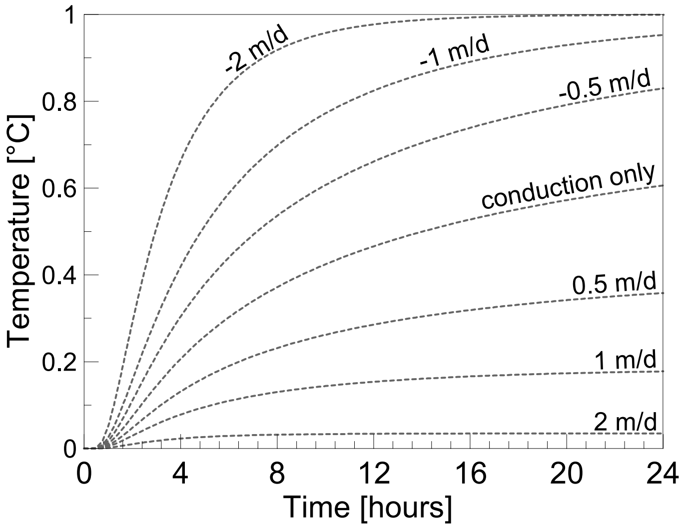

Figure 7: Response of sediment temperature to a sudden step increase of 1°C in water temperature at the top with various water exchange velocities.

However, one major disadvantage of this method is given by the fact that the estimated seepage velocity is assumed to be in steady state, and therefore constant over time. This would only represent an integrative or time averaged water flux which depends on the length of the temperature record. There is a compromise between short and long temperature time series. Short ones offer a velocity value better matching steady state conditions but contain more error due to the influence of the initial temperature condition. This impact decreases with longer time series but the seepage velocity does not reflect possible transient flow conditions. However, this is the parameter of major interest and forward modelling will be used to fit observed temperatures finding best matching value.

3.1.2.6. Using temperature fluctuations

Surface water temperatures are influenced by complex processes coupled with the environment. The sun's extraterrestrial radiation is the major driving force which continuously feeds energy to the earth's surface. However, because of the globe's continuous rotation there is a distinct diurnal rhythm in energy transport causing rhythmic temperature change (day and night). These temperature changes induce periodic heat flow which can be used as a tracer for assessing exchange flows between surface and groundwater bodies. Suzuki (1960) was amongst the first to recognise this fact and he applied a sinusoidal temperature function as an upper boundary condition to the heat transport equation [15] (see page 22). He derived an analytical solution for quantifying water percolation rates under flooded rice fields (paddies). The purpose was to calculate a better water balance leading to an improved understanding of the hydrological process, thus a better irrigation management. His solution relates the change of water temperature over depth to the infiltration velocity of surface water. Reversely, seepage velocity can be estimated by quantifying the ratio of temperature peaks occurring at different depths. Some years later, Stallman (1965) noticed that this solution was an incomplete approximation relying on steady state flow. He developed a more accurate approach also using a lower boundary condition. This assumes a constant temperature for large depths (z positive downwards) given the fact that groundwater doesn't show any significant temperature perturbations. Stallman's (1965) boundary conditions are the following

[22] $$T(0,t) = T_0 + \Delta T \cdot \sin\left(\frac{2 \cdot \pi \cdot t}{P}\right) \quad \text{and} \quad \lim_{z \to \infty} T(z,t) = T_A$$

with T_0 and ΔT being the average ambient temperature [°C] and the amplitude on the surface, respectively, P being the period of considered fluctuations (diurnal ~24 hours = 86,400 s) and T_A representing the average ambient groundwater temperature [°C]. His solution satisfies the heat equation [15] for $0 < t < \infty$ and $0 < z < \infty$ and implies that the system is in thermal equilibrium throughout depth z. The analytical solution is a two-dimensional surface function calculating thermal response (absolute temperatures) to a periodic temperature variation at the surface, depending on sediment depth, thermal properties of the porous media and fluid velocity.

Based on Stallman's (1965) work, researchers have developed modifications and extensions which were then successfully applied to specific problems. Keery et al. (2007) derived an improved analytical derivation of the solution to calculate seepage velocities, but his approach does not allow the determination of directions and also neglects thermal dispersivity. Goto et al. (2005) expanded the original solution in order to calculate the temperature response to an arbitrary but finite series of n trigonometric fluctuations, given the fact that temperature time series usually feature numerous perturbations with different periodicity in superposition. His mathematical formulation is a slight enhancement by providing a simple summation of the sediment thermal response to all these periodic signals in the following formulation (Goto et al., 2005)

[23] $$T(z,t) = \sum_{i=1}^{n} A_i \cdot \exp\left(\frac{v \cdot z}{2 \cdot \kappa_e} - \frac{z}{2 \cdot \kappa_e} \cdot \sqrt{\frac{\alpha_i + v^2}{2}}\right) \cdot \cos\left(\frac{2 \cdot \pi \cdot t}{P_i} - \frac{2}{2 \cdot \kappa_e} \cdot \sqrt{\frac{\alpha_i + v^2}{2}}\right)$$

with the coefficient α_i being

[24] $$\alpha_i = \sqrt{v^4 + \left(\frac{8 \cdot \pi \cdot \kappa_e}{P_i}\right)^2}$$

The parameter v_i represents the velocity of the thermal front and can be transformed into the corresponding fluid velocity by the relationship

[25] $$v = v_z \cdot \frac{\rho_f \cdot c_f}{\rho \cdot c}$$

The following variables are used in the above solution [23]

- A amplitude of temperature perturbation [°C]
- v velocity of the thermal front [m/s]
- v_z water seepage velocity [m/s]
- z depth within the sediment (positive downwards) [m]
- κ_e effective thermal diffusivity of the saturated sediment [W/mK]
- P period of the temperature perturbation [s]
- ρ_f density of the water [kg/m3]
- c_f specific heat capacity of the water [J/kgK]
- ρ density of the saturated sediment [kg/m^3]
- c specific heat capacity of the saturated sediment [J/kgK]

It is important to note that this solution is restricted by assumptions mentioned with the heat transport equation [15] (page 22).

Goto et al. (2005) examined and discussed this formulation and found that the thermal response to temperature fluctuations depend on the direction and velocity of the fluid, the physical properties of the sediment and fluid, and the period of the considered temperature fluctuation. They used two dimensionless parameters: the thermal Peclet number (see equation [11] on page 21) and derived another number related to the three influential factors mentioned above. These can be used to categorise the response in the following way

- Thermal response to heat fluctuations with downward fluid flow

    - heat transport strongly driven by convection ($Pe > 4000$)
    - heat propagation strongly driven by conduction only ($Pe < 0.01$)
    - transition between convection and conduction ($0.01 < Pe < 4000$)

- Thermal response to heat fluctuations with upward fluid flow

- heat transport as a balance of convection and conduction (Pe ~1)
- heat propagation driven by conduction only (Pe < 0.01)
- transition between both mechanisms (0.01 < Pe < 1)

Thermal properties of the sediments depend on many factors such as porosity and composition, and are differ with areas of application. Therefore they have to be either estimated or tested. However, the properties of water are generally well documented. The period of temperature perturbation plays an important role in this case of heat transport because the longer it is, the further a heat wave can travel into the ground. Reversely, short term fluctuations are damped very quickly. As a conclusion, the penetration depth strongly depends on the period of the surface temperature signal. Goto et al. (2005) derived a response formulation for the calculation of amplitude decay and phase shift of the original boundary signal. They found that the amplitude decreases exponentially and phases of the signal shift linearly with depth. Both, however, are strongly influenced by fluid velocity but the second is independent of fluid direction. This method was successfully applied to a hydrothermal mound at the seafloor. Vertical fluid velocity and thermal diffusivity could be estimated quite accurately (Goto et al., 2005).

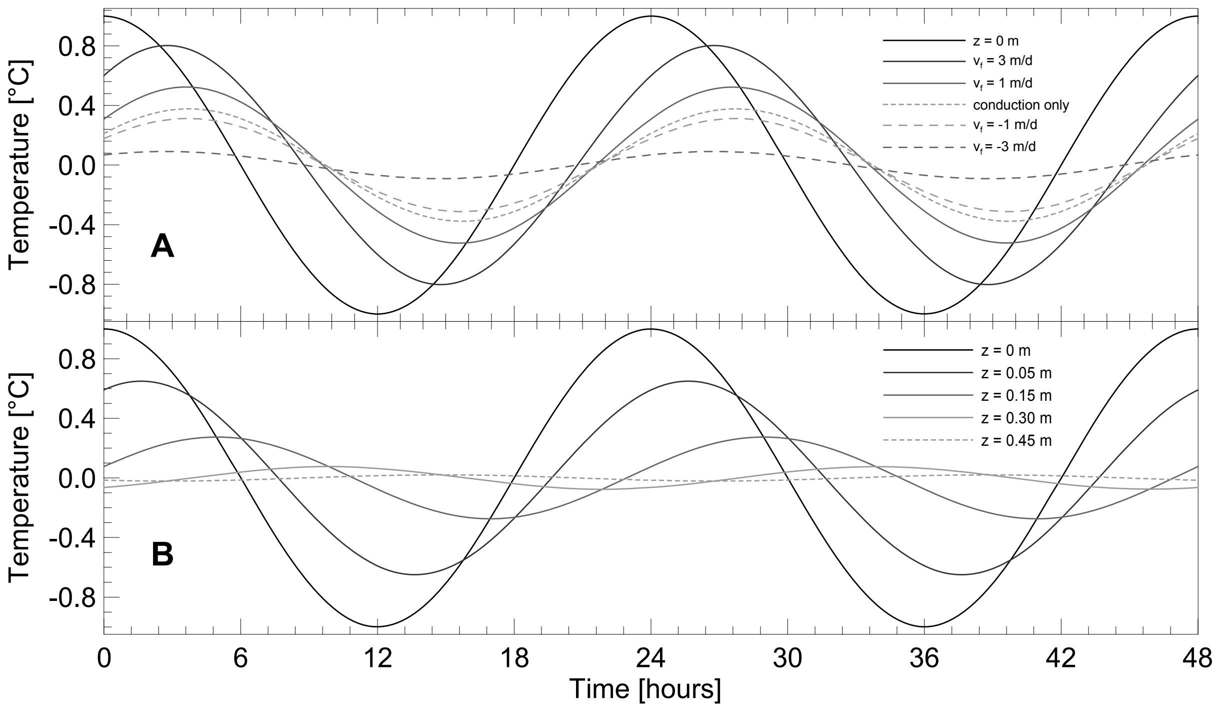

Figure 8: (A) Thermal response of sediment temperatures at the depth of 0.15 m to a diurnal, sinusoidal perturbation (period of 24 hours) in the surface water. The signal is strongly influenced by fluid flow varying in velocity and direction. (B) Temperature depth profile (see legend for depths) under purely conductive conditions (v_f = 0 m/d).

Figure 8 demonstrates the thermal depth response in sediments to a sinusoidal temperature variation with a period of 24 hours at the bottom of the surface water column. The values were calculated using equation [23] (see page 27) and physical properties as indicated in Table 4 (page 53). It is obvious that fluid velocity and direction strongly influence the otherwise purely conductive heat propagation. This impact can be used to quantify the water movement as discussed further.

Amplitude ratio and phase shift solutions

In a similar approach, Hatch et al. (2006) used the same formulation but focused only on the diurnal (period = 24 hours) temperature signal which is most distinct. They developed a new method to calculate the time series of surface water groundwater exchange flux based on periodic temperature measurements in certain depths of the sediments using propagation of daily heat as a tracer. Because it is the most promising approach resulting in a velocity time series, it will be applied in this thesis to data obtained from field measurements. The method itself is quite simple but requires somewhat complex data processing; therefore it will be explained in more detail.

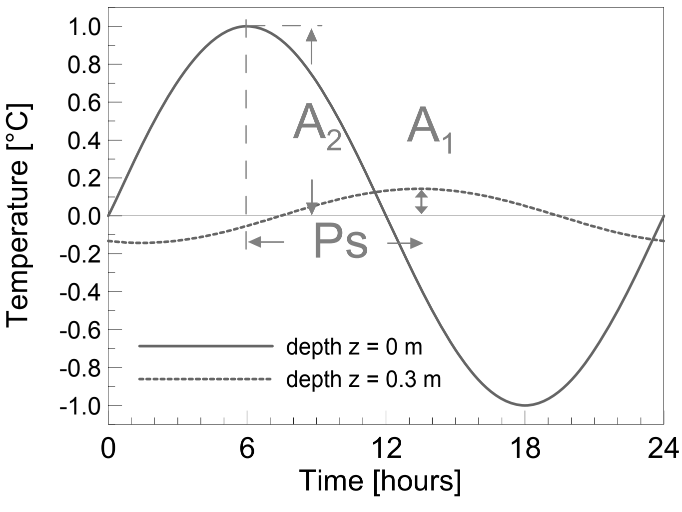

Figure 9: Illustration of the determination of amplitude ratio and phase shift applied to measured temperatures at two distinct depths.

Following Stallman's (1965) solution but using only the daily periodicity of the temperature signal, Hatch et al. (2006) derived two distinct formulations for calculating the same vertical water flux. The equation [23] (see page 27) can be separated into components and solved for amplitude ratio and phase shift of signals measured in two different depths, referred to as 1 (shallow) and 2 (deep). The exponential term multiplied with the amplitude of the original signal describes its damping with depth and can therefore be extracted (Hatch et al., 2006), thus leading to

[26] $$A_r = \frac{A_2}{A_1} = \exp\left(\frac{\Delta z}{2 \cdot \kappa_e} \cdot \left(v - \sqrt{\frac{\alpha + v^2}{2}}\right)\right)$$

with A_2 and A_1 being amplitudes of the deeper and the shallower measurements, respectively, and A_r being amplitude ratio [-] (all other variables see equation [23]). The cosine function which is the next factor multiplied with the original temperature amplitude describes the phase shift and can also be extracted and reformulated as

[27] $$\Delta\phi = \phi_2 - \phi_1 = \frac{P \cdot \Delta z}{4 \cdot \pi \cdot \kappa_e} \cdot \left(\sqrt{\frac{\alpha - v^2}{2}}\right)$$

with ϕ_2 and ϕ_1 being phase of the deeper and of the shallower maximum, respectively, and $\Delta\phi$ the difference. This equation quantifies the difference between the arrival times of a surface temperature peak in two different depths. Figure 9 illustrates amplitude ratio and phase shift definition applied to a synthetically created example.

Because we are interested in the calculation of the actual seepage velocity, both formulations have to be rearranged for the velocity of the thermal front. This leads to a set of equations

[28] $$v_{Ar} = \frac{2 \cdot \kappa_e}{\Delta z} \ln(A_r) + \sqrt{\frac{\alpha + v_{Ar}^2}{2}} \quad \text{and} \quad v_{\Delta\phi} = \sqrt{\alpha - \left(\frac{\Delta\phi \cdot 4 \cdot \pi \cdot \kappa_e}{P \cdot \Delta z}\right)^2}$$

which have to be solved iteratively because the velocity parameter cannot be isolated analytically. Finally, water seepage velocity can be calculated according to

[29] $$v_{Ar,z} = v \cdot \frac{\rho \cdot c}{\rho_f \cdot c_f} \quad \text{and} \quad v_{\Delta\phi} = v_{\Delta\phi,z} \cdot \frac{\rho \cdot c}{\rho_f \cdot c_f}$$

All above equations only contain the relative value of spacing (Δz) between two temperature probes. This means that absolute depth measurement of the sediment is not necessary anymore. The great advantage is that the method has now become relative; hence in case of stream scouring due to e.g. flood events the solution is still applicable (Hatch et al., 2006). In this case, all temperature probes must stay within the sediments for the theory to be valid, since it is based on the heat equation for porous media. According to Hatch et al. (2006), this procedure can theoretically be applied to a times series of any length. However, before extracting the amplitudes and peak times of two time series of temperature measurements it is important to filter for desired oscillations only. This is discussed later in the methodology section.

Sensitivity to probe spacing

This particular method features the advantage of calculating the same fluid velocity from two different mathematical formulations. However, both results should have matching unless there are influencing factors e.g. violated boundary conditions due to natural impacts or erroneous experiment setup. Both solutions can be examined for sensitivity to spacing and physical parameters. As an illustration, Figure 10 (adapted from Hatch et al., 2006) is calculated from equations [26] and [27] (see page 31) and its partial derivations using physical parameters as illustrated in Table 4 (page 53). The plots clearly show that there is different mathematical behaviour of both formulations, and values as well as sensitivity depend on the probe spacing.

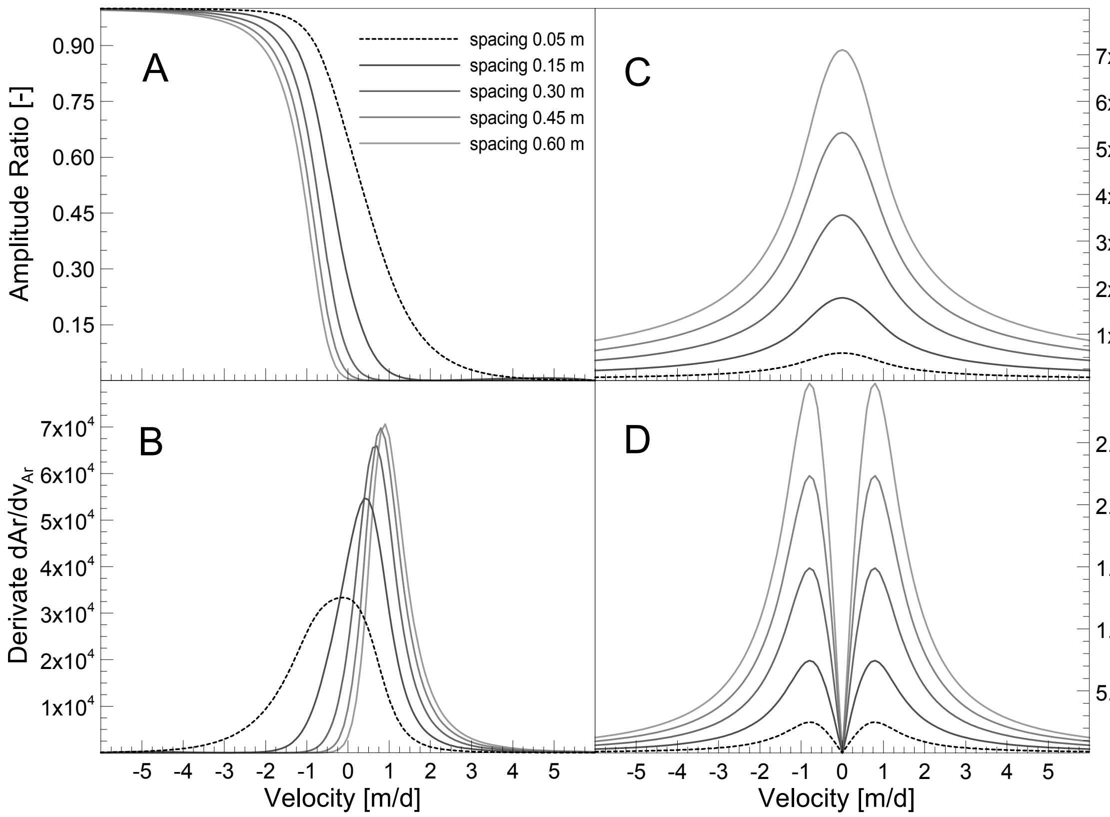

Figure 10: (A) Amplitude ratios versus a range of seepage velocities for three different depths; (B) sensitivity of the amplitude ratio function; (C) Phase shift versus seepage velocity and (D) sensitivity of the phase shift function.

As illustrated in Figure 10, maximum sensitivity for the amplitude ratio function shifts to positive (or upward) fluxes, slightly changing its shape and becoming more sensitive with increased probe spacing. For this solution, best sensitivity for a given thermistor distance between thermistors is reached with low velocities in either upward (more spacing) or downward (less spacing) direction. Hence, this solution features unique values allowing the direction of flux to be determined.

The phase shift formulation is useless under purely conductive conditions, as its sensitivity becomes zero. Also, values are not unique and cannot be used to describe flow direction. However, the advantage is its higher sensitivity with higher velocities in both directions, making it a robust detection tool for fast exchange flows. Greatest sensitivity is reached roughly around ± 1 m/d of water flux. Same as with the amplitude ratio, the solution becomes more sensitive with larger probe spacings as long as a robust signal can still be detected.

The above illustration shows how important probe spacing is in order to detect different ranges of exchange fluxes. It is therefore quite useful to cover multiple depths by installing an array of probes allowing pairs of different thermistors to be selected for evaluation depending on signal strength and thermistor resolution. There is, however, a compromise to be considered because the propagation depth of temperature perturbations strongly depends on its periodicity. This means that oscillations with increasing frequency are filtered with increasing sediment depth, until the signal becomes smooth and amplitudes are below instrument resolution. Thus, the use of daily fluctuations is therefore limited to a certain depth. Precautions can be taken by using an array of temperature probes which are placed in different depths. The advantage is also that each combination of probes offers the calculation of two separate fluid velocity values (Hatch et al., 2006). The recorded temperature signal must be inspected for any distinctly sinusoidal variation featuring an arbitrary but distinct periodicity. After band-pass filtration these can be used to calculate seepage fluxes. However, calculations utilising longer signal periods require sufficiently long data records. The resulting velocity values are averages between the times of neighbouring peaks of the temperature time series taken in two different depths.

3.1.2.7. Physical parameters

Seepage solutions derived from both, amplitude ratio and phase shift equations depend upon the value of several physical parameters (see equations [26] and [27] on page 31). Some of these can be accurately assigned because physical properties of water are known (NIST, 2005). However, the four following sediment parameters can vary with the locations where this method is applied

- n porosity of the streambed [-],
- c_s specific heat capacity of the grain materials [J/kgK],
- κ_s thermal conductivity of the grains [W/mK]
- β thermal dispersivity coefficient of the system [m].

The distribution of each of these parameters is generally heterogeneous within a particular site. This variability could offer equivalent velocity solutions for different sets of parameters. Therefore, solutions of the seepage equations are considered to be highly non-unique and calculations must be restricted to either literature values or results taken from field or laboratory experiments, perhaps using sediment samples. But even these results can be erroneous and not representative of the investigated location but still offer reasonable estimates. Values as taken for this investigation are discussed later.

3.2. Applicability

In this thesis, the investigated system is the shallow surface water body and its adjacent hyporheic zone, which extends further into the subsurface. On the micro scale, this is a very complex environment. Looking closer at a representative volume within this zone illustrates that it contains numerous different organic and inorganic substances in different phases. There are e.g. gravel and sand grains (mainly inorganic solids), various organic sediments (solid phase) originating from plant and animal decay, randomly transported and deposited by flow and there is water (liquid phase), which carries a great amount of solids as well as suspended and dissolved substances such as gases, bacteria, organic molecules, inorganic substances etc. In case of ephemeral stream flow air and water vapour (gas phase) have to be taken into account because the system may be semi-saturated at times. Because of the complexity of interactions between all mentioned factors, mathematical modelling of heat flow on the micro scale involves a huge number of heat sources and sinks to be added to balance equations, e.g. phase changes (latent heat), chemical reactions and biologic activity (biochemical energy). It becomes obvious that at this scale heat is a non conservative tracer and its balance calculation is coupled with various different processes.

The conclusion for modelling of heat transfer is therefore that the micro scale is far too complex to be mathematically described, thus simplifications are needed. All further considerations are done on the macro scale which implies average system properties and therefore eases computing efforts on the spatial and on the temporal scale. Assuming this, the aquatic system can be described as body of porous media (solids) which is fully water saturated and features an unknown seepage velocity of water (liquid) through its voids. For all analytical solutions considered in this thesis water flow is strictly assumed to be one dimensional, referred to the thermistors. The convective conductive heat transport equation (equation [15] on page 22) can be used to mathematically describe the physics of heat flow in such a system. However, it is important to mention that it is restricted to fully water saturated conditions as the equation is single phase only and multiphase flow as well as phase change is physically not incorporated. In terms of heat propagation considered in this work, it is assumed that all internal sources and sinks of heat such as chemical and biologic activity are negligibly small. On the macro scale heat can be considered as a conservative tracer within the limitation of aforementioned conditions, thus making balance calculations much easier.

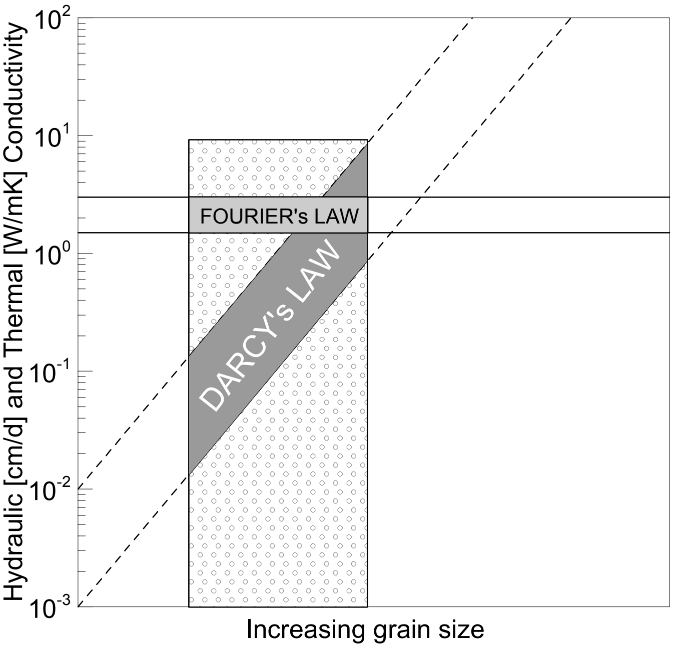

Figure 11: This diagram shows the difference in uncertainty of hydraulic and thermal conductivity values, adapted from Stonestrom (2003).

Modelling with above mentioned simplifications has the advantage of reducing the physical and therefore also the mathematical modelling efforts, thus improving necessary data handling e.g. literature values or the amount of data to be collected in the field. On the other hand such simplifications also result in less detailed model outcome and can contain unknown sources of error. Unfortunately, this reduces the field applicability in case of more complex environments such as multiphase flow. In this case the investigated environment mainly consists of alluvial deposits like inorganic sands, gravels and cobbles. Therefore, the convective conductive heat transport equation represents the closest possible compromise between accuracy and simplification.

Stonestrom et al. (2003) highlight a significant advantage of using heat as a tool for studying the movement of groundwater near streams. The adapted plot (see Figure 11) outlines that in case of using only Darcy's law for flow quantification the required hydraulic conductivity value is a function which depends on the grain size. For field conditions, there is often a large uncertainty in selecting an appropriate value directly influencing flow calculations (note the vertical width of the hydraulic permeability band). On the other hand, heat calculations using Fourier's law requires heat conductivity values which are not a function of grain size or texture. Compared to the traditional Darcy flow model its range of values is also much smaller. This partly originates from the fact that heat travels through all materials (including solids) in a bulk volume of saturated porous media. Contrarily, water flow is forced to follow the tortuous paths between single grains thus causing friction which impacts on the pressure velocity relationship. The only trouble using Fourier's equation is the selection of an appropriate formulation to calculate bulk heat conductivity, as there are distinct models which depend on the geometrical distribution of both, solid and liquid phases.

Temperature measurements are an excellent tool in combination with traditional water level or pressure investigations, as it represents an additional distinct parameter to describe the physical state of an observed system. This can help to constrain modelling parameters because of adding another degree of freedom to the calibration process. Especially in the field of groundwater investigations temperature is an often neglected parameter which potentially offers additional information to enhance field interpretation. Moreover, modelling of heat flow allows the convenient detection of seasonal and long term variations in water flux due to either natural or artificial influences such as climatic conditions or pumping in adjacent wells. Spatially and temporally varying fluxes leading to groundwater recharge can be estimated, which helps to understand the connectivity between surface water and groundwater.

Due to the constant advance in technology temperature logging with special devices has become simple, reliable and inexpensive. Additionally, temperature data is directly available for inspection without much processing efforts such as laboratory work etc. Thus, many interesting investigations based on heat flow have been published and therefore interpretation methods are available. Another great advantage of using heat as a tracer is its natural occurrence and therefore the opportunity for in-situ monitoring without much impact on the experiment. There is no need for the injection of artificial substances such as conservative chemical tracers usually released during field research. In fact, Constantz et al. (2003) exemplified the comparison of heat and bromide and found that both tracers offer quantitatively comparable hydraulic results. The major disadvantage of using heat as a tracer is its limitation to detect only the flow component which is perpendicular to the surface. This is due to the fact that natural heat has to be considered as an area and not as a point source, in shallow aquatic environments. Unfortunately, this limits the true description of the four-dimensional nature of water flow but enables a simple exchange water balance, as only the perpendicular value is required for many purposes. Nevertheless, heat promises to be a reliable tracing tool particularly when used for estimating direction and quantification of vertical water flows through streambed environments within surface waters.

4. Methodology

4.1. Installation equipment

As part of this research project, all necessary test equipment was designed and hand crafted in the workshop of the Water Research Laboratory (WRL) which is a remote campus of the University of New South Wales (UNSW) in Sydney, Australia. Five temperature probes in different depths are used at each location. The probes are equipped with a thermistor and internal computing unit to automatically measure and store temperature data. The probes are also fitted with an infrared communication window at the bottom which can be used together with a USB docking station to easily setup and retrieve the recorded information. Technical details and a sketch of the array are illustrated in Figure 12.

Probe	HOBO Water Temp Pro v2
Range	-20°C to 50°C in water
Resolution	0.02°C between 0°C and 40°C
Accuracy	± 0.2 °C between 0°C and 50°C
Stability	0.1°C drift per year
Response	5 minutes in water
Clock Stability	± 1 min/month (0 °C - 50 °C)
Capacity	42,000 12-bit measurements

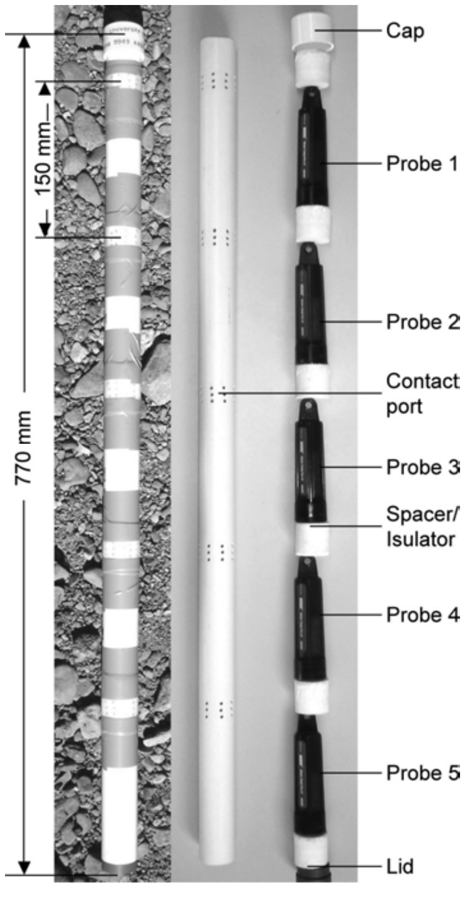

Figure 12 contains technical details about the thermistor and shows the array including dimensions prior and after assembling.

A simple PVC pipe with a diameter of 31 mm was cut to approx. 770 mm length which was required to host all five probes internally. To avoid heat transfer within the pipe, probes were separated by foam spacers featuring very little thermal conductivity. A special lid was fitted to the bottom and a cap to the top labelled with information to allow identification after installation. Three rows of holes were drilled into the PVC pipes at all positions of the internal thermistor to allow water contact and therefore heat transfer to propagate inside the pipe. The distance of 15 cm between each thermistor was used. The holes were covered with polypropylene screen (hole size of 105 µm) to prevent sand from settling inside the pipe which would make disassembling difficult.

Assembling the array was simply done by positioning the probes and spacers inside the pipe one by one gently pushing them down using another pipe with smaller diameter. Two special tools were also hand crafted to allow for easy disassembling in the field: a hook at the end of a long wire equipped with a handle helped pulling out the probes, and a giant cork screw was used to remove the spacers sitting in between. This allowed access to all probes and therefore data could easily be downloaded, inspected and processed.

Diver Type	Mini-Diver DI 501
Level Range	10 m in water
Level Resolution	2 mm
Level Accuracy	5 mm
Compensation	0°C – 40°C
Temp Resolution	0.01°C
Temp Accuracy	± 0.1°C
Capacity	24,000 measurements

Figure 13 contains technical details of the pressure transducers and pictures of the water level data loggers as well as the screened section of the sediment water level measurement pipe.

The final product was an array holding all probes in position ready to be installed in any streambed. The depth of the installation depended on the position of the top thermistor, which was used to measure the stream water temperature above the sediments at the bottom of the water column. All probes were setup to start synchronously, and recorded temperatures continuously every 15 minutes during the entire time of field application.

For further investigations and for verifying results obtained through the temperature method, additional effort was made to measure surface water as well as sediment water heads. Levels were measured using Schlumberger Mini-Diver® data loggers (see Figure 13), also capable of simultaneously measuring temperatures for automatic correction of heads. Surface water measurements were done using the same diameter PVC pipe with holes to allow the level inside to equalise at all times. This also ensured an undisturbed water column in case of turbulent flow conditions outside. Divers were fixed to the pipe using sailing rope to hold in position and prevent from loss in case of flood.

For the sediment level measurement, a long PVC pipe was equipped with a screened section of approx. 30 mm at the bottom leaving space for a sump below to allow fine sediments to settle in case they would enter. Similar to the temperature arrays, all holes were covered in screen for protection from penetration of materials such as sand. The sediment level pipe was also equipped with a lid on top to stop rain falling onto the water column as this could influence the measurements. Additional holes horizontally drilled into the pipe at the top allowed breathing through contact with the atmospheric pressure. All divers were setup with the same sampling frequency as used for the thermistors using a USB docking station. A barometric pressure logger was also installed and used the same sampling period as for all other instruments. This data was necessary to correct all water levels after recording and before interpretation as they contained influences from atmospheric pressure.

4.2. Determination of porosity values

Using heat as a tracer according to the methods described in this thesis requires the determination of some physical parameters unique to the field sites. Only appropriate values can ensure adequate velocity results. It is, however, very difficult to measure the in-situ value of sediment porosity as any mechanical influence would disturb the natural deposition of the streambed, thus leading to repacking of the grains and therefore impacts on the natural porosity. Unfortunately, the methods require at least parameters estimates in order to limit the degree of freedom. In this case, the porosity value firstly influences the specific heat capacity linearly and the heat conductivity exponentially (see section 3.1.2 on page 17), both a considerable cause of erroneous velocity results. To limit the uncertainty of the porosity, sediment samples were taken from the field sites.

This was done by using an open steel pipe of with a diameter of 38.3 mm (and 31.8 mm, see Table 2) which was gently driven into the streambed next to each of the temperature arrays. The pipe was then carefully pulled out and the distance from pipe opening to sediment content inside the pipe was measured from both ends in order to obtain the sample volume. Afterwards, the sample was packed into sealable bags and taken to the laboratory. Each of the samples was placed into a heat proof beaker with known weight. After allowing most of the suspended solids to settle, excess water was removed and the samples were placed in an oven and baked at 110°C to force all water to evaporate. The samples were baked for several hours and they were weighted regularly to make sure all water had vanished. The dry weight of the sample after baking was required to calculate porosities from the following relationship (derived from equation [9] on page 19)

[30] $$n = \frac{V_{void}}{V_{sample}} = \frac{V_{sample} - V_{solids}}{V_{sample}}$$

and with an assumed density of the solid grains of

[31] $$\rho_{solids} = \frac{m_{solids}}{V_{solids}} \quad \text{which leads to} \quad V_{solids} = \frac{m_{solids}}{\rho_{solids}}.$$

equation [30] can be reformulated to calculate the porosity value

[32] $$n = \frac{V_{sample} - \dfrac{m_{solids}}{\rho_{solids}}}{V_{sample}} = 1 - \frac{m_{solids}}{\rho_{solids} \cdot V_{sample}}$$

with m_{solids} being the weight of the baked sediment sample [kg], ρ_{grain} being the density of the grains in the sediment (assumed as ρ_{solids} = 2,650 kg/m^3) and V_{sample} being the total volume of the sample [m^3] after baking. In this case, the solid density is assumed to be known because its range of naturally occurring values is very small. The volume of the sediment in the sample can also be calculated from the cylindrical pipe content as

[33] $$V_{sample} = \pi \cdot \left(\frac{d}{2}\right)^2 \cdot l$$

with d being the diameter of the sample pipe [m] and l representing the length of the pipe which was taken up by sediment content [m].

The sediments in the pipe were compressed thus deviations in grain distribution from the undisturbed sediment may have occurred during sampling. However, the sample volume can also be estimated from the volume scale of the beaker after baking. This method seemed more robust compared to calculating sample volumes using the pipe because some of the sediment was lost during the sampling process. Estimated errors turned out to be lower (see Table 2). Unfortunately, this method can be erroneous and therefore only offer estimates of the undisturbed porosity. However, more realistic porosity values are very difficult to define and values derived from this method are used to limit the number of unknown parameters and hence the number of non-unique solutions.

Location	Units	Location EC	Location DEC	Location HC
Weight of Baked Sample	g	409	227	376
Density of the solids	g/L	2,650	2,650	2,650
Volume of Sample	L	0.246	0.135	-
Estimated Volume Error	L	0.024	0.024	-
Porosity	-	0.37	0.37	-
Estimated Error	%	18	37	-
Volume of Baked Sample	L	0.225	0.130	0.233
Estimated Volume Error	L	0.005	0.005	0.005
Porosity	**-**	0.31	0.34	0.39
Estimated Error	%	5	8	3

Table 2 contains the values as used to calculate the porosity for each location.

4.3. Forward modelling

For the procedure of forward modelling, raw temperature records can be used without the need for further processing. A Matlab script was designed to calculate the temperature response in any depth of the sediment using surface water temperatures as input (see 3.1.2.5 on page 23). The resulting values represent the temperatures time series of the saturated sediment and could be used for the fitting routine in the same script. Fitting the observed to the calculated temperature values was done using multi parameter non-linear curve fitting with the least-squares method. The fitting procedure can be described with the following equation

[34] $$\min_{\vec{c}} \frac{1}{2} \left| F(\vec{c}, \vec{x}) - \vec{y} \right|_2^2 = \frac{1}{2} \sum_{i=1}^{n} \left(F(c, x_i) - y_i \right)^2$$

Recorded water temperatures (vector x) are run through the forward modelling equations expressed as $\vec{z} = F(\vec{c}, \vec{x})$ until fitting coefficients c are found with the minimum deviation between simulated and recorded temperature values (vector y). The method uses the large-scale trust-region reflective Newton algorithm to efficiently find a set of coefficients for the best possible fit (see function *lsqcurvefit* in the Matlab reference). The fit can be characterised using the minimum *Root Mean Square Error* (*RMSE*), a quality parameter which describes the mean deviation between calculated and observed temperature values. It is defined as

$$[35] \quad RMSE(\vec{y},\vec{z}) = \sqrt{\frac{1}{n}\sum_{i=1}^{n}(z_i - y_i)^2}$$

with y being the original temperature series, z representing simulated data and n being the number of data points (or the length of both vectors).

Many parameters in the forward modelling equations can be varied in order to find the best fit. In this case only one physical parameter was actually determined: the porosity of the sediment. As a consequence the degree of freedom for an appropriate set of values was too high. To ensure the uniqueness of the solution, missing physical parameters were taken from publications as explained later in section 4.4.3 (page 50). However, two coefficients were used in this approach: (1) the seepage velocity and (2) the thermal dispersivity. The dispersion value was limited to a maximum of 10% of the system length scale (see page 23 for details). The desired output of both, forward modelling in combination with the fitting process is a constant seepage velocity value which is responsible for the thermal depth response to the water temperatures. This value can be compared to results obtained by the next method offering quasi-transient solutions. Note that the direction of flow derived from the forward modelling equations as indicated by the signum is reversed in the presentation section for better comparison. For details about the fitting process see the Matlab syntax of script E which is attached to the appendix (page 112).

4.4. Transient solution

4.4.1. Signal sampling and processing

Temperature fluctuations in surface waters are a result of periodic and random energies (e.g. climate, weather change, cloud cover, shadows etc) with plentiful frequencies. All these influences contribute to the recorded signal hence obscure the diurnal signature. The earth's rotation and therefore insolation feature a periodicity which is very distinct compared to other regular or random events. In addition, the sun is our main source of natural heat energy and its signal is strong compared to heat consumed or released by different processes. The pure diurnal temperature signal should quite accurately comply with a time invariant sinusoidal wave having a period of 24 hours (86,400 seconds). This specific signature is therefore most suitable for the evaluation of water flow because its period is distinct. Furthermore, it matches the upper boundary condition which is used to find an analytical solution for solve the heat transport equation [22] (see page 27). However, for seepage calculations it is crucial to use only the diurnal temperature perturbation. It can be extracted using a special filtration process with the purpose of cancelling undesired frequency components. Filter design is a complex task and part involving extensive knowledge about signal processing. It will only briefly be discussed as it exceeds the frame of this thesis.

4.4.1.1. Fourier Transform

Signal processing can be applied to inspect, investigate and modify any data obtained by environmental monitoring. The Fourier Transform (FT) is often used as a basis for these processes which include filtration or spectral analysis. It transforms any arbitrary continuous time signal from time domain to its frequency domain. That is because Fourier assumed that any signal of limited extend can be described as a finite sum of time-invariant sine and cosine functions with different period and amplitude coefficients (Kanasewich, 1981). This complies with the above mentioned approach of energy superposition in recorded temperature time series. More generalised, this means that arbitrary periodic sequences can be represented as a sum of complex exponential sequences (Oppenheim, 1989). Following this approach, periodicities and magnitudes of the signal components can be identified and desired parts can be extracted or modified.

Environmental variables such as temperature are normally sampled discretely rather than recorded continuously. Therefore, the general Fourier Transform must be reformulated as it can also be expressed as summation approximating the integral of a continuous function. The following formulation is generally used to transfer an arbitrary finite signal with N samples from time domain to frequency domain (Oppenheim, 1989)

[36] $$X(\omega) = \sum_{t=0}^{N-1} x(t) \cdot e^{-j \cdot \omega \cdot t \cdot \frac{2 \cdot \pi}{N}} , \quad \omega = 0,1,2,...,N-1$$

The inverse form is synthetically derived and is represented by the following equation which transforms the signal from frequency domain representation back to its time domain

[37] $$x(t) = \frac{1}{N}\sum_{\omega=0}^{N-1} X(\omega)\cdot e^{j\cdot\omega\cdot t\cdot\frac{2\cdot\pi}{N}}\ , \quad t = 0,1,2,...,N-1$$

The above transformations are known as Discrete-Time Fourier Series (DTFS) and they features extensive mathematical properties such as linearity, shift of sequence, duality, symmetry etc (Oppenheim, 1989). In this case, the most important properties of the DTFS are considered for further temperature signal processing

- Convolution Theorem: The result of multiplication of two periodic sequences is equivalent to the periodic convolution sum of their representative transform

  [38] $$x_1(t)\cdot x_2(t) \rightarrow \frac{1}{N} X_1(e^{j\cdot\omega}) \otimes X_2(e^{j\cdot\omega}) \quad \text{and} \quad X_1(e^{j\cdot\omega})\cdot X_2(e^{j\cdot\omega}) \rightarrow x_1(t)\otimes x_2(t)$$

- Time reversal: Reversal of a signal in the time domain corresponds to conjugation of the same signal in the frequency domain

  [39] If $x(t) \stackrel{F}{\longleftrightarrow} X(e^{j\cdot\omega})$, then $x(-t) \stackrel{F}{\longleftrightarrow} X(e^{-j\cdot\omega})$

However, the DTFS equations form the basis for the Discrete-Time Fourier Transform (DTFT). The DTFT can be computed electronically using its most efficient algorithm which is widely known as the Fast Fourier Transform (FFT), and it is implemented in much scientific software for convenient use.

As mentioned above, continuous signals are usually sampled periodically which results in records with discrete values. Choosing the sampling frequency is an important consideration as it influences the length of the data set as well as the detection quality of the desired signal period. The higher the sampling frequency the better is the detection quality. Unfortunately, longer data records require more handling effort and computational resources e.g. memory space, calculation speed etc. However, the Nyquist frequency can help to find the best suitable compromise. It defines the lowest frequency component which can reliably be determined which depends on the sampling time (Oppenheim, 1989). The relationship is given as

[40] $$f_{Nyquist} = \frac{1}{2\cdot\Delta t_s}$$

In this case, the accurate description of signals with the frequency of 1 cpd [3] is required. The

3 cpd = cycles per day: frequency unit related to Hertz (Hz) by the factor of 86,400.

maximum necessary time between samples is therefore 0.5 days. If sampled at lower rates (more time spacing), the diurnal signal cannot uniquely be identified resulting in inappropriate signal estimates after the digitisation process (known as aliasing). However, a sampling time of 15 minutes (approx. 0.0104167 days, sampling frequency 96 cpd) was selected as a compromise which maximises signal quality and minimises data handling effort. According to [40], this sampling rate allows the reliable detection of signal components with frequencies up to 48 cpd.

4.4.1.2. Signal filtering and re-sampling

A filter is a system which modifies certain frequencies of a signal relative to others (Oppenheim, 1989). This can be used to eliminate all temperature signals interfering with the diurnal cycle as these are considered to be noise. More accurately, a band-pass filter passes signal components which are in a certain width of the frequency range. It can be designed to maintain all desired and cancel all unwanted spectral influences. This helps to clearly expose the diurnal sinusoid in case of appropriate bandwidth selection (pass band approx. 0.9 – 1.1 cpd). Unfortunately, the DFT postulates that sinusoidal components of the transformed signal in the frequency domain are time-invariant. This means that frequency and amplitude of each signal component does not change with time because they are coefficients describing the corresponding sinusoidal function values. These conditions are invalid in this case because daily temperature fluctuations propagate trough the sediment and experience modifications such as decrease in amplitude and a shifting in phase. More importantly, calculations are based on these variations as water velocity strongly impacts on these. In this case, the Short-Time Discrete Fourier Transform (STDFT) can be used because it focuses only on small sections (widows) of the time series. The STDFT is defined as (Oppenheim, 1989)

$$[41] \quad Y(n,\omega) = \sum_{t=0}^{N-1} x(n+t) \cdot w(t) \cdot e^{-j \cdot \omega \cdot t}$$

In other words, a shifted signal *x(n+t)* can be seen through a window *w(t)* with width N and stationary origin. The STDFT is computed for each step n after the section *x(n+t)* of the signal is multiplied with the window function *w(t)*. The advantage is that the original signal's local properties are more accurately reflected by focusing on small sub-sequences where sinusoidal signal components are less variable with time. For the purpose of accurate signal description the window should be as narrow as possible. On the other hand, a narrow window results in lower resolution of the frequency response. The window length is therefore a compromise between frequency resolution and time resolution (Oppenheim, 1989). Unfortunately, selecting a short time window of the sequence is equivalent to the multiplication of a rectangular window with a part of the sequence having the same number of samples. Additionally, filtration of signals requires modifications to the frequency domain by multiplying a weighting function to alter the coefficients of the signal components. The mathematical properties of the DTFS make these procedures more complicated because multiplication in either the frequency or time domain result in periodic convolution of the representative response in the other domain. Hence, transformation results can be significantly distorted due to the transformation response of the window. This impact is referred to as spectral leakage and it can be minimised by designing the shape of the window to match specific signal processing purposes (Harris, 1978). Valid transform boundary conditions such as convergence of the transformed window function must be ensured.

The shape of the window defines the frequency response and it is usually tapered to zero at both ends. As the shortened signal sequence is multiplied with the window function, time as well as frequency domain are weighted according to the principles of the transform, e.g.

[42] $$y(t) = w(t) \cdot x(t) \quad \text{and} \quad Y(e^{j\omega}) = \frac{1}{N} W(e^{j\omega}) \otimes X(e^{j\omega}).$$

Hence the problematic fact is that parts of the original signal's values are faded and this induces loss of information at the window edges. To avoid this, the window can be applied in an arbitrarily overlapping manner (Harris, 1978) and results can be added due to the linearity of the transform. The significant increase of computational resource is rewarded with preservation of signal information. If expressed in polar form, magnitude and phase response of the system input and output are related by

[43] $$\left|Y(e^{j\omega})\right| = \left|W(e^{j\omega})\right| \cdot \left|X(e^{j\omega})\right| \quad \text{and} \quad \angle Y(e^{j\omega}) = \angle W(e^{j\omega}) + \angle X(e^{j\omega}).$$

Clearly, modifications of amplitude coefficients in the frequency domain also cause alterations to the component's phases, thus results in a phase response of the filter (Smith, 2007). As a consequence the inversely transformed signal experiences a phase distortion. This manifests itself as a shift of the component's phase. In this case, the phase impact on the filtered temperature records is undesired and must be avoided. The method requires exact phase values to evaluate accurate time shifts between the peaks of two signals recorded in different depths. Forward-backward filtering provides a solution with true signal phase preservation (zero-phase filtration) but only for this case because of finite signal extend. The signal is filtered in both directions resulting in squared magnitudes and cancelled phase distortions (Smith, 2006).

The “Filter Design & Analysis Tool” implemented in Matlab was used to create a band-pass filter considering the previous discussion. This tool eased the complexity of signal processing by providing implemented functionality such as analysis of the amplitude and phase response. A cosine tapered window (Tukey window, Filter order 576 and α = 0.75) offers the advantage of smoothly cancelling the boundary frequencies without reducing the desired pass gain (Harris, 1978). The filter was designed to allow all energy between 0.9 cpd and 1.1 cpd to pass and a cosine shaped side slope to fade boundary frequencies with a width of 0.3 cpd, as suggested by Hatch et al. (2006). The filter was applied to all recorded temperature time series to extract the diurnal temperature sinusoid. See script A (page 106) attached to the appendix for more details.

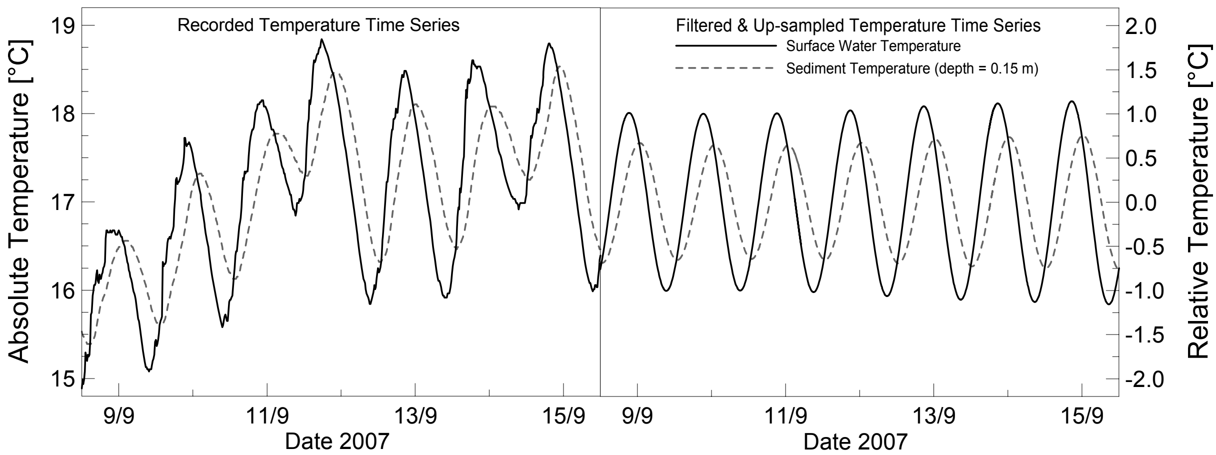

Figure 14 exemplifies a sequence of original and band-pass filtered temperature signal (recorded in surface water and in sediment depth of 0.15 m).

A pair of filtered diurnal signals (see Figure 24) quite accurately complies with the Stallman (1965) boundary condition and offers amplitude ratios and phase shifts values which can then be extracted and evaluated according to the theory. However, all signals are up-sampled from the original sampling time of 15 minutes (96 cpd) to 3 minutes (480 cpd) after filtration using a low pass interpolation algorithm implemented in Matlab. The up-sampling must be performed after filtration because most undesired frequency components are eliminated and values of the diurnal sinusoid can be interpolated much better. The accuracy of the desired temperature peak and time values depends on up-sampling because discrete time steps of 15 minutes (900 seconds) may not match with the time of the actual peak. On the other hand, amplitude values are less variable than phase values, especially in the vicinity of the sinusoid's peak. Hence, amplitude derived velocity solutions are less sensitive to the temperature sampling time.

Hatch et al. (2006) illustrate that the filtration process induces errors at the beginning and at the end of each time series due to the adaptation of initial filtering conditions. It is suggested to simply delete the first and the last three days of the filtered signal to avoid false results. The error in the final results which was caused by filtering have been investigated by Hatch et al. (2006) and were found to be within the range of approximately 2 % and therefore quite insignificant.

4.4.1.3. Spectral Analysis

The DTFT can also be used to estimate the amplitude spectrum or spectral density (SD) of arbitrary recorded signals. The SD is an expression of the average energy per frequency unit found within the original signal. It can be calculated in the following way (Stearns et al., 1996)

$$[44] \quad SD(\omega) = |X(\omega)| = \frac{1}{N} \cdot \sum_{t=0}^{N-1} \left| x(t) \cdot e^{-j \cdot \omega \cdot t \cdot \frac{2 \cdot \pi}{N}} \right|$$

The above discussion about windowing is equally applicable to spectral analysis. The result of the use of a rectangular window is called periodogram, and otherwise it is referred to as modified periodogram. The convolution of window and sequence transformations causes distortions such as spectral leakage (Kanasewich, 1981) which severely depend on window shape and can thwart the spectral density calculation. To minimise this effect, many windows have been designed for different purposes (see Harris, 1978). The spectral energy given by equation [44] is calculated for each windowed sequence and results are time averaged (Oppenheim, 1989). However, computation of all energy spectra used in this thesis was performed with TSOFT (Van Camp & Vauterin, 2005), a free software package for the inspection of time series. This software uses the Hanning window as sequence weighting function.

Spectral plots can be created from spectral analysis results showing signal energy as a function of frequency. They are helpful for the examination of dominant frequencies contained in the original signal. These frequencies can easily be identified because they appear as outstanding peaks and exhibit high energy of signal components with the corresponding peak frequencies. If the investigated signal contains a nonzero mean, its spectrum shows energy at zero frequency. This is referred to as the “DC component” [4] of the signal. The accuracy of the measuring device is contained in this value if it is linear over the range of measured values. Spectral analysis can support the determination of physical origin of features encoded in signals, thus improve the understanding of the investigated system. In this case, spectral analysis was used to identify natural impacts on temperature and level data. It was also helpful to determine the required width of the band-pass filter in order to ensure that all required signal components are passed and noise is cancelled.

4.4.2. Calculation of seepage velocity

A Matlab script was designed to extract amplitude ratios and phase shifts from two corresponding signals recorded at different sediment depths (see section B on page 107). The values of the filtered temperature time series were processed by a local maxima/minima detection algorithm which used the deviation between adjacent temperature values to detect peaks. Peaks are local extremes best indicated by signum change of its deviation value. Identified peaks feature distinct times and amplitude values which were stored for maxima and minima separately. This was necessary to avoid confusion because the corresponding peak simultaneously searched for in the second (deeper) signal could occur later than the next peak value of the same signal. All maxima and minima as well as absolute occurrence times were collected and stored as amplitude ratio and phase shift time series. Furthermore, a different Matlab script utilised these values and iterated through both equations [28] (see page 31) in order to find two independent seepage velocities (see section C on page 109). The script was also equipped with all physical parameters values as necessary for the calculation. Resulting values were unique water seepage velocities representative for the time between two peaks at different depths. Consequently, the time values centred between peaks were also calculated and appointed to the corresponding velocities.

4.4.3. Sensitivity to physical properties

The two heat equations utilise a number of physical variables which could only be estimated from literature values. The three most uncertain physical parameters are heat conductivity,

[4] DC stands for “Direct Current” and originates from electronics. In case of general signal processing, this term is used to describe the offset of a signal from zero.

heat capacity and thermal dispersivity. Table 3 contains the range of values for three main rock materials which were found in Maules Creek: Andesite, Basalt and Granite.

Parameter	Unit	Andesite	Basalt	Granite	Maules Creek
Heat Capacity	kJ/kgK	0.81 – 0.82	0.54 – 2.14	0.25 – 1.55	0.6 – 0.9
Heat conductivity	W/mK	1.35 – 4.86	0.44 – 3.49	1.25 – 4.45	1.0 – 3.0
Dispersivity	m	-	-	-	0.0 – 0.06

Table 3 illustrates the range of physical properties of representative rock materials found in Maules Creek.

These values were found in Schön (1996) and confirm a limited range. The composition of rock fragments in a sedimentary environment can be highly variable, thus these values may not represent the actual field values. A laboratory test as well as mineralogical investigations was beyond the scope of this thesis. On the other hand, there are two independent velocity solutions which could be used to restrain parameters by matching both results. However, a matching set of velocities may be found for various sets off different physical parameters. In order to estimate the individual influence on seepage values the sensitivity of each of these parameters was examined. At first, amplitude ratios and phase shifts were calculated for three distinct velocity values (0.5 m/d, -0.1 m/d and -0.5 m/d) using a defined set of physical parameters and equations [26] and [27] (see page 31). Afterwards, the same equations were used to re-calculate seepage velocities, varying the value of only one distinct parameter in the range between minimum and maximum value as given in Table 3. This was done for all combinations of velocities and parameters and the results are displayed in Figure 15. Columns represent same physical parameters and rows show the same three distinct velocities. It is clearly visible that the specific heat capacity of the solid matrix contributes to the smallest error when varied in the limits of its possible range (see Figure 15 plot A, D and G). The thermal conductivity is somewhat more sensitive (see Figure 15 plot B, E and H) and the dispersivity value exhibits strongly divergent seepage results (see Figure 15 plot C, F and I). As a consequence, the specific heat capacity was set to a representative mean value of 750 J/kgK. The thermal conductivity was then used to find an appropriate fit of both solutions, and was appointed the value of 1.8 W/mK. The choice of both indicates little Granite content or organic sediment according to Schön (1996). As a matter of fact, organic solids were evident in the sediment which was sampled for the porosity tests.

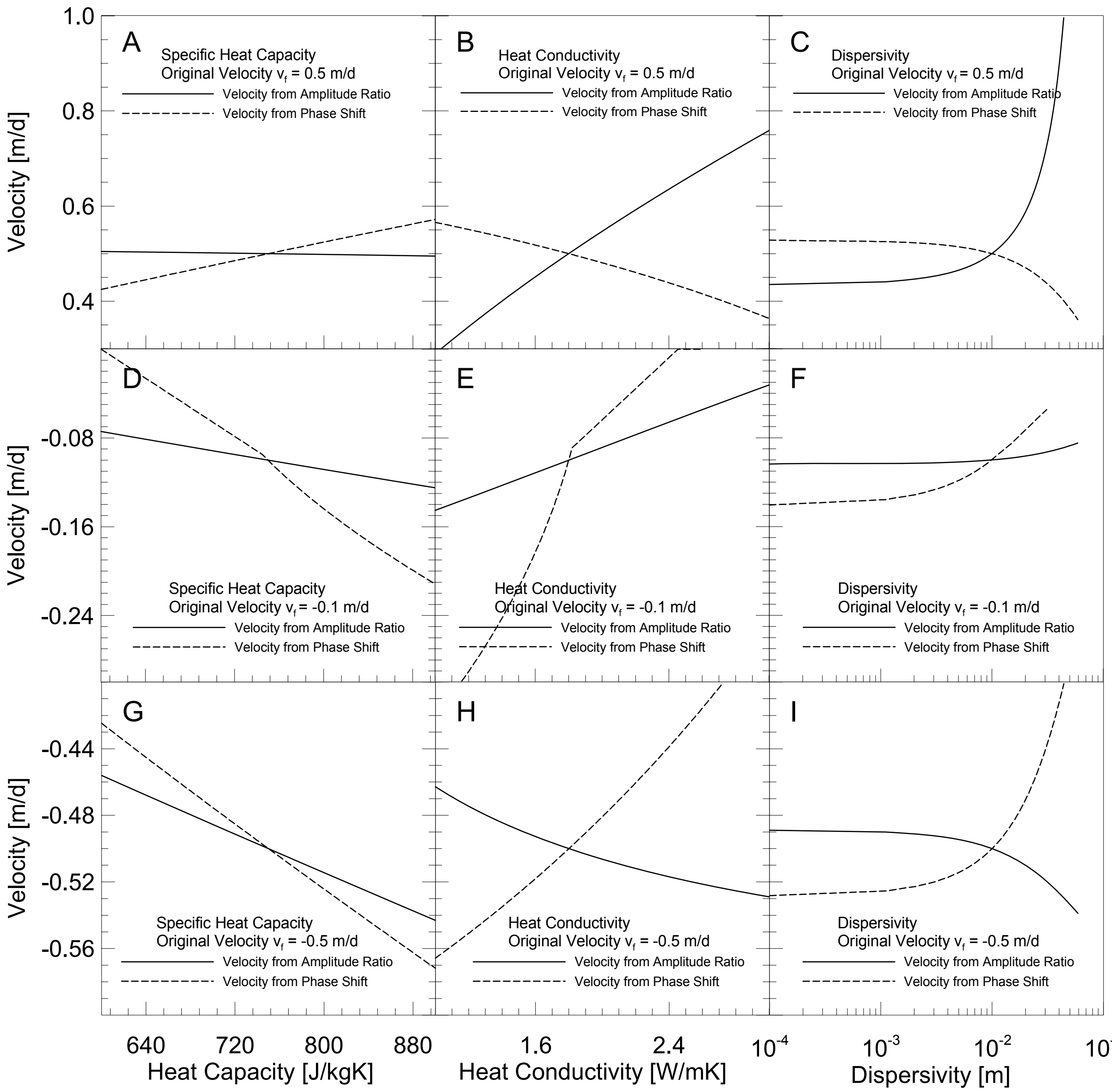

Figure 15: Sensitivity of three distinct seepage velocities (0.5 m/d, -0.1 m/d and -0.5 m/d in the rows, respectively) to the main unknown physical parameters of the locations (heat capacity, heat conductivity and thermal dispersivity in columns, respectively).

As discussed in chapter 3.1.2.4 (see page 21) the thermal dispersivity is treated in literature in a somewhat controversial way, but there are a number of recent publications focusing on its mathematical description and the fact that its mechanism differs from the one widely used for solute dispersion (e.g. Metzger et al., 2004; Nakayama et al., 2005; Testu et al., 2007). This particular parameter is generally difficult to estimate, especially in field environments. Unlike the rock properties, it is the only parameter which is considered to vary with locations of the installations. However, it is thought to be a scale dependent problem and maximum values of approximately 10% of the experimental length scale were found appropriate (Neuman, 1990). For all these reasons it can be used to explain any further abnormality between both seepage equations.

Parameter	Symbol	Unit	Values
Density of water	ρ_w	kg/m^3	998
Density of sediment	ρ_s	kg/m^3	2,650
Spec. heat capacity of water	c_w	J/kgK	4,183
Spec. heat capacity of sediment	c_s	J/kgK	750
Thermal conductivity of water	κ_w	W/mK	0.6
Thermal conductivity of sediment	κ_s	W/mK	1.8

Table 4: This table contains physical parameters which were used for the calculation of seepage velocities.

4.5. Numerical methods using VS2DHI

The analytical solution of the heat equation as explained in section 3.1.2 (page 17) is restricted to a set of certain boundary conditions. These are most likely violated in realistic situations, thus errors are introduced. Unfortunately, the heat transport equation is only analytically solvable under distinct circumstances. Therefore, the application of the heat method to field problems may be limited if these conditions are unknown. Numerical schemes for the solution of the differential heat transport equations are required to investigate influences because arbitrary boundary conditions can be applied. In this case, the condition which is most likely violated is that there could be an additional horizontal flow component. The software VS2DHI (Healy et al., 1996) was used to evaluate and study the influence of horizontal streambed flow on the vertical results of the analytical solutions. The package was designed to calculate two-dimensional heat transport problems in variably saturated porous media. It is freely available from the U.S. Geological Survey and features an interactive graphical user interface, allowing the easy setup and application of geometrical groundwater models, grid, boundary conditions and physical parameters (Hsieh et al., 2000). The additionally included post-processor helps the user to set simulation parameters and to visualise the results after running the simulations.

4.5.1. Mathematical and physical basis

The software package was originally designed to simulate solute transport in porous media considering variably saturated but single (fluid) phase flow problems only (Lappala, 1987). However, additional functionality in order to handle energy transport was added later by Healy (1996). The heat balance is calculated using the following equation

$$\frac{\partial(\theta c_f + (1-n)c_s)T}{\partial t} = \nabla \cdot K(\theta)\nabla T + \nabla \cdot \theta c_f D_H \nabla T - \nabla \theta c_f vT + qc_f T^* \quad [45]$$

with the parameters

- Θ fluid saturation [-]
- c_f specific heat capacity of water [J/m^{3}K]
- c_s specific heat capacity of the solids [J/m^{3}K]
- T temperature [°C]
- K thermal conductivity tensor of the bulk medium [W/mK]
- D_H hydrodynamic dispersion tensor [m^2/s]
- v advective fluid velocity [m/s]
- q in- or exfiltration of fluid at source or sink [-/s]
- T* temperature of infiltrating fluid at source [°C]

The left hand term represents the change of energy stored in a certain bulk volume over time. Terms on the right side stand for (1) thermal conduction, (2) hydro-thermal dispersion, (3) advective energy transport by fluid movement and the last one (4) is a point source and sink term for injection or removal of fluid and energy.

An important parameter is the hydrodynamic dispersion tensor defined for two dimensions by Healy (1990) as

$$D_H^{xz} = \alpha_T |v| \delta_{xz} + (\alpha_L - \alpha_T)\frac{v_x v_z}{|v|} \quad \text{with} \quad \begin{cases} x = z \rightarrow \delta = 1 \\ x \neq z \rightarrow \delta = 0 \end{cases} \quad [46]$$

with α_L and α_T being the longitudinal and the transversal dispersivity coefficients [m], v_i and v_j representing velocity components in the two-dimensional space and δ is Kronecker's delta. The impact of different dispersivity values on the analytical solution will be examined.

The heat balance of a bulk consisting of porous media strongly depends on fluid flow. Mass conservation is applied to a representative volume in the following way

[47] $$\int_V \frac{\partial(n\rho\theta)}{\partial t} + \oint_A (\rho v) dA - \int_V (\rho q) dV = 0$$

With the assumption of a small enough volume that values can be considered constant throughout space the equation can be simplified to

[48] $$V \frac{\partial(n\rho\theta)}{\partial t} + \oint_A (\rho v) dA - \rho q V = 0$$

Furthermore, Darcy's law is utilised to transfer water levels (pressure) into a flow velocity

[49] $$v = -K k_r(h) \frac{\rho g}{\mu(T)} \frac{\partial H}{\partial L} \quad \text{and} \quad H = h + z$$

with K being the intrinsic permeability of the medium [m^2], k_r the relative permeability as a function of pressure head, H the total potential of the liquid [m] and, as a major difference to the analytical solution, the viscosity μ [Pas] being an empiric function of temperature (Healy, 1996)

[50] $$\mu(T) = 0.00002414 \cdot 10^{\frac{247.8}{T+133.16}}$$

Equation [49] and [50] can be substituted in equation [48] and for cubic (3D) or square (2D) cells the flow across the faces can be approximated leading to

[51] $$V \frac{\partial(n\rho\theta)}{\partial t} - \sum_{k=1}^{4} \rho^2 A_k K k_r(h) \frac{g}{\mu(T)} \frac{\partial H}{\partial L_k} - \rho q v = 0$$

An additional energy transport caused by gas or water vapour is considered negligible in all simulations using the above formulations. In some cases, this may introduce errors to the heat balance due to the possibility of e.g. energy transport by vapour or consumption by phase change etc. In this case, all simulations will be run under fully saturated conditions only and errors are therefore prevented. Additionally, fully saturated conditions simplify the above equations considerably because values for saturation (Θ) and relative hydraulic permeability (k_r) become equal to 1.

In VS2DHI the non-linear flow equation [51] is solved together with the heat equation [45] using the cell centred Finite-Difference Method (FDM). This solution scheme features discretisation (approximation) which is centred in time (Crank-Nicholson method) and in space, thus avoids numerical dispersion. However, numerical oscillations within the solution may still occur unless the following criteria recommended by Healy (1990) is met

[52] $$\frac{|v|\Delta z}{|D_H^{zz}|}+\frac{|v|\Delta x}{|D_H^{xx}|}\leq 2$$

This is thought to be a guideline especially applicable to sharp gradient values. In this case, the temperature simulations will be run with sinusoidal (smooth) temperature signals and this condition can be relaxed.

4.5.2. Model setup

A two-dimensional model was setup to represent a vertical slice of the streambed. The upper boundary of the model maps the top of the sediments and the bottom of the water column. Width and depth were chosen to be 5 m and 2 m, respectively, as this would be large enough to represent the investigated environment. Vertical and horizontal discretisation is 0.02 m and 0.04 m. Observation points were placed at the depth of 0.15 m, 0.31 m, 0.45 m and 0.61 m because these are similar depths used during the field application. The total duration of the simulation was 3 days with time steps of 1 minute which equalled 4,320 steps to be calculated for each simulation. As an upper boundary condition a constant flux of 1 m/d with sinusoidal temperature fluctuating between 19 °C and 21 °C (amplitude of 1 °C) was applied to all models.

Parameter	**Symbol**	**Unit**	**Value**
Saturated hydraulic conductivity	k_s	m/s	1.0×10^{-4}
Anisotropy Ratio	k_{zz}/k_{xx}	-	1
Specific Storage	S_s	1/L	0
Spec. Volumetric Heat Capacity of Water	c_w	J/m^3 °C	4,174,634
Spec. Volumetric Heat Capacity of Sediment	c_s	J/ m^3 °C	1,987,500
Thermal Conductivity of Saturated Sediment	κ_s	W/m °C	1.5
Porosity of the Sediment	n	-	0.3

Table 5 contains physical parameters which were used for numerical simulations.

Five different dispersivity values (in this case: $\alpha = \alpha_L = \alpha_T$) were selected to be important for the simulation as they would be worst case scenarios: (1) α = 0 m, (2) α = 0.015 m, (3) α = 0.03 m, (4) α = 0.045 m and (5) α = 0.06 m. For each of these values the simulation was run

10 times using different left boundary conditions with increasing horizontal fluid inflow between 0 m/d and 2 m/d (in steps of 0.2 m/d). For the case of zero flow, the right and left boundaries were set to no energy flux (J = 0), and for all other cases a constant temperature of 20 °C was applied. This boundary temperature may not represent real streambed situations but was kept invariant to prevent horizontal heat flow anomalies. Also, the observation points were placed “downstream” just before fluid outflow to avoid influences of the left boundary condition on the observed temperature signal and to simulate an infinite horizontal extend of the streambed. The right boundary condition was always assigned the same velocity as the left one, and the bottom one always had a fluid velocity of 1 m/d (same as the top). For these boundaries the temperatures were chosen to be the default model outflow values. A sketch of the model setup and resulting velocity vectors caused by the velocity boundaries is pictured in Figure 16. All simulations were run using the set of physical parameters as noted in Table 5.

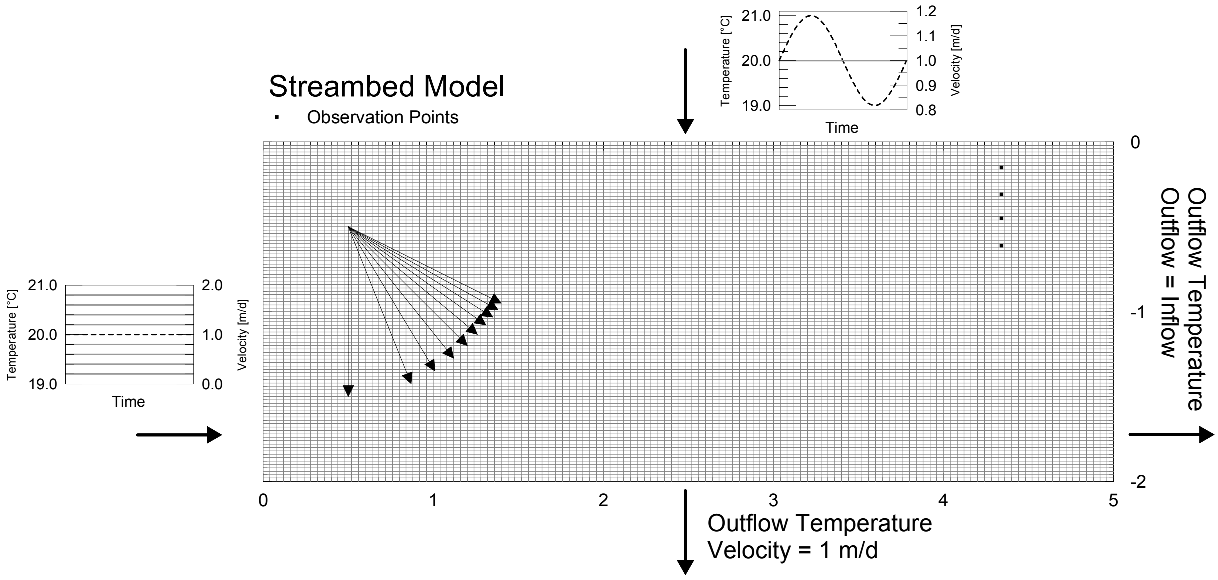

Figure 16 illustrates the setup of the numerical model and its boundary conditions.

Altogether, a total of 50 simulations were run and simulated temperatures at all observation points were recorded. These values were used to run through the same peak picking script in Matlab as used for the analytical method. Afterwards, seepage values were iterated using the quasi-transient method explained in section 3.1.2.6 (page 26). Simulation outcomes are presented later in section 6.5 (page 84) together with the field results.

5. Field Application in Maules Creek

The previously described methods using diurnal heat as a tracer was applied to the field and tested as part of a major research project. This was funded by the Cotton Catchment Community's Cooperative Research Centre in Australia. The Maules Creek catchment (see Figure 17) was selected as field site and various different research projects were carried out in the same place. This offered additional data monitored by a weather station especially setup for research purposes. The catchment area is situated westwards of the Great Dividing Range in the North Western Slopes and Plains. This area is part of the Namoi Valley which belongs to the state of New South Wales. It is extensively used for large scale farming of cotton but also other useful plants such as barley, wheat and soy. However, limited surface water resources and ongoing drought conditions force farmers to extract groundwater for irrigation. Moreover, management of water allocations and licenses is currently ignoring hydrogeological features like linkages between surface and groundwater which are unique to this particular catchment area. This malpractice has been causing a severe drop in groundwater table and is suspected to also deplete water resources. Water demand for farming is increasingly big due to the growth of water intensive plants.

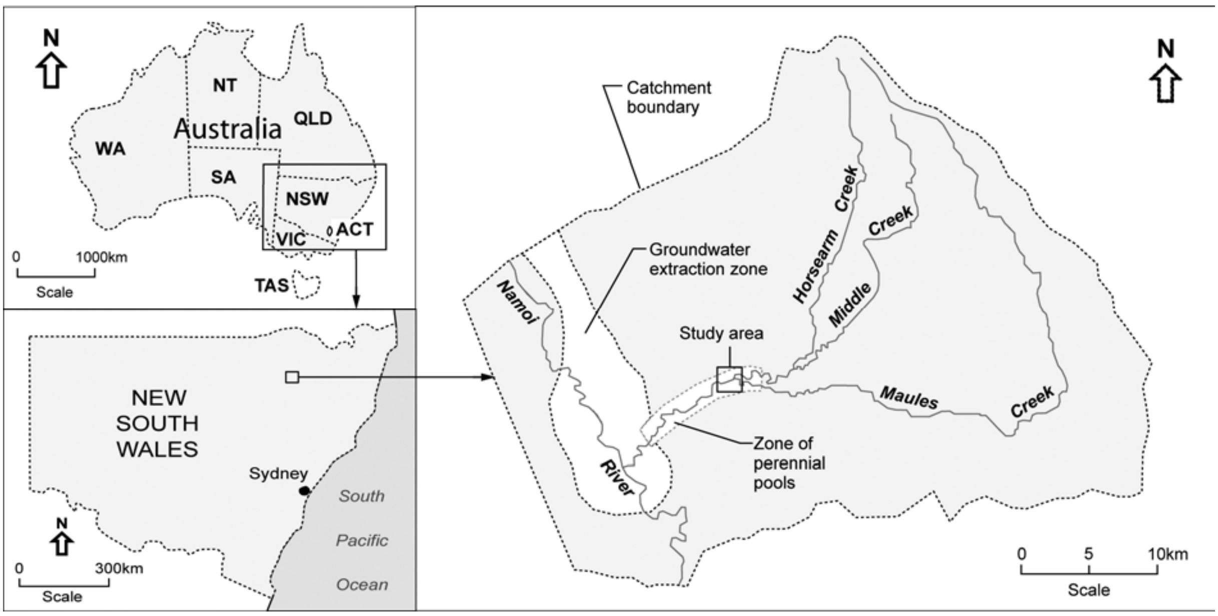

Figure 17 shows maps of Australia, New South Wales, Maules Creek catchment area and the study site (follow enlargements).

5.1. Description of the catchment

The Maules Creek catchment covers a surface area of approx. 1,600 km^2. Only after continuing rain events, surface runoff from Horsearm Creek, Middle Creek and Maules Creek accumulate and discharge into the Namoi River. Further westwards, the Namoi then feeds the Darling River, Australia's longest river flowing thousands of kilometres to its confluence with the Murray River and water finally discharges into the ocean. The catchment area is bound to the north by the Nandewar Ranges, a volcano of tertiary age with Mount Kaputar (1510 m) being Australia's highest peak outside the Great Dividing Range. The New England Fold Belt defines the eastern boundary and to the south west, Gins Leap Gap and a range of hills limit the catchment. Figure 17 illustrates the estimated catchment boundaries.

On a larger scale the area is part of the Upper Namoi Valley, a large transmissive alluvium which is used for groundwater pumping to support agricultural production in very fertile soils. The southern and central part is underlain by Permian volcanic bedrock (Andersen and Acworth in prep., 2008). The Maules Creek geology is composed of Tertiary alluvial sediments with medium to heavy clays and lenses of sand and gravel accumulated to a thickness of up to 20 m. On top, a layer of Quaternary sediments with sands, gravels and boulders is between 10 m and 15 m thick and approximately 500 m wide. It is described as unconfined aquifer highly connected to the surface water bodies. Moreover, most of the bores in this area are thought to extract from this unit (Sinclair, 2006).

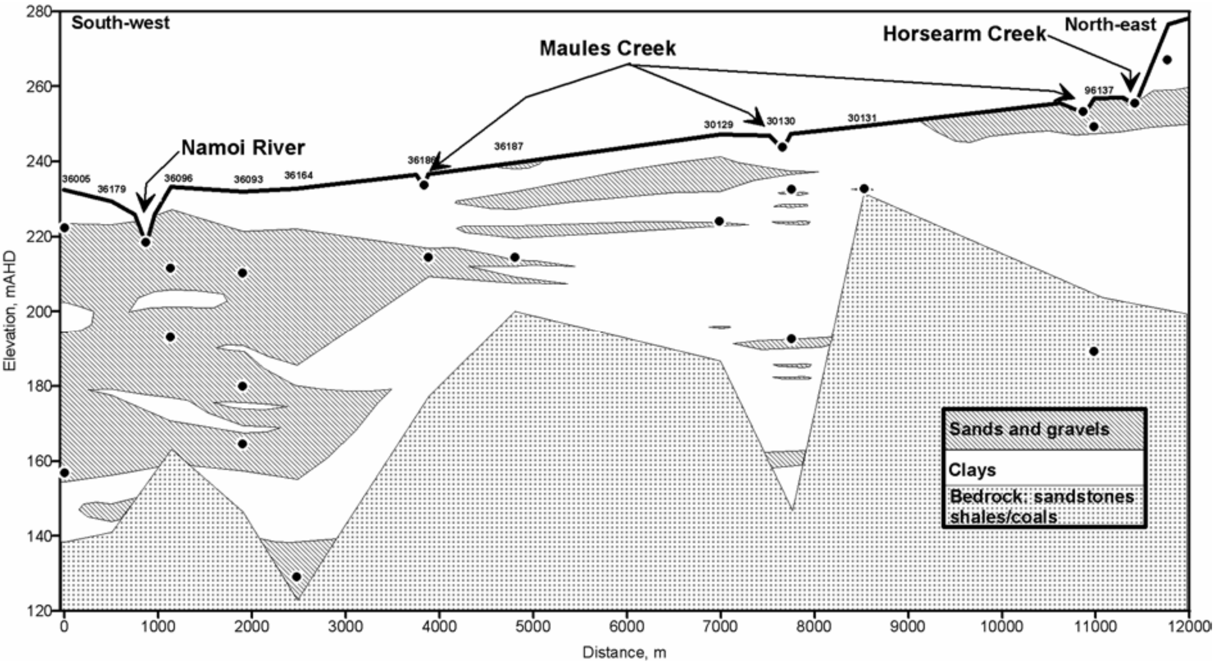

Figure 18 shows a hydrogeological cross section through Maules Creek (Andersen, 2007).

The active channel in Maules Creek can be described as ephemeral stream because surface water flow can only be observed after substantial rain in the catchment area upstream. However, a series of perennial pools is located between Horsearm Creek, just upstream the confluence with Maules Creek, and downstream Elfin Crossing. Recent investigations suggested that there is groundwater discharge in the area (Andersen, 2007) which may feed these ponds. Despite higher than average rainfall, stream flow has been declining which is found to be a consequence of unsustainable nearby groundwater extraction (Sinclair, 2006). Figure 19 outlines the study area and contains exact positions of all installations as well as the boreholes used (Abbreviations: EC - Elfin Crossing, HC - Horsearm Creek, DEC - Downstream Elfin Crossing).

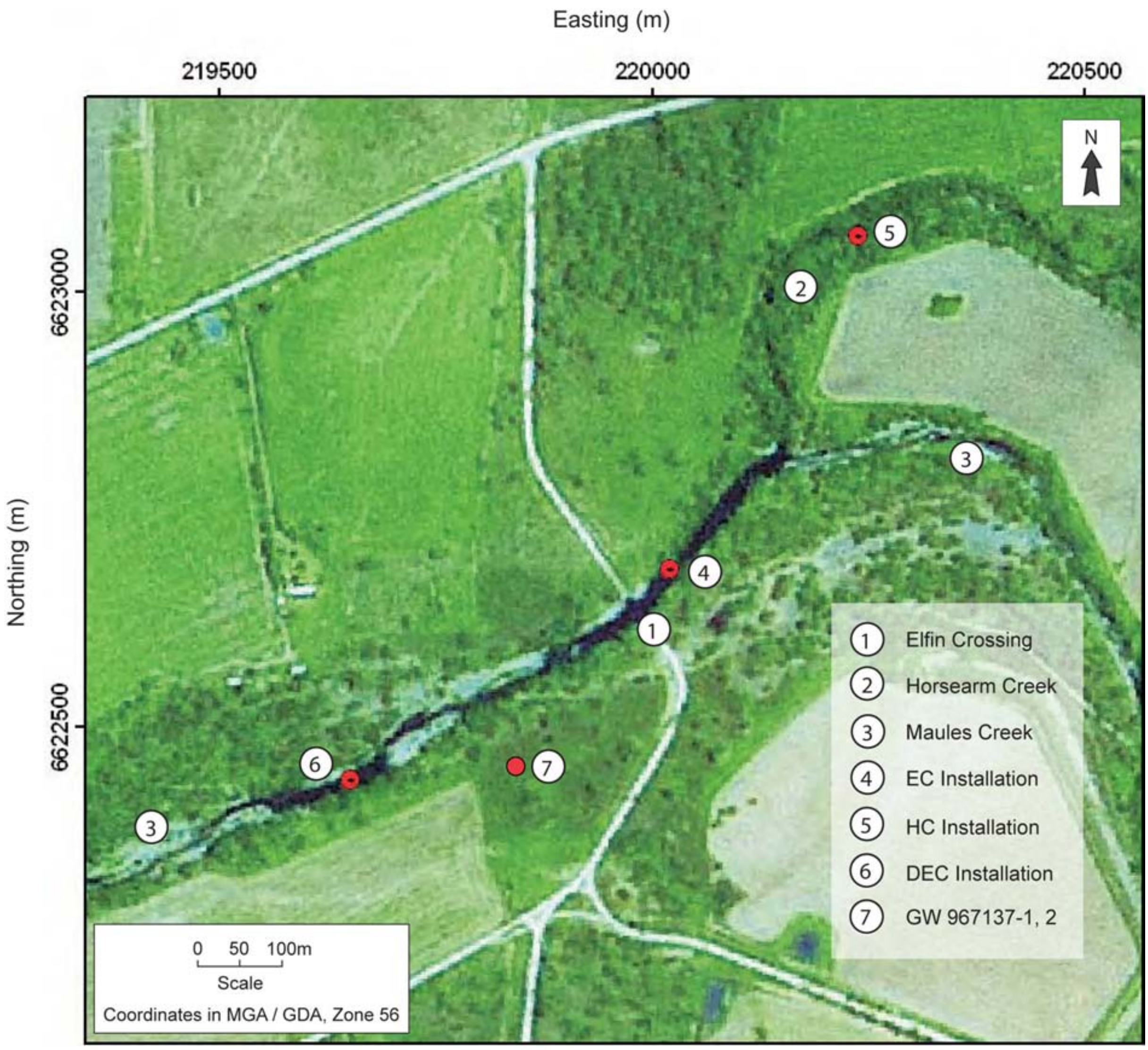

Figure 19 pictures a map of the Maules Creek study area including locations installations.

5.2. Field work and installation procedure

Several field trips to the Maules Creek catchment area were done during the time of investigation. The first field trip at the end of August 2007 was necessary to choose appropriate field sites for the installation of the temperature arrays and the level measurements.

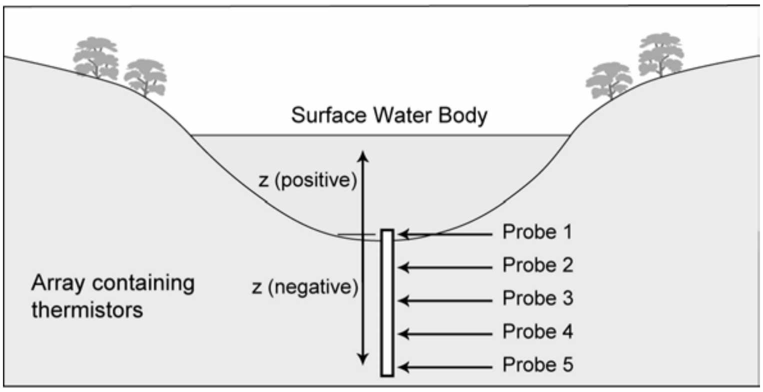

Figure 20: Illustration of the installation in the streambed of surface water bodies.

The procedure of installing the temperature probes was done in the following way: a simple steel pipe with an inner diameter of 38 mm was fitted with a PVC drive point snugly fitting into the opening at the bottom. The pipe was driven into the sediments using a heavy post rammer (see picture in Figure 23) until the required depth of approx. 0.75 m was reached. The steel pipe was now in place and a metal rod which was longer than the pipe could be used to knock out the drive point at the bottom. Then, a readily assembled temperature array was pushed under water to allow air to escape and water to settle inside. It was immediately fed into the top opening of the steel pipe and gently pushed down using another same sized PVC pipe until it reached the bottom. Afterwards, the steel pipe was gently twisted and slowly pulled upwards, always keeping the array in place with the second PVC pipe. Furthermore, the position and safety of the installation were checked and impacts to the surrounding sediment such as depressions were removed by hand. All water level instruments were installed in the same way using a post rammer and the steel rod with driving point. Additionally, a star picket was used to secure surface water and sediment level installations. Finally, instruments were setup and affixed in order to hold in place inside the pipes. All measurements, dimensions and times were noted and related to the current surface water level.

A second excursion was done in October 2007 to make sure that all installations were still in place and functioning. This trip was also useful to observe any changes in the flow regime. The installations were accurately surveyed using RTK differential GPS (Trimble 5800 equipment). Horizontal and vertical positions were recorded as coordinates of Zone 56 in Map Grid Australia (MGA), and refer to the Geocentric Datum of Australia (GDA). The vertical positions were required to transfer all water levels from relative to absolute values which improved interpretations such as water level comparison and gradient calculations. As visible throughout all field trips, Maules Creek was dry and surface water flow could not be observed. However, the surface water ponds which were used for the installations did not change but levels had decreased.

Location	Unit	EC	DEC	HC	GW 967137
Figure 19	#	4	6	5	7
Northing	m	6622681.486	6622439.594	6623063.842	6622451.684
Easting	m	220020.232	219651.198	220237.344	219845.794
Elevation	m	252.760	251.698	255.720	258.780
Hor. Accuracy	m	0.009	0.008	0.352	-
Vert. Accuracy	m	0.015	0.012	0.759	-

Table 6 contains positions of installations obtained by the GPS survey in Maules Creek (Zone 56, MGA/GDA).

5.3. Location Elfin Crossing (EC)

This location (see Figure 23) was chosen because it was easily accessible by car because it was located next to the road crossing the creek. An apparently stagnant pond of surface water was used for the installation of one temperature array containing probes, and surface water as well as sediment level measuring devices. This pond was the last significantly large surface water body as part of the series of larger ponds extending from Horsearm Creek to downstream of Elfin Crossing (see Figure 19). Therefore, it was thought to be losing water to the ground and assumed to be fed by horizontal surface water inflow from the pools at Horsearm Creek flowing through the highly permeable alluvial sediment. The water at this site was quite murky and smelled of organic compounds. Installing the temperature array at this particular location was convenient, but the depth of the sediment water level pipe was limited to approx. 0.720 m below the stream channel by cobbles preventing the drive point from penetrating any deeper. This nicely indicated the nature of sediment layering and variability of grain size dis-

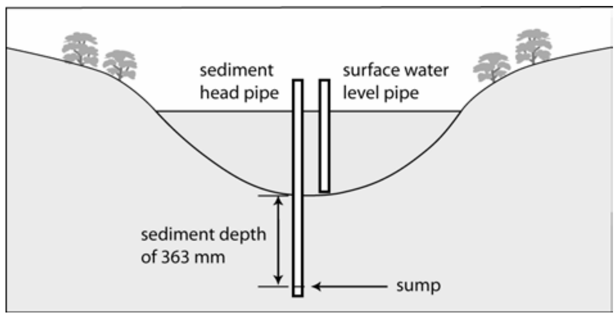

Figure 21: Sketch of the water level installation at Elfin Crossing.

tribution in the streambed environment. The installation responsible for level recordings consisted of a star picket with an attached PVC pipe which secured the logger in place.

5.4. Location Downstream Elfin Crossing (DEC)

The Maules Creek streambed was completely dry downstream Elfin Crossing. However, a single pool was discovered as being the last significant surface water pond along this reach. The location was exposed to sunshine for most of the day as the streambed was quite wide. A temperature array as well as a surface water level logger was installed right in the centre of the pond. Furthermore, between the locations EC and DEC there are two groundwater monitoring locations GW 36913-1 and 2 installed by the DWE [5] (see Figure 19 on page 60). Casing GW 369137/1 is screened in the shallow aquifer in a depth of 8 – 11 m, and GW 369137/2 is screened in of approx. 69 m depth reaching the deeper alluvium. The monitoring stations are setup to automatically and continuously record groundwater levels every three hours by the department. Additionally, a flow gauging station directly located at Elfin Crossing offered daily surface water level and flow values. All this data was requested from the department for the period of investigation and could be utilised in the discussion section. However, there was no surface water flow recorded throughout the entire period of installation and recording.

5.5. Location Horsearm Creek (HC)

The site at Horsearm Creek (HC) was only accessible by foot, walking up Maules Creek along the pools in the dry streambed. The site was located under big trees growing along the side of the creek keeping it a shadowy environment throughout most of the day. The instruments were intended to be installed in the last pond upstream because the

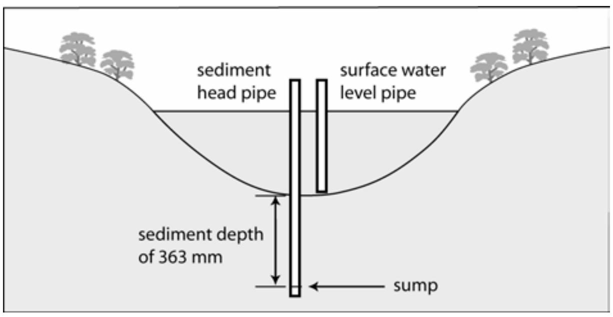

Figure 22: Sketch of the level installation at Horsearm Creek.

[5] DWE: Australian Government Department of Water and Energy, New South Wales

sediments were covered in red colour as a result of iron oxide precipitation. This was suggested to originate from anoxic groundwater rich in Fe^{2+} discharging at the location. Unfortunately, many cobbles in shallow depths prevented the steel pipe to penetrate deep enough to ensure an adequate installation. This indicated a practical limitation to applications of the heat method. After trying various locations, a large pool which offered a thick layer of sandy sediments was found suitable for the installation of the array. Water in the pond was unbelievably clear which indicated that this could be a possible groundwater discharge zone. Surface water and sediment level measurement pipes were installed next to the array and equipped with data loggers.

Figure 23 contains pictures of the installations taken at each location. Table 7 illustrates the depth of each thermistor at every single location. Values are referred to the boundary between sediment and water (positive: up; negative: down).

Location	**Elfin Crossing**	**Downstream Elfin Crossing**	**Horsearm Creek**
Probe 1	0.00 m	0.00 m	0.15 m
Probe 2	-0.15 m	-0.15 m	0.00 m
Probe 3	-0.30 m	-0.30 m	-0.15 m
Probe 4	-0.45 m	-0.45 m	-0.30 m
Probe 5	-0.60 m	-0.60 m	-0.45 m

Table 7 contains the absolute depths of each temperature probe at all locations.

Figure 23: Preparation of temperature arrays, installations at Elfin Crossing, downstream Elfin Crossing and Horsearm Creek (clockwise from top left).

6. Presentation of results

After about two months of continuous recording, a last field trip was done to Maules Creek in November 2007. All installations were disassembled and all instrument data was downloaded. Temperature and level data was continuously measured between approx. 29th August 2007 and the 2nd November 2007. Data was recorded by field instruments as described in the field application chapter 5 (see page 58) and processed as explained in the methodology section 4 (see page 38). The following chapter presents the results obtained from this environmental monitoring.

6.1. Climate data and water temperatures

The majority of larger temperature changes at the earth's surface are induced by climatic conditions. Therefore, climate data from the weather station is considered to be an additional and valuable source to enhance further presentations, discussions and interpretations. Figure 24 shows unprocessed data like air temperature, solar radiation, relative humidity, rainfall and surface water temperatures recorded during the entire time frame of investigation. Plot A clearly illustrates sun radiation input and its effect on the ambient air temperature. It is obvious that temperature fluctuations result from solar radiation which is occurring regularly on a daily basis, as the globe is constantly rotating with the same speed. The average maximum daily solar insolation was around 1,000 W/m^2 showing little variation which indicated minor cloud cover during the time of investigation. Air temperatures illustrate strong daily oscillations with amplitudes greatly varying between approx. 5 and 25 °C. The lowest and highest recorded temperatures were 1.4 °C and 34.7 °C, respectively. The average temperature during the time of recording was 17.5 °C and higher than the average temperature for spring seasons (BOM, 2008). The air temperature also contained additional energies like fluctuations with longer than diurnal frequency. This originates from the change in macro climate such as low and high pressure events passing by the point of measurement.

Graph B shows the corresponding time series of relative humidity and rainfall. The relative humidity was highly variable between a maximum of 95.5 % and a minimum of only 8.3 %. The average value was calculated and equalled 52.1 %. The relative humidity is obviously coupled to the air temperature but its trend is of course reversed. There was some minor rainfall in August and September 2007 which was probably due to locally developed thunderstorms because radiation input is not significantly reduced. This would indicate longer periods of cloud cover and therefore larger scale weather events. However, the climate station was situated next to the Namoi River approx. 12 km westwards of Elfin Crossing at the main position where most of the research project took place.

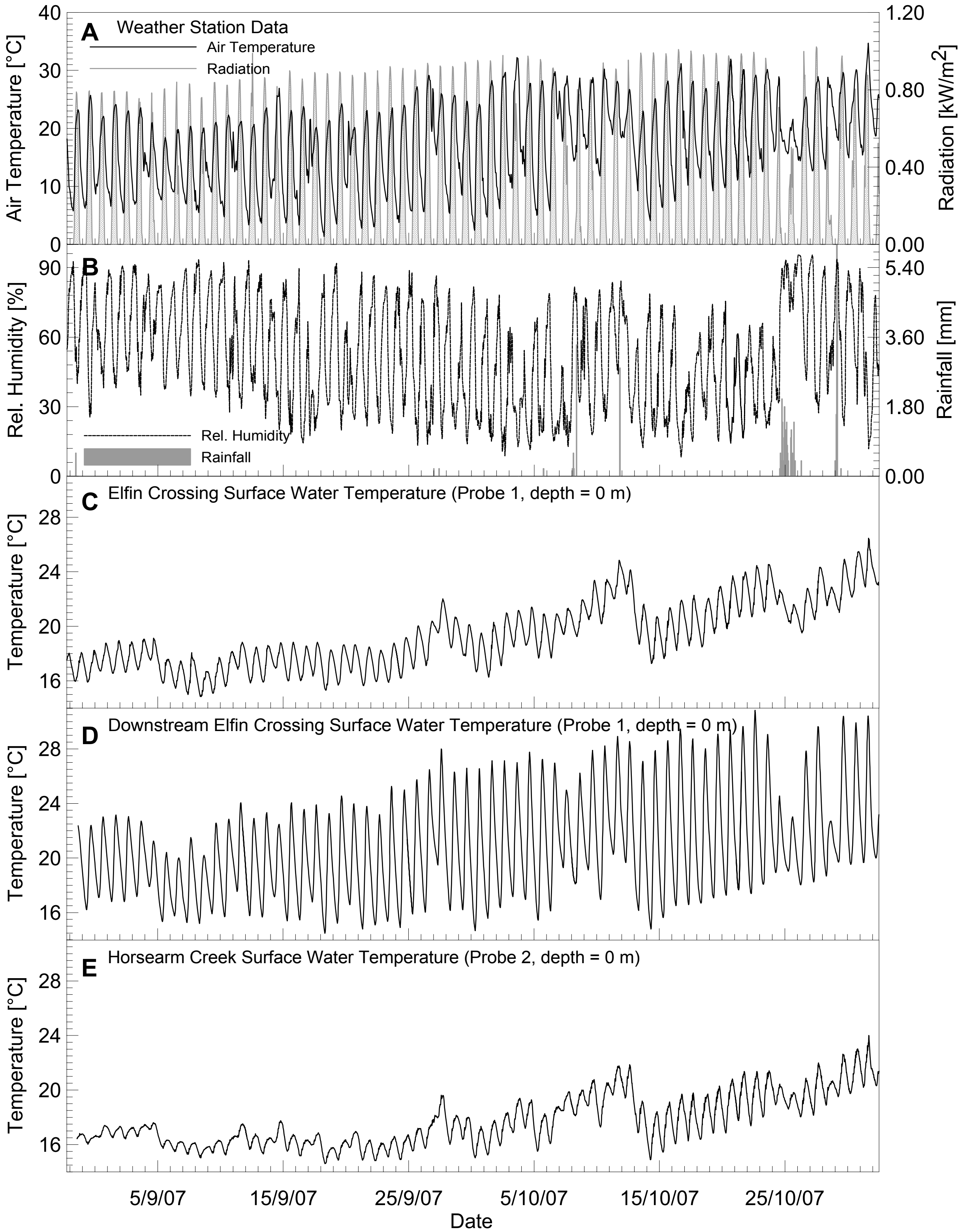

Figure 24: Time series of climate data recorded by the weather station as well as surface water temperatures at all locations.

It is important to notice that temperature, humidity and rainfall are phenomena with capability to significantly change on the temporal and spatial scale. Therefore, data recorded by the climate station does not entirely characterize values at Maules Creek. However, long term weather events such as more continuous rainfall on the 25th or the 29th of October 2007 can be assumed to offer reasonable values for the Maules Creek region. This also applies to air pressure because spatial change is much less significant.

Plots C, D and E display the surface water temperatures measured at the three different locations which were described in chapter 5 (page 58). The frequency of water temperature oscillations in all locations is obviously equal to the ones recorded in the air. However, amplitudes are quite different reflecting various environmental conditions which will be discussed later. Temperature maxima, minima and averages were 26.5 °C, 14.8 °C and 19.3 °C for Elfin Crossing, 30.8 °C, 14.5 °C and 20.8 °C for downstream EC and 24.8 °C, 14.4 °C and 17.9 °C for Horsearm Creek, all calculated for the period of investigation. There were amplitudes of approx. 2-3 °C at Elfin Crossing which was quite constant with time. Quite differently, water temperatures downstream EC oscillated with amplitudes between 4 °C and up to 12 °C between day and night time. Interestingly, temperature perturbations at Horsearm Creek were of a comparable magnitude to the ones at EC, but amplitudes varied stronger throughout time. They were between 0.5 °C at the beginning and approx. 4 °C at the end of the recording period. Also clearly noticeable is the fact that night time minima of all recorded surface water temperatures show the same long term trend when compared to each other.

6.2. Surface water level results

All recorded water levels were originally thought to be usable to verify seepage results obtained from the heat method and, in combination, for estimations of streambed hydraulic conductivity. Quite surprisingly, the raw surface water and sediment water level data contained some remarkable features which will be discussed in more details. Firstly, all recorded water level data had to be cleaned from atmospheric pressure influences. Afterwards, they could be referred to the Australian Height Datum (AHD) using the GPS survey results. This process transferred levels into absolute values and allowed easy comparison between locations (see Table 6 on page 62).

Figure 25 contains barometric pressure (plot A), rainfall (plot A) and surface water levels (plot B, C and D) as recorded in all investigated surface water bodies throughout the time of installation. The highest, lowest and average atmospheric pressure at the point of recording (altitude of approx. 227 m AHD) was 1,001.6 hPa, 976.4 hPa and 988.6 hPa, respectively. The pressure series shows fluctuations with various frequencies all superimposed. Clearly visible are daily water level fluctuations, and the origine of these will be discussed later. The barometric record also illustrates the pass of longer lasting trends which are caused by high and low pressures as part of the meteorologic macro climate. Most rainfall occurred during times of low barometric pressure as pointed out in the plot.

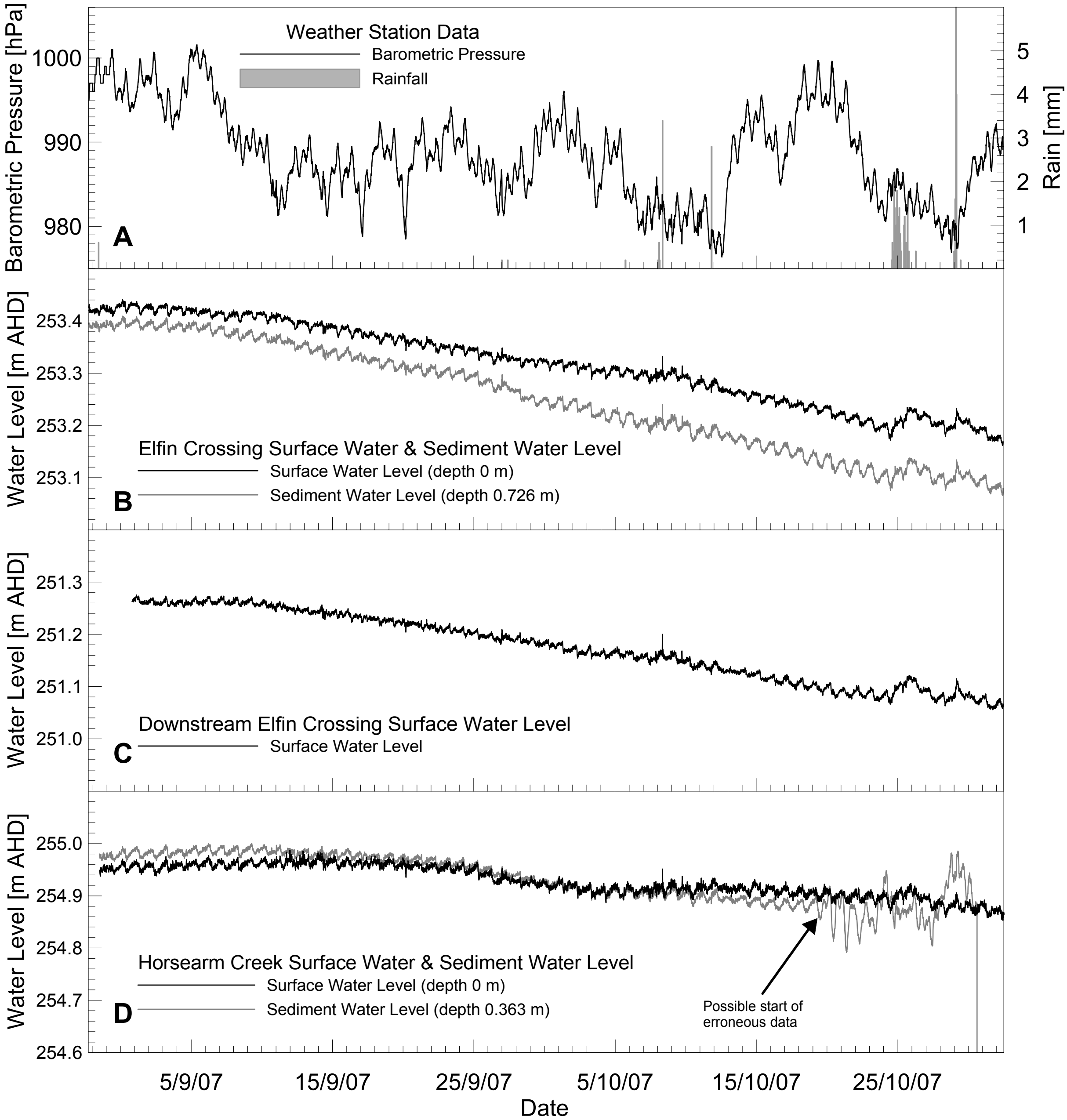

Figure 25 shows barometric pressure and rainfall data as well as surface and sediment water levels.

Graph B, C and D display the recorded surface and sediment water levels at all three locations. Unfortunately, the instrument measuring the sediment water level at Horsearm Creek stopped functioning around the 20th October 2007. The manual level measurement was done only before disassembling at the end of the recording period. Therefore the values cannot be referred to the AHD, thus levels cannot accurately be compared with all other recordings. However, all plots indicate the same decreasing trend. The magnitude of decrease at Elfin Crossing and downstream EC are similar compared to the signal at Horsearm Creek behaving differently. A quick but short response of levels to four rainfall events with 4.4 mm (around the 8th), 2.8 mm (12th), 13.8 mm (around the 25th) and 4.8 mm (29th) are clearly visible in October 2007. The amount of accumulated rainfall was approx. 40.2 mm during the entire period of investigation. Especially the longer lasting rain around the 25th of October 2007 caused a consistent but delayed rise in surface water levels. However, there was much less response to rain events at Horsearm Creek.

6.3. Temperature results

Spectral analysis was also performed, particularly with the temperature results recorded at Elfin Crossing. Figure 26 illustrates clearly that propagation depth of oscillations strongly depend on the frequency. This is also formulated in the exponential term of Stallman's analytical solution (equation [23] on page 27). In general, the lower the frequency (larger scale temperature changes) the stronger is the temperature signature and the further the penetration into the streambed. The decline of signal strength can be noticed by inspecting the peaks visible at 1 cpd in Figure 26. All five thermistors are located in different depths (see Table 7 on page 64) and illustrate a peak which is strongest at the same frequency. They are a distinct result of diurnal temperature changes caused by solar day and night. However, temperature oscillations recorded by probe 5 were damped down to a spectral value of approx. 0.2 °C. This is well above the resolution but reaches the accuracy limit of the thermistors. Also, this does not concern further results because filtering eradicates the accuracy (which is part of the DC component) from the recorded values. Higher frequencies exemplify the signature of noise caused by the instrument as well as experiment environment.

Filtering as described in chapter 4.4.1 (page 43) was performed on all recorded temperature time series. As a representative example of the outcome, only the surface water and sediment temperature in a depth of 0.60 m at Elfin Crossing are displayed in Figure 27.

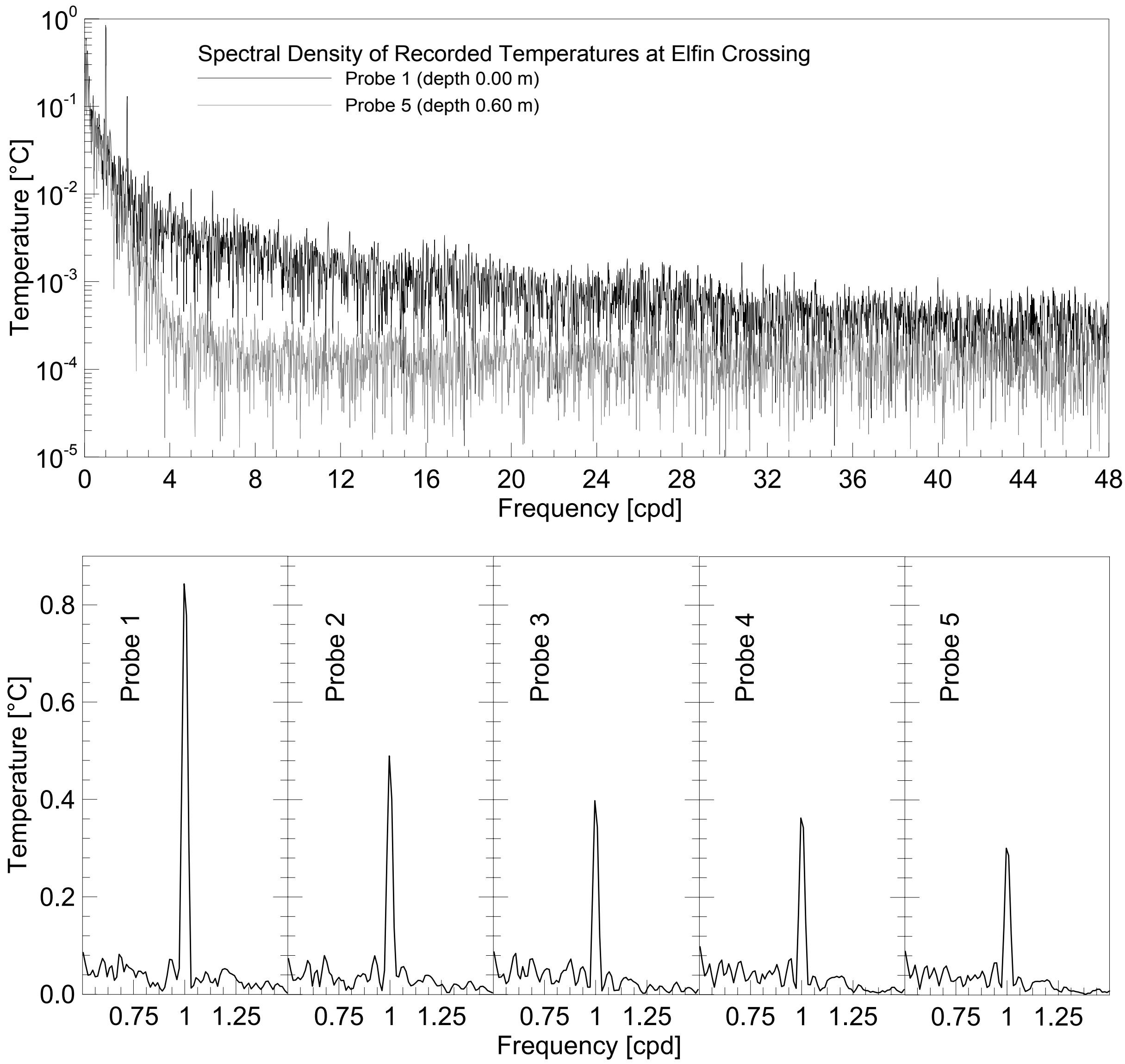

Figure 26 illustrates spectral density of temperature time series recorded by five different thermistors and depths at Elfin Crossing.

There is a clear variation of oscillation amplitudes in both signals, which indicates the variability of water velocity. The “cut off” dates at the beginning and the end are illustrated as a dashed grey line in Figure 27. After filtering the signal was up-sampled by the factor 5 which resulted in a new sampling time of 3 minutes (180 seconds). All amplitude ratios and time lags of each individual temperature peak were now available for extraction. As discussed in the methodology, these values could be used to calculate the velocity of vertically percolating water.

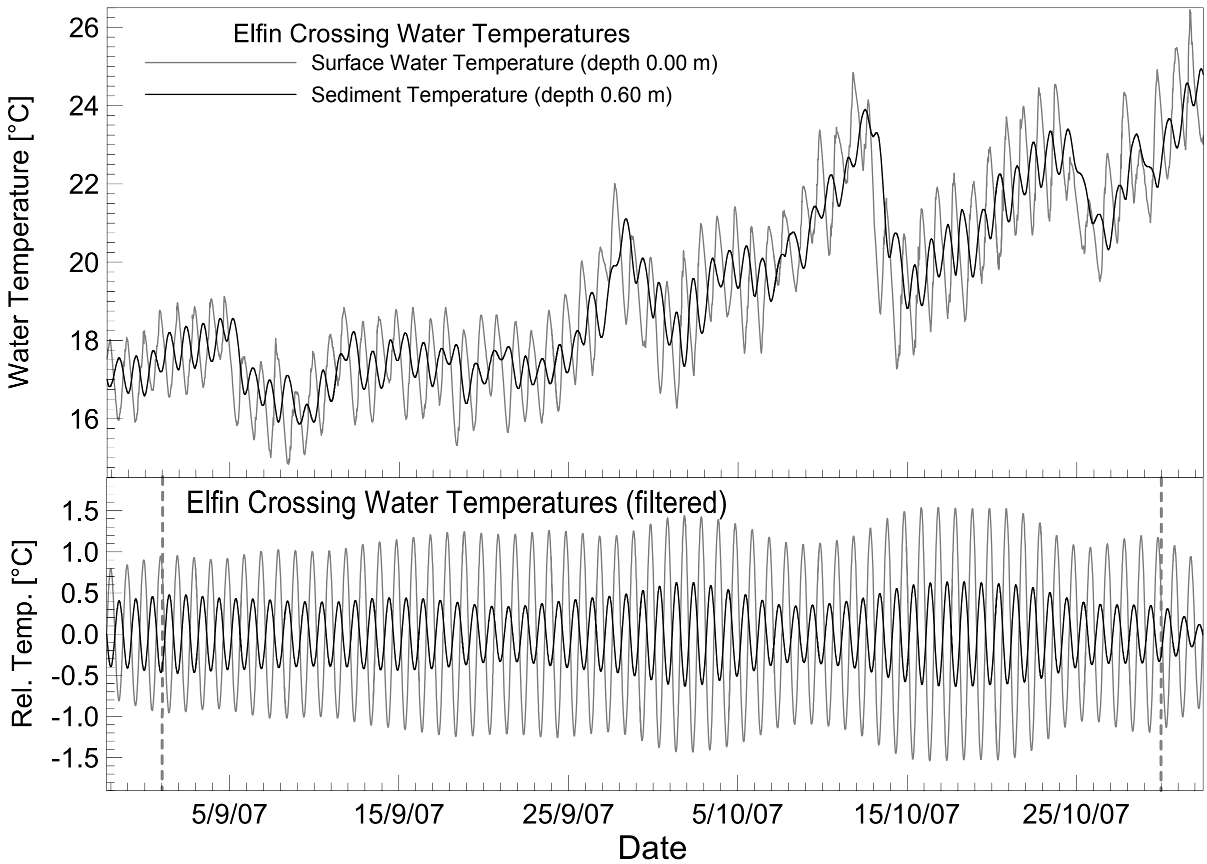

Figure 27: Raw and filtered temperature time series recorded by probe 1 and 5 at Elfin Crossing.

6.4. Velocity results

6.4.1. Elfin crossing

For the calculation of the vertical water seepage or exchange velocity, a pair of processed temperature signals is required. Each array contained 5 temperature probes thus offering a combination of 10 different seepage velocities for evaluation. In all cases it was decided to only use the first probe (surface water temperature) in combination with the probes in different depths. This is because the focus was given to surface water groundwater exchange rather than hyporheic flow profiles. As a consequence, there were four and eight results obtained from each array by the steady state and the transient method, respectively.

All original temperature recordings could directly be utilised without any further processing of the signal in order to iterate through the forward modelling and fitting routine. Temperatures recorded at the four distinct depths in the sediment were calculated using equation [18] and [19] (page 24). In order to find the best fit between simulated and recorded values the two variables seepage velocity and dispersivity were adjusted. Figure 28 demonstrates the quality of fit for Elfin Crossing using an extraction of the total sampling time. Results were calculated from 6,213 sampled temperature values for the probe combinations 1/2 (plot A), 1/3 (plot B), 1/4 (plot C) and 1/5 (plot D). The root mean square error (RMSE) is included for comparison of the quality of fit (Beta = dispersion coefficient).

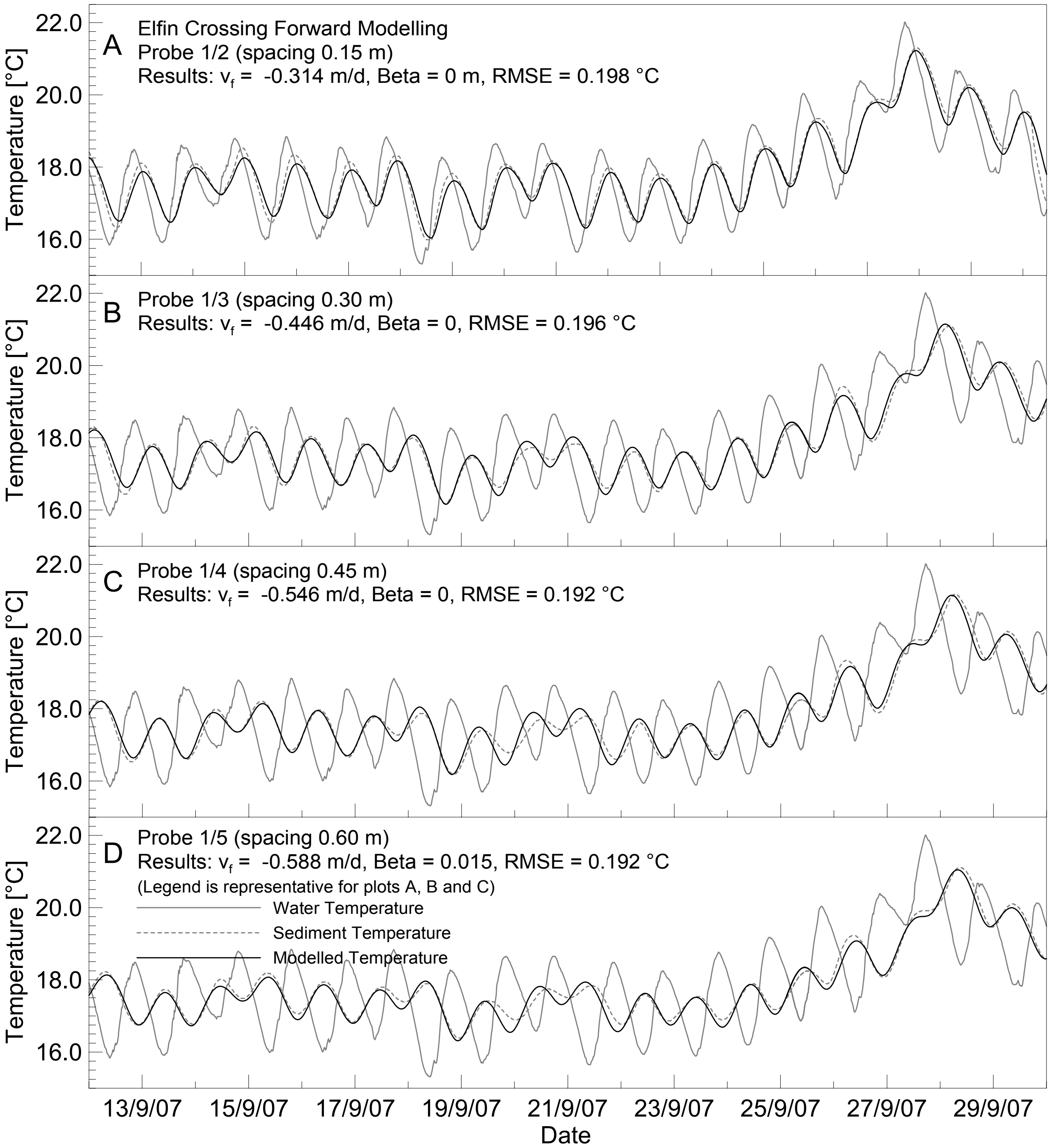

Figure 28 demonstrates the quality of fit using an extraction of modelled temperatures.

Forward modelling results matches the measured temperatures at Elfin Crossing quite well as indicated by the RMSE values. These approach the accuracy of the thermistors which is approx. 0.2 °C. Most perturbations are nicely replicated but for some peaks the simulated and the recorded values differ in magnitude and also show a slight phase shift. This is most probably caused by the values of the real velocity and thermal dispersion varying with time, compared to the assumption of a steady state system for the computation. It is interesting to observe that this simulation method is capable of describing signal perturbations with an arbitrary temperature signature. The seepage results calculated from four different instrument pairs are consistently increasing with depth. For continuity reasons, this seems impossible for truly vertical flow.

Pair of Thermistors		**1 / 2**	**1 / 3**	**1 / 4**	**1 / 5**
Spacing	m	0.15	0.30	0.45	0.60
Seepage	m/d	-0.314	-0.446	-0.546	-0.588
Dispersivity	m	0	0	0	0.015
RMSE	°C	0.198	0.196	0.192	0.192

Table 8 shows the parameters and results used for and obtained from the forward modelling approach at Elfin Crossing.

The transient seepage results for Elfin Crossing are displayed in Figure 29 together with the water temperatures, rainfall and the independently recorded level gradient. In this case, dispersion coefficients were used to manually match results derived from both solutions as good as possible. The dispersion values proved to have a significant impact on calculated velocity results. However, they are somewhat inconsistent suggesting that the first pair produces results which have to be interpreted with care. Please note that the water level gradient is displayed using a descending axis for better comparison with the velocities below. All gradient values were derived from surface water and sediment water levels recorded by a different instrument but in the vicinity of the temperature measurements. Seepage velocities calculated for thermistor pairs 1/2, 1/3, 1/4 and 1/5 are displayed in plot C, D, E and F, respectively. Clearly, all vertical water exchange velocities were in the range between -0.2 m/d and -0.65 m/d indicating surface water loss to the streambed. This fact is confirmed by the forward modelling results calculated using the same pairs and results are illustrated in the corresponding plots. It can be observed quite clearly that the forward modelling results reflect an average of the quasi-transient value. Moreover, there is a trend of decreasing velocity during the period of investigation which is especially evident in shallow depths. Velocity values evaluated from pairs with more spacing show an overall stable trend. Again, the depth increase previously noted is also apparent in the transient data.

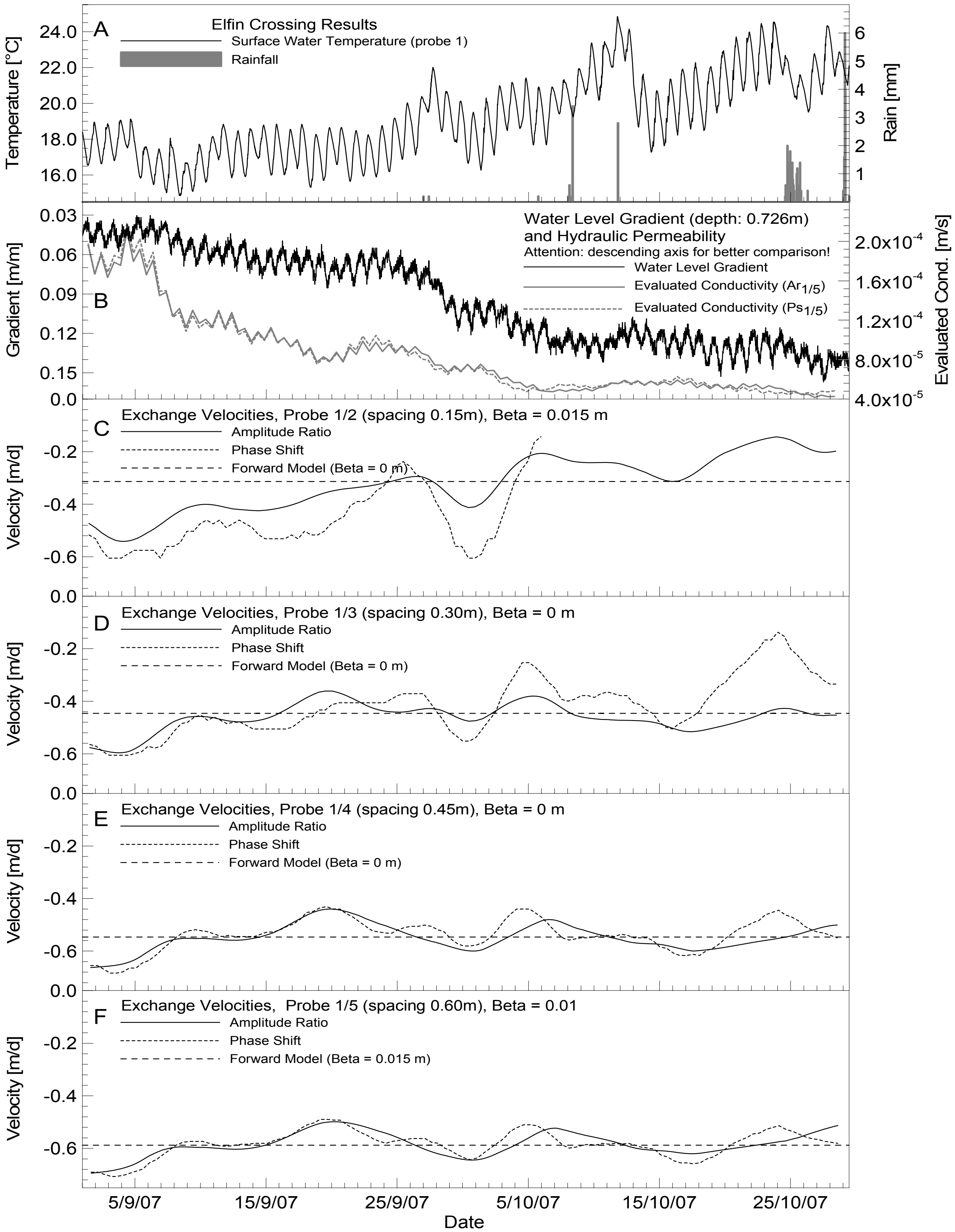

Figure 29 displays the original water temperature (A), water level gradient (B) and all final velocity results derived from amplitude ratios and phase shifts (C, D, E and F) at Elfin Crossing.

Quite differently to the seepage results obtained from the heat methods, the water level gradient increased during the time of investigation (plot B). Both results were evaluated from independent physical sources, thus applying Darcy's law (see equation [2] on page 5) allowed the estimation of the streambed hydraulic conductivity (evaluated conductivity). In order to obtain appropriate results, gradient values had to be averaged for the time period between corresponding temperature peaks as used for the velocity calculation. Only pair 1/5 was used for this process because the depth (0.6 m) was closest to the depth of the level measurement (0.726 m) in the near vicinity. Graph B shows the hydraulic conductivity results which decreased from approximately $2x10^{-4}$ m/s to $4x10^{-5}$ m/s. The timely decline in streambed conductivity is quite significant, and it is surprising to observe that it goes along with a fairly constant vertical loss of water. However, these values must be interpreted with care because they are a result of recordings taken at two different points in the hyporheic zone.

6.4.2. Downstream Elfin Crossing

Results for the location Downstream Elfin Crossing were evaluated using both methods and are plotted in Figure 30 (forward modelling with 6,133 data points) and Figure 31 (transient solution). The same probe combinations as for EC were used for this location. Figure 30 graph A, B and C illustrate that the fitting quality decreases (note the RMSE values) until no valid solution was found for thermistors pair 1 and 5 (see graph D). It is quite noticeable that in all cases the best fits were found for the maximum dispersivity value which was restricted to 10% of the length scale. The possible explanation for this is that model conditions were stressed.

Probes		**1 and 2**	**1 and 3**	**1 and 4**	**1 and 5**
Spacing	m	0.15	0.30	0.45	0.60
Seepage	m/d	-0.609	-0.519	-0.525	-0.016
Dispersivity	m	0.015	0.030	0.045	0.060
RMSE	°C	0.379	0.516	0.873	0.697

Table 9 demonstrates the parameters and results used for and obtained from the forward modelling method applied to location DEC.

An extraction of temperature values is also displayed in Figure 30 for comparison. Results derived from the first three probe combinations indicated vertical downward water loss to the streambed with a flow rate between approx. -0.55 m/d and -0.60 m/d (see Table 9 for details). However, the last solution (pair 1/5 in plot D) cannot be evaluated probably because its oscillations were damped below thermistor accuracy.

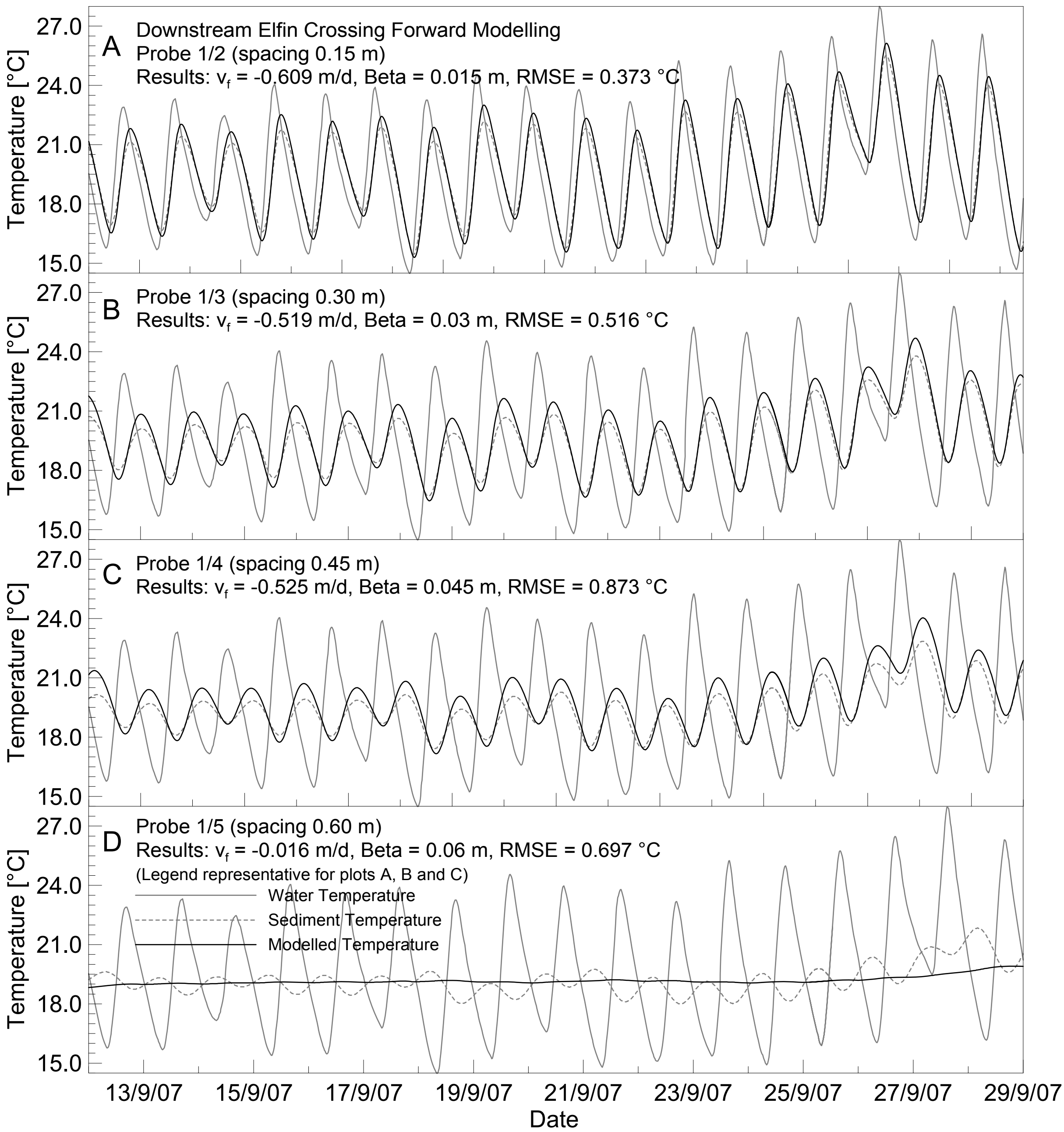

Figure 30 illustrates an extraction of the forward modelling results computed for probe combinations 1/2 (A), 1/3 (B), 1/4 (C) and 1/5 (D) at the location DEC.

Transient results were combined with additional information to improve the presentation and interpretation of the aquatic system at this location (see Figure 31). The surface water level in plot B illustrates a quick response to the recorded rain events. In fact, the water level increased just after the rain, and the decline response was fairly rapid within approx. 1.5 days (see 25th of October 2007). However, the total trend shows a constant decrease in groundwater level of approx. 0.2 m starting at the 9th September 2007.

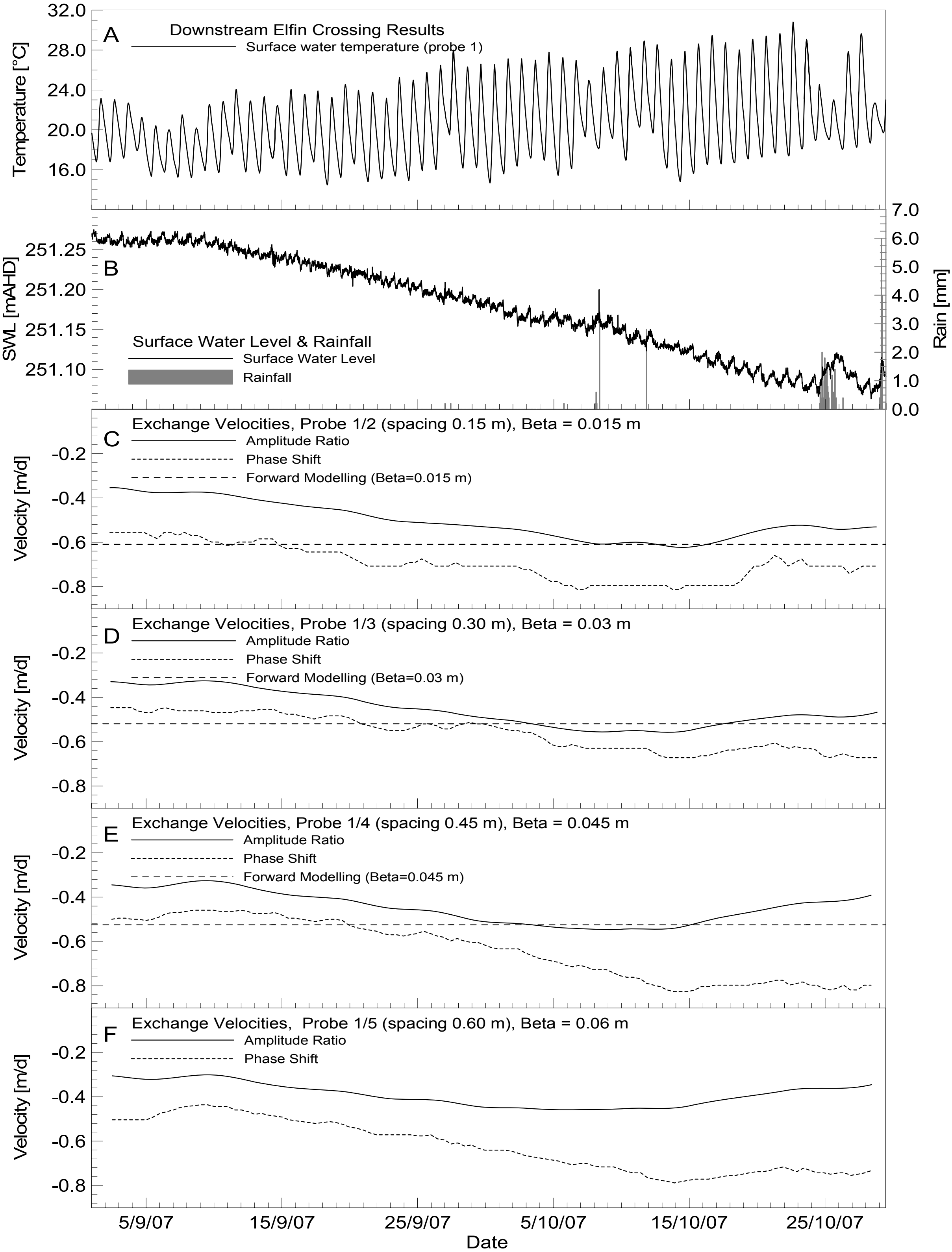

Figure 31: Diagram showing the original water temperature (A) and the final seepage results derived from amplitude ratios and phase shifts (C, D, E and F) at location DEC.

Velocity results as pictured in Figure 31 plot C, D, E and F illustrate a remarkable feature: both series derived from amplitude ratios and phase shifts initially show the same trends but do not exhibit matching values. In fact, velocities derived from phase shifts are much higher than the ones obtained from amplitude ratios. Towards the end of the time, both results diverged even more, especially between pairs 1/4 and 1/5. The difference between both solutions cannot be explained using different thermal properties at this location in order to match both. Thermal values would be considerably different, which is impossible because sediment properties should be quite comparable in this area of Maules Creek as they originated from the same source. It was therefore concluded that diverging seepage values were a result of violated boundary conditions of the analytical solution. The most important violation to be considered is the influence of horizontal flow. This is an assumption which requires the need for further investigation and will be dealt with later in this thesis.

The comparison with plotted forward modelling results also suggested that the transient solution contained sources of errors. The invariant values do not represent average values of either of both analytical solutions but exhibit a value which is in between. This fact also contributes that there is a need for the examination of possibly violated boundaries.

6.4.3. Horsearm Creek

The third location investigated using the heat method was Horsearm Creek. At this location, the temperature records were divided into two sections because the water level gradient indicated a change in direction from upward to downward (see Figure 25 page 69). The cut of the series was done at the 30th September 2007 leaving two temperature time series with 3,114 and 3,025 values. The results were calculated using the same methods and illustrated in Figure 32, Figure 33 (forward method) and Figure *34* (transient solutions).

It is important to mention that two probes in this array had to be discarded from the calculations: Probe 1 was outside the sediment detecting temperatures in the surface water body together with probe 2 (see Table 7 on page 64). Temperature signals recorded by probe 5 were unusable because they featured values below instrument resolution, thus offered possibly inappropriate values. Due to this loss, only the probe combinations 2/3, 3/4 and 2/4 were used for presentation and interpretation. Again, forward modelling results are plotted and listed in Figure 32, Figure 33 and Table 10. Part one (Figure 32) illustrates that water in the sediment flowed downwards between pair 2/3 but upwards between 2/4 and 3/4. However, the best fit for water flow in the second part was found for consistent downward flow through the streambed as displayed in Figure 33. The solution diverged towards the end of September because the flow direction changed. This doesn't agree with the steady-state nature implied by the forward modelling approach and illustrates the limited field applicability of this method.

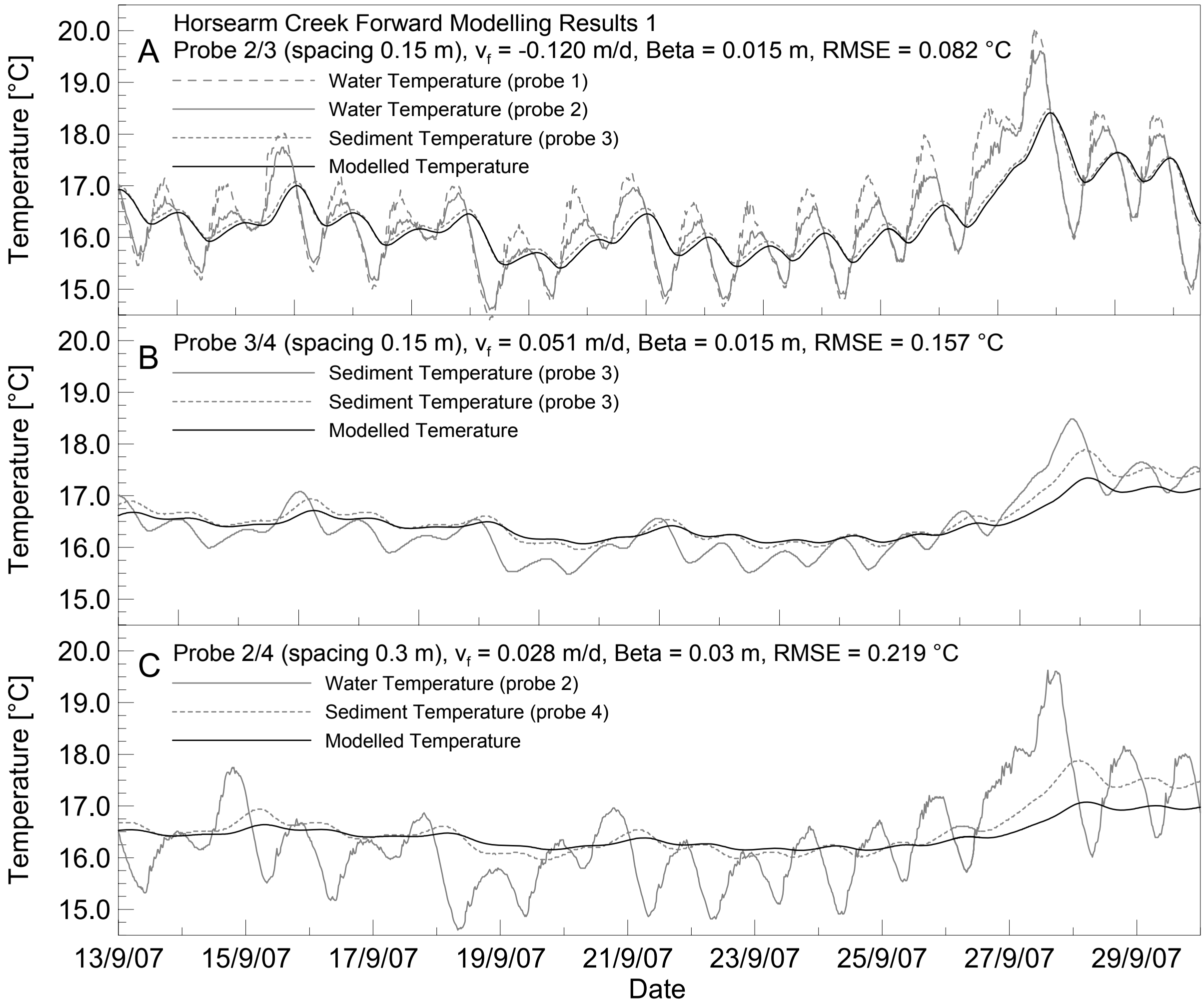

Figure 32 exhibits an extraction of forward modelling results calculated for probe combinations 2/3 (A), 3/4 (B) and 2/4 (C) at location HC using the first time period.

Transient results are plotted in Figure 34. Sediment water levels were not usable towards the end of the record because the device stopped functioning before the manual level was taken as a reference. An estimated measurement could be extracted from field notes, which included dimensions and initial water level manually taken after installation. Additionally, the survey accuracy is quite low due to the trees blocking satellite contact (see Table 6 on page 62). However, values are accurate enough for comparison with the other installations. Figure 34 demonstrates that the sediment water level decreased more than the surface water level. As a result, the level gradient reversed, indicating change of flow direction from upwards to downwards between points of measurement in the period of recording. It is important to mention that water levels were not recorded at the same position as the temperatures, but in the near horizontal vicinity with a vertical spacing of 0.363 m. Same as at the other locations the water levels exhibit a rapid response to rainfall events.

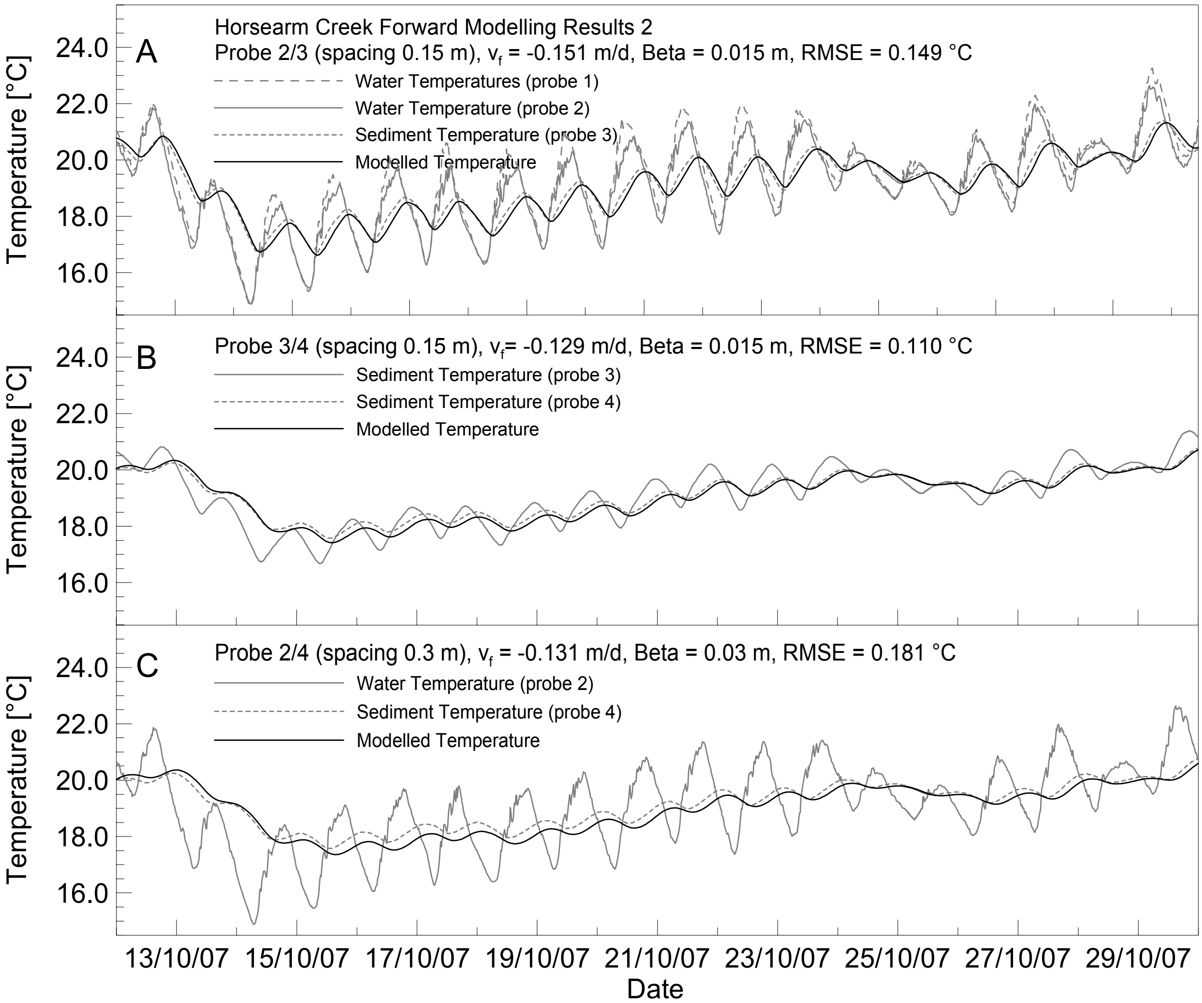

Figure 33 illustrates an extraction of Horsearm Creek forward modelling results calculated for probe combinations 2/3 (A), 3/4 (B) and 2/4 (C) and the second period..

Transient exchange velocity solutions are displayed in Figure 34, plot C, D and E. Contrarily to the invariant solutions, thermistor combinations 3/4 and 2/4 exhibited a vertical downward flow between -0.1 m/d and -0.2 m/d throughout the period of recording. Phase shift results differed significantly from amplitude derived velocities as values were between -0.3 m/d and -0.4 m/d. There was a consistently increasing trend in downward velocity magnitudes for both solutions as well as all thermistor pairs. Confusingly, the forward model predicted a slightly gaining system between pair 3/4 (plot D) and 2/4 (plot E) for the first period of simulation. This is in disagreement with the quasi-transient solution and has to be examined. The second period shows matching values for results obtained by both heat methods. Troughs and peaks in the phase shift plot of probe pairs 2/3 and 3/4 were caused by the fact that the method sensitivity is limited for low velocity magnitudes (see Figure 15 on page 52).

Results between 28/08/2007 and 30/09/2007 (3,114 temperature sampling values)				
Probes		**2 / 3**	**3 / 4**	**2 / 4**
Spacing	m	0.15	0.15	0.30
Seepage	m/d	-0.120	0.051	0.028
Dispersivity	m	0.015	0.015	0.03
RMSE	°C	0.082	0.157	0.219
Results between 01/10/2007 and 01/11/2007 (3,025 temperature sampling values)				
Probes		**2 / 3**	**3 / 4**	**2 / 4**
Spacing	m	0.15	0.15	0.30
Seepage	m/d	-0.151	-0.129	-0.131
Dispersivity	m	0.015	0.015	0.03
RMSE	°C	0.149	0.110	0.181

Table 10 shows the parameters used for and results obtained from the forward modelling approach for temperatures recorded at Horsearm Creek.

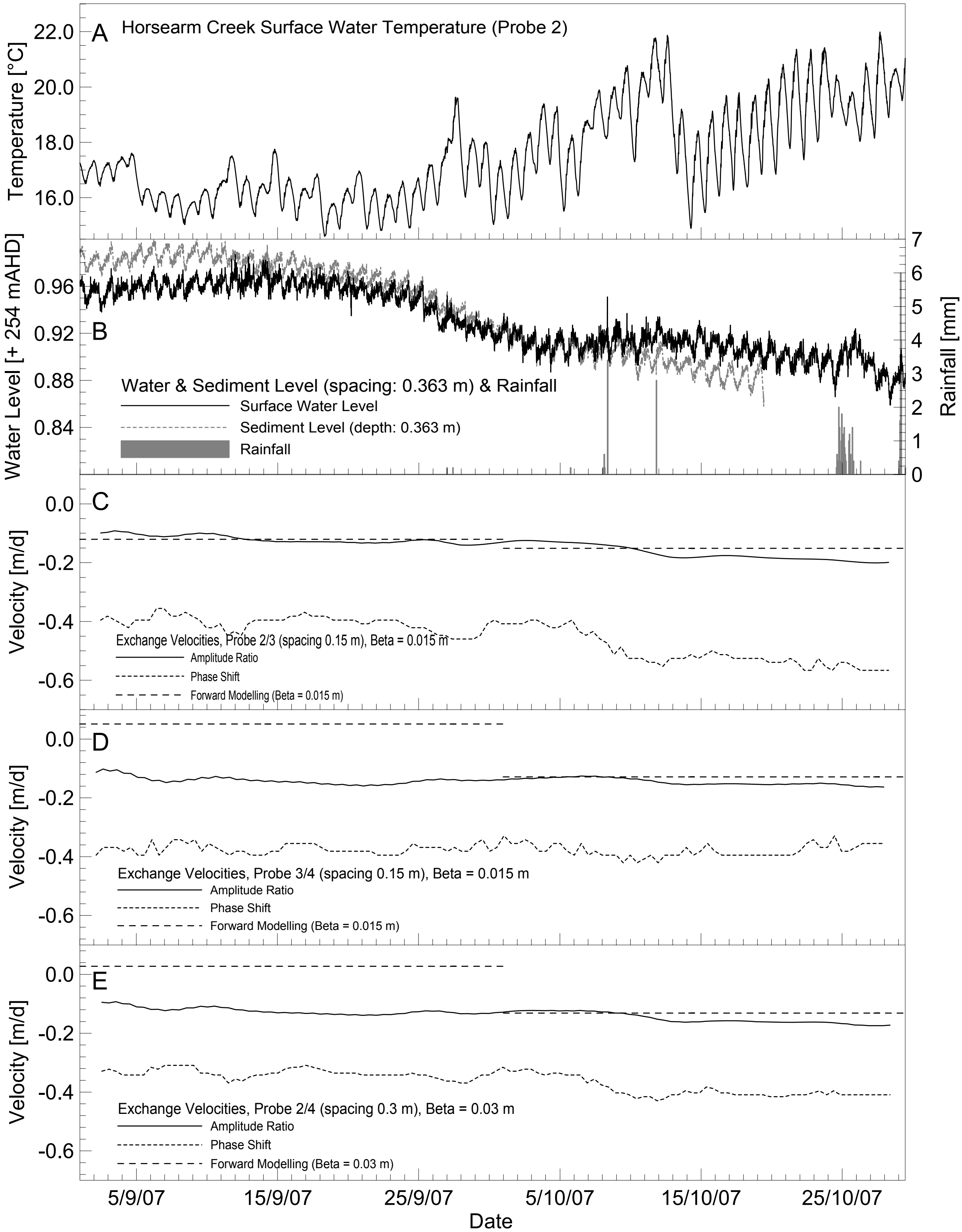

Figure 34 shows the original water temperature (A) and water levels (B) as well as seepage results derived from amplitude ratios and phase shift values (C, D, E) at location HC.

6.5. Numerical results

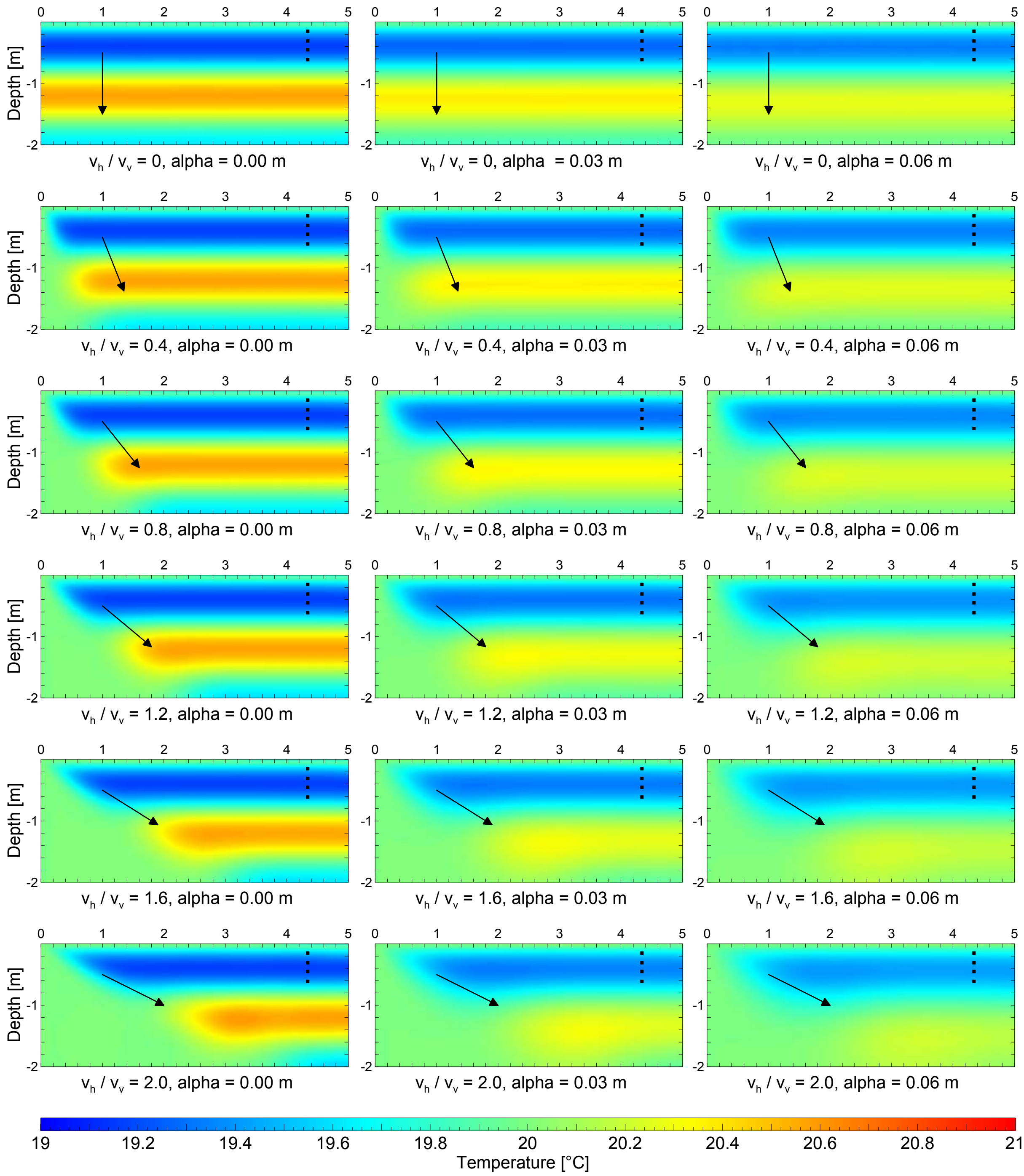

Figure 35 shows an extraction of the numerical simulation results. Vectors denote the direction but not magnitude of fluid flow.

The outcome of the numerical heat transport simulations as discussed in section 4.5 (page 53) is exhibited in Figure 35 and Figure 36. The images were taken as post-processor snapshots at the end of the particular computation period. Vertical heat flow anomalies as seen in the images probably originated from the corner policy of the boundary conditions. Clearly, an increase in thermal dispersion caused enhanced spreading of heat, thus lowering temperature amplitudes and shifting peak phases due to the propagation of the sinusoidal temperature signature. All recorded temperature observations were processed by a peak picking script in order to use the amplitude ratio and phase shift values for iteration of seepage velocities. Each value in Figure 36 was an average calculated as a result of all temperature peaks which occurred in the entire simulation time.

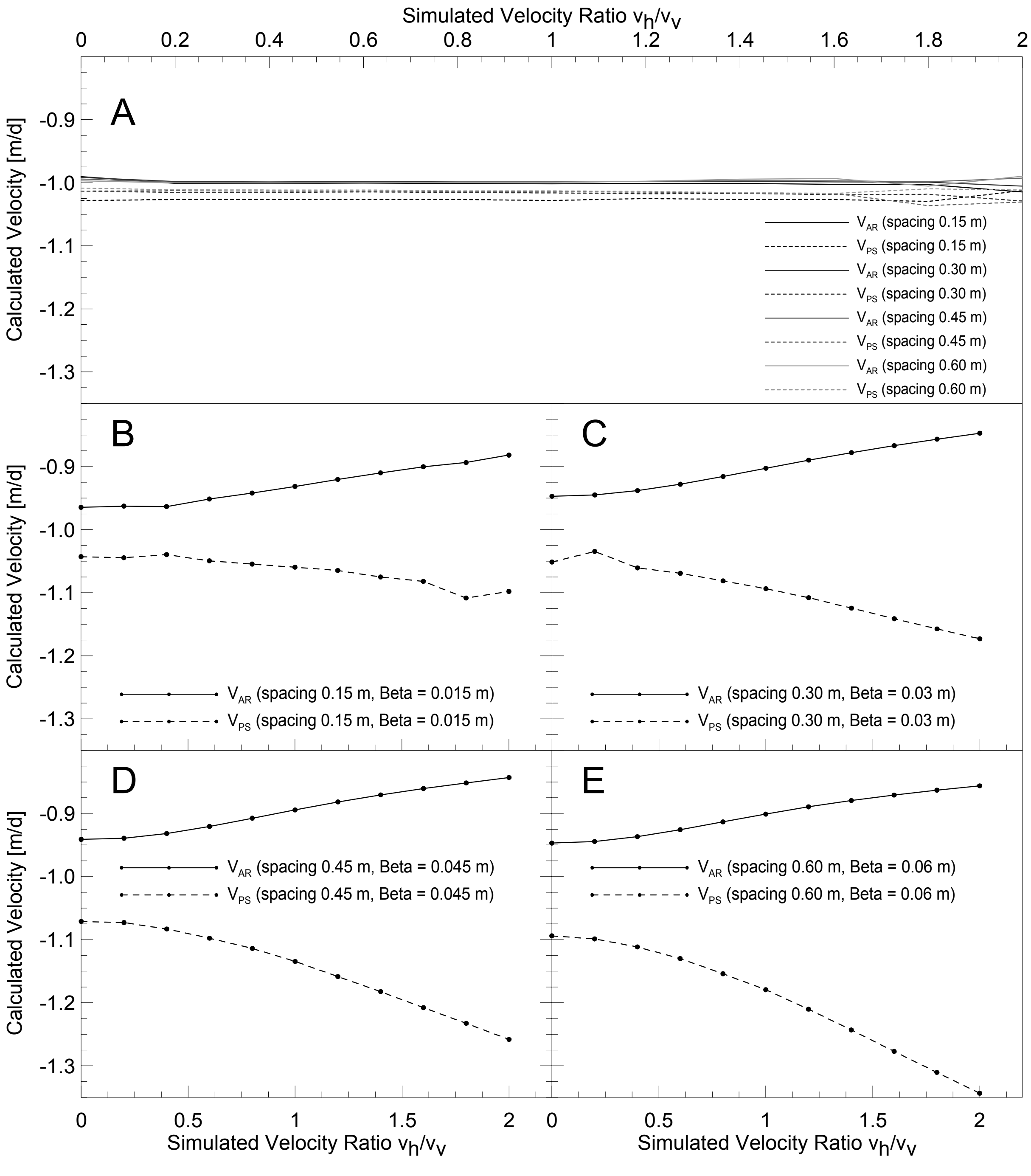

Figure 36 summarises results of the heat transport simulation with different velocity ratios and dispersivity coefficients.

The impact of horizontal flow and thermal dispersion on the analytical solution is considerable. Plot A demonstrates that the influence of horizontal streambed flow does not alter the analytical and one-dimensional solution unless heat dispersion is relevant. The diverging solutions at purely vertical flow exhibit that both methods are based on different mathematical approaches concerning the dispersivity value. Moreover, flow simulations considering both, longitudinal and transversal dispersion coefficients offer variant results after recalculation. This is because of the purely vertical formulation of the analytical solution which clearly restricts its capability for field application because results diverge and exact quantification becomes impossible. It can be seen in Figure 36 plot B, C, D and E that the higher the horizontal flow the more significant the impact on the recalculated velocities. The relationship between horizontal flow and amplitude derived result is non-linear, thus an increase in velocity ratio forces the solution to decrease. However, these values appear to be independent from dispersion coefficient and probe spacing. Unlike these findings, solutions derived from phase shifts increase with more thermal dispersion and flow ratio. Looking at the field results recorded at Maules Creek, it can be concluded that heat dispersion is definitely present and has to be considered when the method is applied to the field.

7. Discussion

The following list includes the major questions concerning surface water groundwater interactions and the new heat method. This thesis aims to answer these trying to also find out about the flow situation in Maules Creek.

- How does climate and especially heat flow influence aquatic systems?
- How can heat transfer and resulting temperature signals be used to characterise the connectivity of aquatic systems?
- Are all or some of the surface water bodies connected to the groundwater table?
- Does heat offer reliable results when used as a tracer to quantify exchange flow?
- Is there water exchange between the surface water pools and the groundwater at Maules Creek?
- What is the variability of water exchange through the streambed?
- How can the connectivity between both water sources be characterised?

This section discusses the results previously presented and tries to answer all above questions about the heat method and about water exchange in Maules Creek.

7.1. Climate data and water temperatures

Figure 37 shows an extraction of climate data recorded in the period between the 15th and the 25th of October 2007 for closer inspection. Clearly, it can be seen in plot A that temperature rises as soon as the insolation starts at the beginning of each solar day. Also, temperature peaks show a slight but constant phase shift compared to peaks in radiation. This is probably due to heat storage being released after radiation decline by various different objects on the surface environment mostly featuring larger specific heat capacity than air. The zoomed data neatly visualises the inverse relationship between temperature and relative humidity. Sudden changes in air temperature as obvious early in the morning on the 17th and the 20th of September are suspected to be driven by the local climate.

In Figure 24 (see page 66) it is interesting to see how conditions like surface water body size and surrounding environmental conditions are reflected in the recorded surface water temperatures at each location. It is obvious that the pond at Horsearm Creek was located in a shady location and temperature perturbations measured in the surface water pool are mainly induced by heat transfer through the interface between water and air.

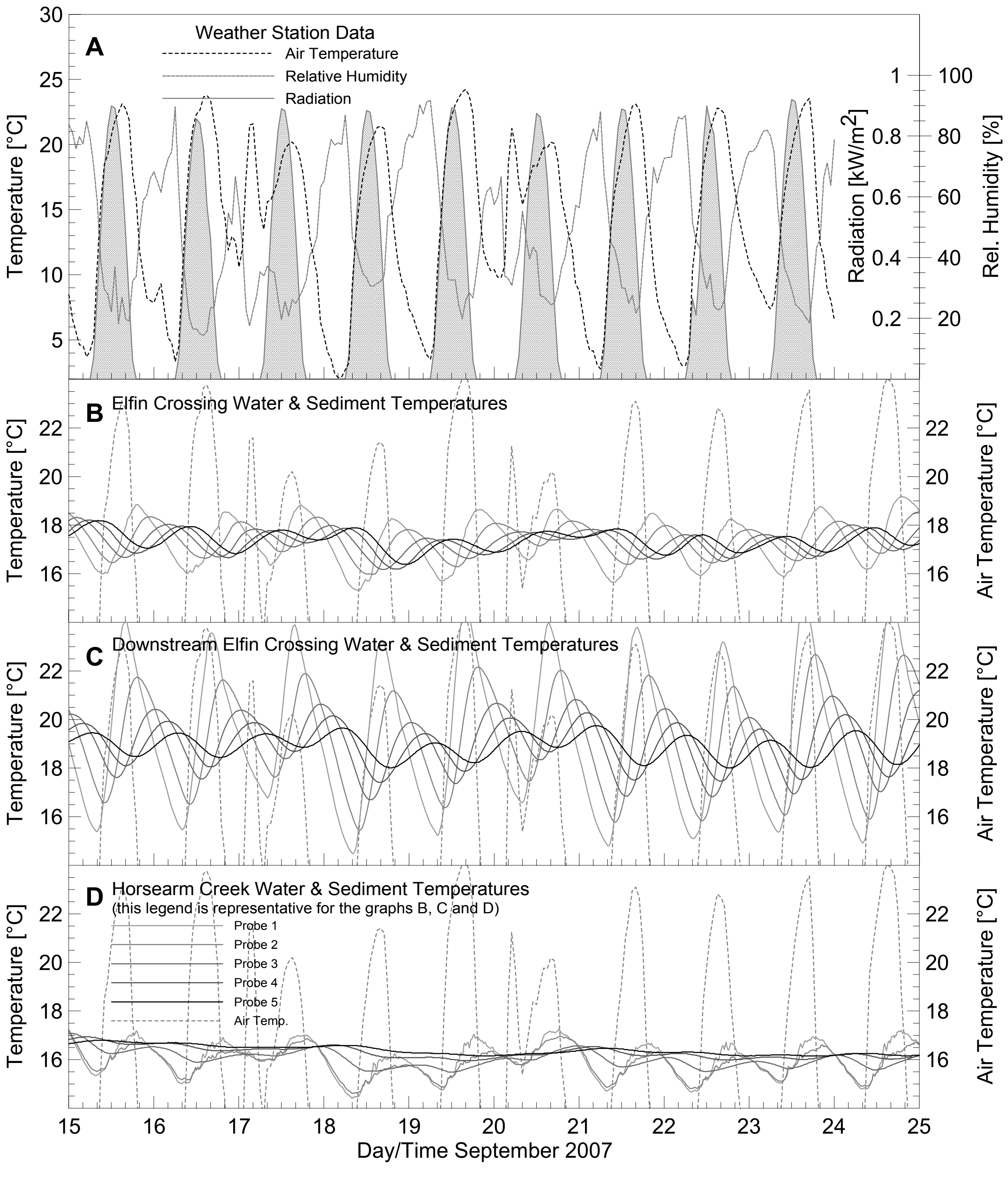

Figure 37 illustrates a time period extracted from climate recordings and water as well as sediment temperatures in September 2007.

The extreme temperature signal in the pool downstream Elfin Crossing clearly illustrates that warming is also induced by sun radiation penetrating into the water body. The evidence can be seen in Figure 37 especially on the 18th and 19th September 2007, because water temperatures were much higher than the ambient air temperature at noon. The amplitude difference between the signals of the three surface water bodies was quite significant. The reason for this could be found in the different surface area to volume ratio of the ponds, which is much lower downstream Elfin Crossing (shallow surface water pond with large surface area). However, a direct comparison of energy input by these two different processes cannot be performed. This would depend on various factors: the penetration depth of radiation, which is influenced by dissolved substances (colloids) defining the turbidity, the surface area and intensity of radiation. Additionally, water at Horsearm Creek was much clearer than the water downstream Elfin Crossing thus energy components resulting from the different heat transfer processes cannot be distinguished.

Graph B, C and D illustrate surface water and sediment temperatures recorded in the four different depths at all locations (see Table 7 for exact values). At this level the following heat balance is visible: oscillations in air temperature are damped down in water because of the difference in specific heat capacity of liquid water approx. 4.81 kJ/kgK (NIST, 2005) compared to dry air with approx. 1.005 kJ/kgK (WPI, 2008), respectively. If the pond is located in a shady position such as Elfin Crossing or Horsearm Creek, surface water temperature maxima are located on the descending branch of the air temperature which indicated that heat transfer between air/water was more dominant than heat through absorption of sunlight. However, slight peak time lags were due to the complexity of natural processes as part of the local climate.

The location downstream Elfin Crossing (plot C) is the best example for the theory of diurnal heat propagating into the surface water sediment. These field results obviously conform to the theoretical solution of the conductive convective heat transport equation [23] (see page 27). The main features are decreasing amplitude and increasing time lag of the signal with depth. Figure 38 (plot B) contains unexplainable and inappropriate features: temperatures recorded by probe 2 and 3 are lower than the ones measured by thermistors in the deeper sediment. This does not match the theory and no reasonable explanation could be found.

Figure 38 shows air temperature, relative humidity, radiation and water as well as sediment temperatures recorded at all three locations for the time period between 15th October and 25th October 2007. As visible, the depth response at Horsearm Creek is damped down much quicker, especially considering the fact that the depth of the array was less than at the two other locations. Also, the deepest temperature signal recorded by probe 5 (see Figure 37 plot D) exhibits temperatures which were generally higher than the average of the other thermistors. According to Silliman et al. (1995) this can indicate groundwater discharge because the signal is damped quickly by upwards flowing water having a constant temperature. Figure 38 plot D exemplifies a period with bigger amplitudes in October.

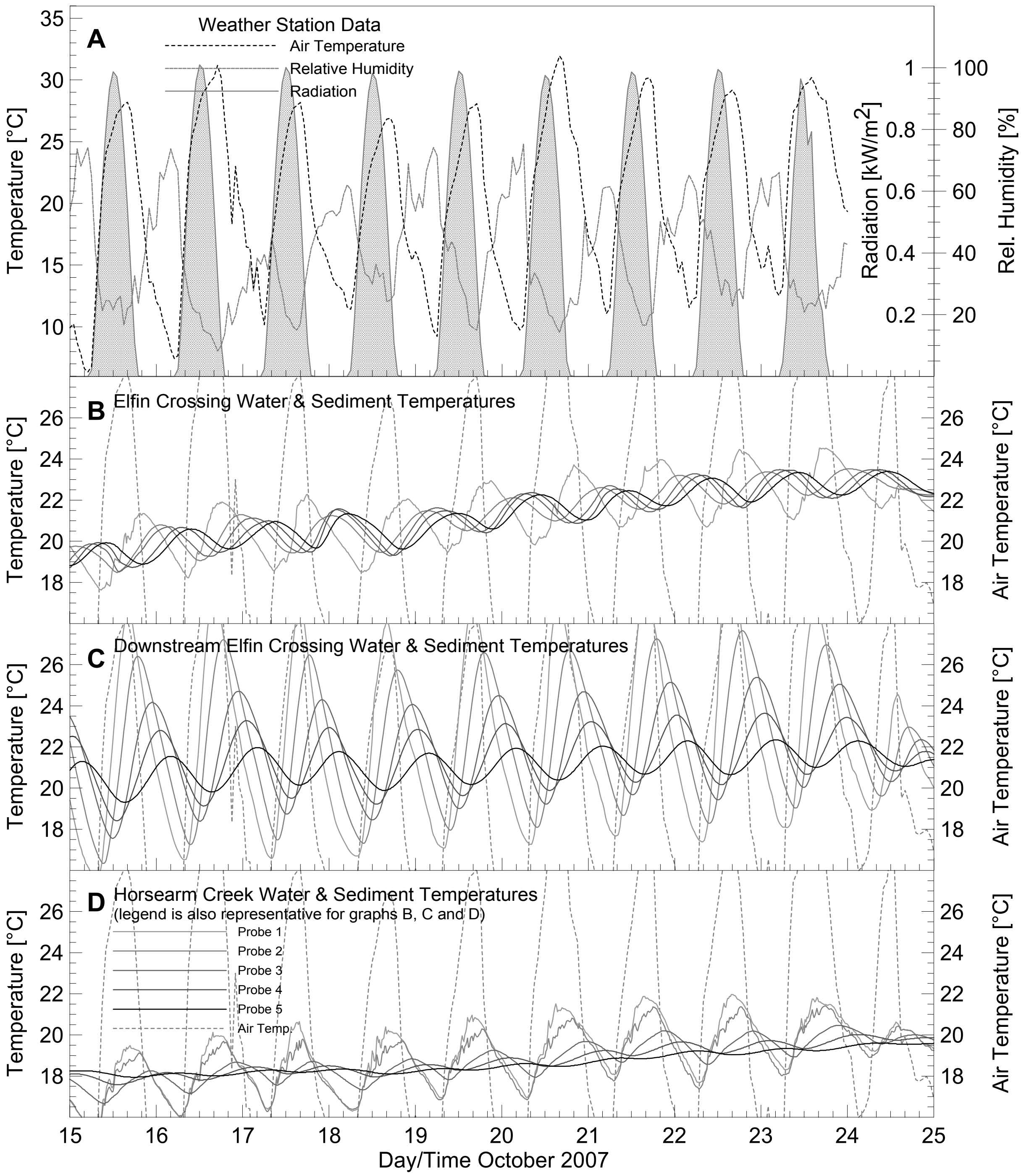

Figure 38 shows an extraction of air temperature, relative humidity and radiation recorded in October 2007.

Referring back to Figure 24 plot E (page 67) it can be interpreted from the simple heat balance of water in the pond that groundwater discharge at HC must have decreased. This is evident looking at the fact that daily oscillations in air temperature show constant amplitudes (plot A), a signature similar to the ones at EC (plot C). However, oscillations at HC confirm significant damping with time. The first two probes at HC directly measured water temperatures. Probe 1 (0.15 m above streambed) logged higher values than probe 2 during the day (as seen in Plot D) which means that heat propagated from the top of the water body to the bottom.

Figure 24 (page 66) demonstrates that the trend in night time minima of the ambient air temperature is reflected in the minima of all investigated surface waters. This result shows the following phenomenon: surface water bodies warm up during the day. The value of the heat capacity of water is approx. five times higher than heat capacity of the surrounding air. This encourages heat storage and retention in the water bodies, which means that heat is accumulated during the day and slowly released after the air temperature drops below the one of the water body. After that heat flow reverses and is released into the air, thus water bodies in all three locations cooled down slowly. However, there is a difference in the rate of cooling down which generally depends on the surface area of the water body for heat transfer, and its volume for the amount of heat which is stored. This mechanism could be a reason for the fact that the pool at EC (see plot C) showed similar amplitudes than Horsearm Creek pond, despite the fact that it was located in a much sunnier position. More energy is stored because the volume of water was much bigger, thus requiring much more time for heating and cooling resulting in smaller amplitudes of the diurnal temperature oscillation.

7.2. Water levels

The barometric pressure time series as seen in Figure 25 (page 69) contained energies with numerous frequencies. However, clearly visible were longer term changes usually caused by lows and highs as part of the atmospheric macro climate. Very interesting is the fact that strong atmospheric pressure fluctuations with diurnal frequency were recorded. These are also clearly reflected in all surface water and sediment water level recordings, which can be seen in the same plot. To further examine these effects, spectral density analysis was performed on barometric pressure as well as the surface water level at Elfin Crossing as an example representative for all other locations.

Figure 39 contains spectral results calculated from the entire data set of atmospheric pressure, water and sediment level recorded at Elfin Crossing. The second plot shows an enlargement only focusing on the range between 1.5 cpd and 2.5 cpd. Note that the barometric pressure axis is reversed. The spectral density graph clearly exhibits obvious energy peaks at a frequency of 1 and 2 cycles per day. This is caused by atmospheric tides (Palumbo, 1998), whose influence on surface and groundwater levels are not very well researched up to date. However, similar features were also found in boreholes and analysed by Acworth in prep. (2008). In general, atmospheric tides are caused by two different mechanisms: the gravitational pull of the sun and the moon on the gas molecules in the atmosphere and, much more influential, daily heating and cooling of the atmosphere, thus causing barometric pressure changes due to expansion and contraction.

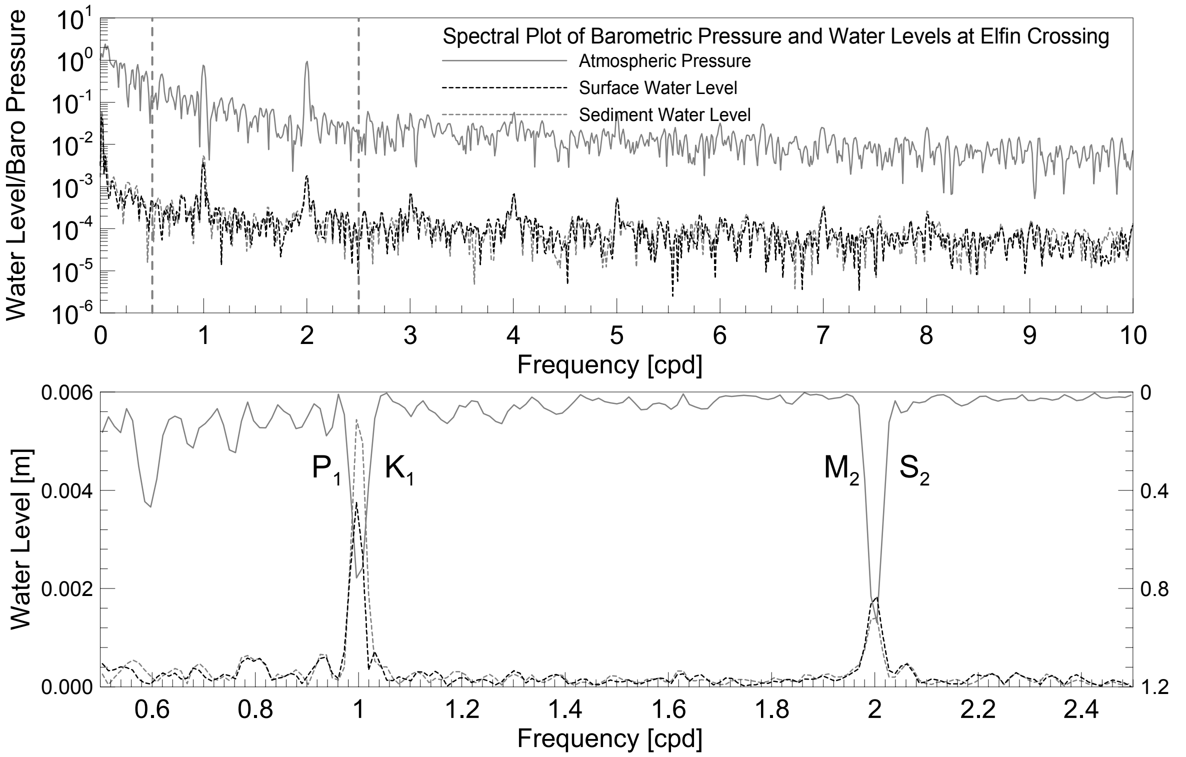

Figure 39 illustrates spectral analysis of barometric pressure, surface water and sediment water level at Elfin Crossing.

The frequency resolution of the barometric pressure data was poor after performing the Fourier Transform. This originated from a short length data set with a length of approx. two months. However, the two significant level peaks found in Maules Creek data were compared to literature values calculated from much longer data sets by Merritt (2004). Both results were illustrated in Table 11. Low spectral resolution of the Maules Creek results caused slightly differing values. The same reason is responsible for the fact that P1 and K1 as well as M2 and S2 are visually combined in one peak as seen in Figure 39. Higher resolution would separate these peaks, however published results were matched with surprising accuracy. Both peaks were found to be a combination of lunar (gravitational) and solar (heating) influences with diurnal (K1 and P1) and semidiurnal (M2 and S2) frequencies (Merritt, 2004). It is not known why the diurnal peak of barometric pressure (K1, P1) which is smaller than the semidiurnal peak (M2, S2) influences water levels in an inverse manner. However, the stronger response of the sediment water level can be explained in the following way: as the barometric pressure increases stress is being shared between the rock matrix as well as the water within the pores. This means that water in the sediment is under less stress than water in the installed pipe causing a higher gradient between the pipe and the streambed and therefore more water flowing out of the installation. The result is a more significant level response in the sediment as visible in Figure 39.

Component	**Unit**	**Frequency at Maules Creek**	**Frequency by Merritt, 2004**	**Explanation**
P1	cpd	0.99609375	0.99726206	Main solar diurnal
K1	cpd	1.00781250	1.00273794	Lunar-solar diurnal
M2	cpd	1.99218750	1.93227356	Main lunar semidiurnal
S2	cpd	2.00390630	2.00000000	Main solar semidiurnal

Table 11 compares frequencies of atmospheric tide components as found in Maules Creek with published values.

The diurnal barometric pressure oscillations feature amplitudes of approximately 4 hPa. The water level dropped fairly rapid at around 10:00 as a response to the increase in barometric pressure every morning as visible in Figure 40. Please note that surface water and sediment water levels were assigned to different axes on the left side using the same scale for better comparison. The level recovery lasted much longer. However, there was no obvious influence of the semidiurnal pressure peak on the water levels (occurrence at approx. 22:00). The magnitude of level change was approx. 2 cm, thus well above the range of instrument sensitivity (~0.2 cm). It was interesting to conclude that this change of water column must have been pushed into the streambed leading to a significant amount of water volume exchange with the hyporheic zone on a daily basis. Penetration depth can be calculated as approx. 5 cm (using a porosity value of 0.4), if the following assumptions were applicable: the area of water penetration is approximated by the surface area of the water body and water movement is vertical and not sidewards. These level changes certainly impact on many natural processes like biochemistry in the hyporheic zone. Apparently, no research has yet been done to investigate the effects of barometric tides on surface water bodies and the surrounding groundwater.

Barometric pressure perturbations as caused by atmospheric tides were obviously significant enough to directly imprint on all investigated water levels (Figure 25 on page 69). This lead to the straight forward conclusion that water levels at these specific surface water ponds must have been part of the continuous subsurface water table. They were directly connected to the surrounding groundwater, or in other words, the ponds were windows to the groundwater table. The evidence was given by the fact that recovered from tidal depression. This particular phenomenon would probably not have occurred if these ponds were surface water bodies trapped above an impermeable layer and therefore disconnected from the surrounding groundwater table. However, it did not solve the task of flow quantification but helped towards the conclusion that the temperature probes recorded temperatures in the fully water saturated sediment. The recovery from atmospheric tides can therefore be used as a tool in any surface water body to answer the question of connectivity between surface water and groundwater.

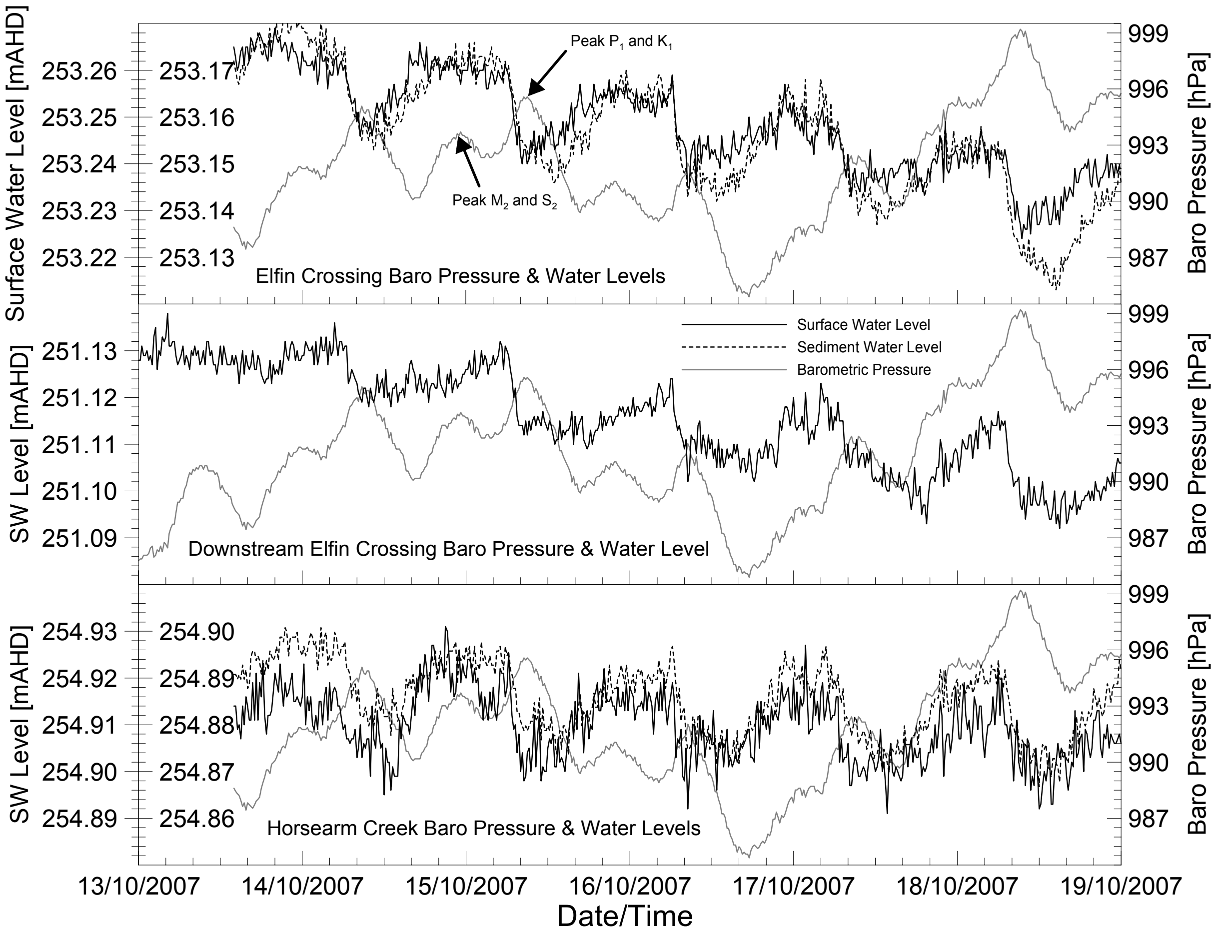

Figure 40 shows the influence of atmospheric tides on surface water and sediment water levels at all locations.

Water levels downstream Elfin Crossing illustrated a steady decline with time, as seen in Figure 25 (page 69). This effect was probably caused by alluvial gradient flow and recharge of aquifers further downstream because no surface runoff was recorded. A drop in levels due to evaporation was considered negligible because ponds were connected and water loss could be replaced by the surrounding reservoir. Water levels were slightly increased by rain obviously falling in the catchment area. A single peak visible in all level data on the 8th October proved to be the response to a quick and intense rain event with about 3.5 mm water. In contrast, levels at Horsearm Creek further upstream illustrated less decline. Subsurface geological properties are most probably responsible and it seemed that there was a flow barrier between the locations downstream and upstream. This would explain the fact that downstream levels decreased more than upstream levels in the same time. Rapid level response to rainfall indicated that there was high connectivity.

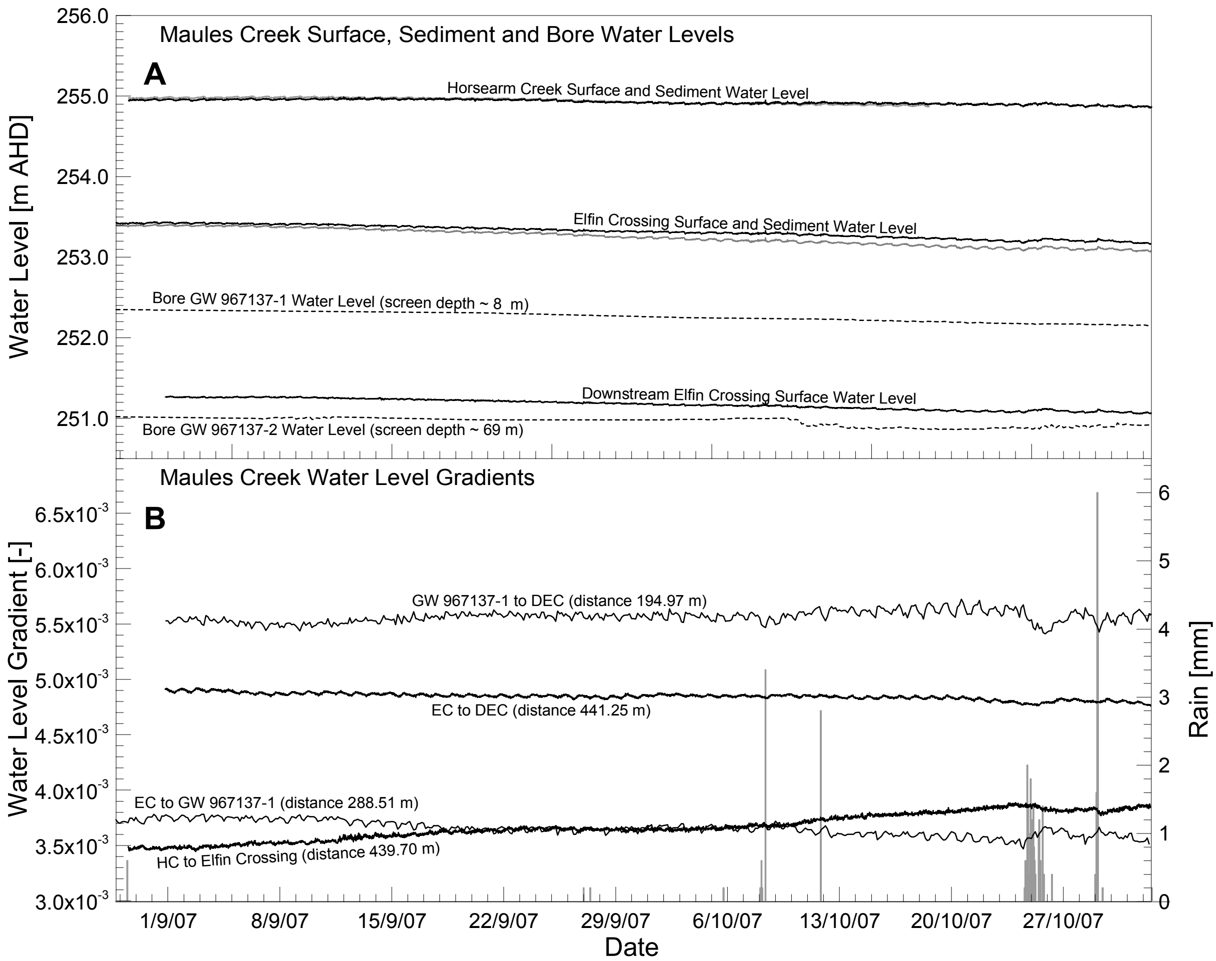

Figure 41 shows all water levels (A) and calculated water level gradients (B).

All recorded surface water levels are summarised in Figure 41 plot A, and the corresponding water level gradients were calculated and plotted in B. Andersen (2007) conducted a survey measuring water level elevations in all ponds along the creek, and concluded that there must be horizontal gradient flow through the creek streambed. Levels in Plot A are consistent with this finding. The water level logged in bore GW 967137/1 screened in the alluvium corresponds with the constant spatial drop of levels along the creek confirming that the pools were connected to the surrounding groundwater table. Additionally, plot B shows that all gradients downstream the confluence declined during the investigation. Quite differently, the gradient between HC and EC increased in the same time. This confirms that there was active water flow discharging from this area, and that there must be a flow barrier probably located near the confluence. Rainfall seemed slightly increase levels and gradients in October 2007 due infiltration of surface runoff causing groundwater recharge. It is obvious that this particular part of the catchment area is a highly variable and strongly coupled hydrogeological system.

7.3. Water exchange velocities

Comparing the temperature time series recorded at the three different locations allowed the qualitative interpretation that both, Elfin Crossing and downstream EC definitely lost water to the streambed. This was evident because heat was carried into the streambed by vertical water movement. Contrarily, the temperature signal at Horsearm Creek in graph D shows much faster damping with depth. This is especially obvious considering the fact that the last thermistor was only located 0.45 m below the streambed surface compared to 0.6 m at all other locations. The clear colour of the water in the pond, the fact that water sampling indicated rapid decrease of dissolved oxygen with depth and chemical observations like the occurrence of iron precipitation (Fe^{2+} oxidation) at the sediment surface, all this supported the hypothesis of discharging groundwater (Andersen, 2007). Groundwater outflow and feeding into the large pool could also be interpreted from the simple heat balance as mentioned in 7.1. However, the array could not be installed at the point where outflow was anticipated because cobbles in the streambed prevented the penetration. It was therefore placed further downstream where it obviously received a slightly losing signal. This illustrates the variability of streambed exchange flow.

All values calculated from phase shifts exhibited significant fluctuations in compared to the more stable lines obtained from amplitude ratios. It is interesting that abnormalities in velocities derived from the same solutions but using different thermistor pairs were of similar nature. As a consequence, this must be caused by water flow rather than the instruments. Furthermore, the effect of signal processing using the filter as explained in 4.4.1.2 (page 46) was done by Hatch et al. (2006) with the conclusion that errors were negligibly small. However, at Horsearm Creek both seepage solutions offered consistently different results for each pair of probes. Surprisingly, water velocity results generally showed the same overall trend with time. The numerical investigation suggested that diverge of both solutions was caused by an additional flow component in the horizontal direction. Hence, heat was carried horizontally as well and additional thermal dispersion resulted in further spread and consequently reduced the temperature amplitude and shifted the peak phase. This means that thermal dispersion must have been present as a mechanism. Moreover, horizontal groundwater flow could be detected using this method but this influence made exact quantification impossible. However, it can be concluded that the more divergent the results the higher the velocity ratio thus the more significant the horizontal flow component. Contrarily, results downstream Elfin Crossing featured an increasing deviation with time. This possibly indicates that horizontal flow increased, again highlighting the variability of the flow regime. Oscillations between each pair of solutions and abnormalities were visibly damped with depth. Furthermore, seepage values increased with depth as illustrated by the forward modelling results. All these features indicated that there is further need for research and validation of using heat as a tracer under distinct circumstances. A laboratory experiment is suggested to improve interpretation of results, thus enhancing field application. Ideally, the heat equation must be equipped with an additional term accounting for horizontal flow and solved accordingly. Unfortunately, this goes beyond the framework of this thesis.

At Elfin Crossing another phenomena required examination: vertical water flow decreased but the level gradient increased during the investigation which can be seen in Figure 29 (page 8). The result was significant temporal change of the evaluated streambed hydraulic conductivity. This can be caused by clogging due to sedimentation and filtration of fine grained organic matter (Su et al., 2004). Observations at the point of disassembling confirmed that the streambed was covered in a layer of organic sludge, which could also be found in the corresponding sediment sample used for the determination of the porosity value. Furthermore, the turbidity of the water and the observation of animals using this pool for drinking and bathing suggested that there was microbiological activity due to high nutrient contents. The installation procedure was thought to have caused an additional impact as the streambed was penetrated by the steel pipe and impacts to the sediment surface area were manually removed. This possibly caused the dispersion of fine grained material previously covering the sediment which would result in a change of conductivities. Using only the Darcy method to estimate exchange flow would have caused erroneous values because it only considers constant hydraulic conductivity values. An additional consideration about this phenomenon is the fact that pressures and temperatures were recorded using different devices at different spatial points in the streambed. As a consequence the mathematical combination of these values must be interpreted with care because hyporheic flow is usually complex and dynamic. For a future improvement of the method application it is suggested to utilise divers instead of thermistors only as they record both, water levels and temperatures at the exact same spot. This could offer two independent physical parameters for the evaluation with the heat and the Darcy method, thus allowing an improved spatial profile and temporal evaluation of water flow and streambed hydraulic conductivities.

The increase of velocity with depth at Elfin Crossing (see Table 8 page 74) is noticeable and does not make sense from a fluid continuity point of view. The analytical method strictly assumes homogeneous distribution of physical parameters, an assumption which is rarely met in field situations. In this case the increase could be caused by a decrease in porosity with depth. However, further investigations like inspection of streambed layering and porosity depth profiles are necessary to confirm this interpretation.

7.4. Method Limitations

Both temperature methods were applied to all recorded temperatures and results can be compared in the presentation section. The forward modelling method illustrated appropriate results which were consistent with the quasi-transient values for the location Elfin Crossing and downstream. However, the RMSE features values which are comparable in magnitude were noticeably close to the accuracy of the probes. At DEC the best fit for all pairs was only found applying the maximum value the dispersion coefficient was restricted to and the quality of fit was much worse than at location EC. A comparison with the transient solution offered the following possible explanation to this approach: (a) the water velocity changed significant enough with time to impact on the quality of fit, (b) there was horizontal flow violating the model boundary conditions. Another limitation could be extracted from the problem which occurred at Horsearm Creek. Solutions using probe 4 were not satisfying because they exhibit completely different results for the first time period. This was possibly caused by the relative temperature accuracy between the two thermistors which were used for calculation, thus the fitting process delivered faulty velocity values. Each device featured a measurement accuracy of ±0.2 °C. The absolute accuracy value was advertised by the manufacturer as almost invariable in the range of measurements presented in this thesis. Hence, the relative error of temperatures recorded by two thermistors can be as high as ±0.4 °C in the worst case. As a consequence, this offset can disturb velocity vales obtained by the fitting process and it can be concluded that forward modelling requires either strong oscillations or relies on precision temperature measurement. To avoid this issue in the future, the thermistors must be calibrated before they are deployed in the field.

Contrary to the forward modelling observations, the transient method offered reasonable values, despite the fact that results derived from both solutions diverged. In this case, the thermistor accuracy was part of the DC component as part of the general signal offset and was simply removed by the filtration process. Therefore, the precision of the velocity results depended on signal processing and on the temperature resolution of the device. It was important to recognise that seepage calculations obtained from the transient method reflected an average of the flow between peaks. More precisely: velocities represented an average value for the time between arrival of the thermal front at two devices in different depths. Consequently, temporal resolution of velocity results was limited by the travel time of heat, which in turn depended on the spacing and depth of the installation.

All results calculated from amplitude ratio and phase shift exhibited variations and differed more or less. Several reasons for these observed deviations can be stated

- a small but consistent velocity deviation between amplitude ratio and phase shift derived results may be due to heterogeneities in the distribution of physical parameters
- velocity deviations observed between a pair of solutions are probably caused by the complex nature of water flow constantly changing in space and time, impacting differently on the amplitude and phase of the temperature signal
- larger deviations between solutions as offered by one pair of probes could originate from violated boundary conditions like horizontal water flow and heat dispersion.

Disadvantages of both methods can be characterised in the following way

- Results offered only a two-dimensional (spatial and temporal) “window” looking into the complex nature of water flow and heat transport in porous media, thus interpretations were restricted by limited dimensionality.
- The complex character of “real” field situations could cause unknown violation of boundary conditions and therefore distort results obtained by the analytical solutions. Field conditions should be verified to backup solutions e.g. by monitoring water levels and gradients in order to ensure correct interpretation.
- Solar radiation as a source of diurnal heat has to be considered as an area source. This means that only vertical flow can be reliably quantified, in case of insignificant heat dispersion. However, the irreversibility of thermal dispersion can be used to indicate horizontal flow.

8. Conclusion

The use of heat as a tracer to quantify the exchange between surface and groundwater was examined in theory and practice. Special devices were constructed and installed and periodically recorded temperatures in distinct depths of the streambed at Maules Creek (Australia). Additionally, adjacent surface water and sediment water levels were measured in order to provide more information supporting the interpretation of both heat methods. Sediment samples were taken and the porosity value was evaluated in the laboratory. The values of heat capacity and heat conductivity of the sediment solids are usually in a narrow range and were therefore extracted from publications. Moreover, discrete-time signal processing and model fitting was applied to the raw temperature records. Additional filtering of the temperature data revealed clear diurnal temperature variations which could be used to compute a time series of water exchange velocities. The combination of all different field results helped to improve interpretation of the complex flow processes at Maules Creek. Despite the computational effort, both heat methods provided reliable velocity results.

Forward modelling assumes steady state conditions and therefore offers only an average of the temporally changing velocity. Required computational effort is reasonable and results are more an estimate rather than a description of the flow process. Violation of the boundary conditions such as great variability in vertical or additional horizontal flow impairs the fitting and thus impacts on the result. The correctness of results is also limited by the accuracy of the thermistors which should be calibrated before application. However, sediment depth responses to arbitrary temperature perturbations in the surface water can be described quite accurately without the need for sinusoidal compliance.

Using temperature fluctuations to quantify fluid propagation involved the application of complex data handling and signal processing. Major advantages were the two independent solutions and the fact that results could produce a proper picture of temporal variability in water flux. Horizontal flow components could also be detected but results should be treated with care because boundary conditions were stressed in this case. Temporal resolution is limited as single values were time-averages depending on a number of factors such as probe spacing, water velocity, oscillation amplitude and physical parameters. The correctness of results was independent from the accuracy of thermistors because this could be considered as constant value within the range of recorded temperatures.

Diurnal water level fluctuations were found in all investigated surface water bodies at Maules Creek. They were examined using spectral analysis which helped to explain that atmospheric tides caused these diurnal level oscillations. Atmospheric tides are barometric pressure changes caused by a several influences like the gravitational pull of planets as well as gas expansion under the influence of solar atmospheric heating. The effect on levels contributed to the conclusion that surface water bodies were windows to the groundwater. However, the impact on water levels was suspected to cause streambed water flow thus most likely influenced biochemical hyporheic processes.

Results from Maules Creek suggested that the streambed is directly connected to the groundwater. At Elfin Crossing water vertically penetrated through the streambed with a velocity between -0.2 m/d and -0.7 m/d. The loss of water is possibly fed by alluvial flow into the same pool from a source upstream. The location downstream Elfin Crossing demonstrated the same magnitude of flow but solution magnitudes greatly diverged. Contrarily, the pond at Horsearm Creek illustrated different results. Although temperature measurements were damped quickly with depth it was still found to be a losing section with velocities between -0.1 m/d and -0.4 m/d. Same as at location DEC, both solutions deviated considerably. A numerical model illustrated that significant horizontal flow causing additional heat dispersion was responsible for this anomaly. The forward modelling method failed to provide a reasonable result because of stressed boundary conditions and limited accuracy of thermistors. Although surface water flow was not evident during the entire time of investigation there still was groundwater flow draining from the permeable alluvial aquifer in the direction of the Namoi River. This was indicated by streambed water flow calculated with both heat methods, and by the steady decrease of water levels in the pools as well as in the shallow borehole. Both, water levels and streambed velocities suggested that there must be a flow boundary somewhere near the confluence of Maules and Horsearm Creek. This was concluded because flow downstream was consistently faster and levels decreased more rapidly than in the pool at Horsearm Creek further upstream. The hydrogeological system illustrated rapid increase and decline of water levels to rainfall events indicating high connectivity. However, temperature results alone only allowed quantification of flow at a particular point. Even the comparison of velocity results derived from various locations did not help to capture a larger picture of the flow regime. The description of the hydrogeological system on this scale required monitoring of additional parameters like water levels, which can be interpreted in combination with flow velocity. The method using heat as a tracer offered reliable results which were much more certain in magnitude than the traditional Darcy estimation. It therefore evinced to be a robust tool when used to quantify vertical and detect horizontal water movement thus can improve water balance calculations.

9. References

ABS, 2006. Water Account, Australia, 2004-05. Australian Bureau of Statistics (Australian Government), http://www.abs.gov.au/AUSSTATS/abs@.nsf/DetailsPage/4610.02004-05?OpenDocument.

Acworth, I.R. and Brain, T., 2008. Calculation of barometric efficiency in shallow piezometers using water levels, atmospheric and earth tide data. University of New South Wales

ADFAT, 2006. TRADE 2006. Australian Department of Foreign Affairs and Trade (Australian Government), http://www.dfat.gov.au/trade/trade2006.

Alexander, M.D. and Caissie, D., 2003. Variability and comparison of hyporheic water temperatures and seepage fluxes in a small Atlantic salmon stream. Ground Water, 41(1): 72-82.

Andersen, M.S. and Acworth, I.R., 2006. Geochemical and geophysical sampling campaign at Maules Creek - Data report for 2006.

Andersen, M.S. and Acworth, I.R., 2006. Preliminary investigations of surface-water groundwater interactions in the Maules Creek catchment, Namoi Valley, NSW, Australia

Andersen, M.S. and Acworth, I.R., 2007. Hydrochemical investigation of surface water groundwater interactions in a sub-catchment in the Namoi Valley, NSW, Australia

Andersen, M.S. and Acworth, I.R., 2007. Surface water groundwater interactions in an ephemeral creek in the Namoi Valley, NSW, Australia - Controls by geology and groundwater abstraction

Anderson, M.P., 2005. Heat as a ground water tracer. Ground Water, 43(6): 951-968.

Becker, M.W., Georgian, T., Ambrose, H., Siniscalchi, J. and Fredrick, K., 2004. Estimating flow and flux of ground water discharge using water temperature and velocity. Journal of Hydrology, 296(1-4): 221-233.

BOM, 2008. Climate Information. Bureau of Meteorology (Australian Government), http://www.bom.gov.au/climate/.

Braaten, R. and Gates, G., 2003. Groundwater-surface water interaction in inland New South Wales: a scoping study. Water Science & Technology, 48(7): 215-224.

Bravo, H.R., Jiang, F. and Hunt, R.J., 2002. Using groundwater temperature data to constrain parameter estimation in a groundwater flow model of a wetland system. Water Resources Research, 38(8).

Bredehoeft, J.D. and Papadopulos, I.S., 1965. Rates of Vertical Groundwater Movement Estimated from Earths Thermal Profile. Water Resources Research, 1(2): 325-&.

Brunke, M. and Gonser, T., 1997. The ecological significance of exchange processes between rivers and groundwater. Freshwater Biology, 37(1): 1-33.

Chen, W.P. and Lee, C.H., 2003. Estimating ground-water recharge from streamflow records. Environmental Geology, 44(3): 257-265.

Chen, X.H. and Yin, Y.F., 2001. Streamflow depletion: Modeling of reduced baseflow and induced stream infiltration from seasonally pumped wells. Journal of the American Water Resources Association, 37(1): 185-195.

Constantz, J., Cox, M.H. and Su, G.W., 2003. Comparison of heat and bromide as ground water tracers near streams. Ground Water, 41(5): 647-656.

Constantz, J., Stewart, A.E., Niswonger, R. and Sarma, L., 2002. Analysis of temperature profiles for investigating stream losses beneath ephemeral channels. Water Resources Research, 38(12).

Constantz, J., Stonestrom, D., Stewart, A.E., Niswonger, R. and Smith, T.R., 2001. Analysis of streambed temperatures in ephemeral channels to determine streamflow frequency and duration. Water Resources Research, 37(2): 317-328.

Constantz, J., Thomas, C.L. and Zellweger, G., 1994. Influence of Diurnal-Variations in Stream Temperature on Streamflow Loss and Groundwater Recharge. Water Resources Research, 30(12): 3253-3264.

Dahm, C.N., Grimm, N.B., Marmonier, P., Valett, H.M. and Vervier, P., 1998. Nutrient dynamics at the interface between surface waters and groundwaters. Freshwater Biology, 40(3): 427-451.

DNR, 2008. NSW Department of Natural Resources (Australian Government), http://www.dnr.nsw.gov.au/.

Domenico, P.A. and Schwartz, F.W., 1990. Physical and Chemical Hydrogeology. John Wiley and Sons, New York. 1990. 824.

Fawcett, R.J.B., 2007. Seasonal climate summary southern hemisphere (autumn 2006): drought returns to Australia. Australian Meteorological Magazine, 56(1): 55-65.

Findlay, S., 1995. Importance of Surface-Subsurface Exchange in Stream Ecosystems - the Hyporheic Zone. Limnology and Oceanography, 40(1): 159-164.

Goto, S., Yamano, M. and Kinoshita, M., 2005. Thermal response of sediment with vertical fluid flow to periodic temperature variation at the surface. Journal of Geophysical Research-Solid Earth, 110(B1).

Gregory, S.V., Swanson, F.J., McKee, W.A. and Cummins, K.W., 1991. AN ECOSYSTEM PERSPECTIVE OF RIPARIAN ZONES. Bioscience, 41(8): 540-551.

Harris, F.J., 1978. Use of Windows for Harmonic-Analysis with Discrete Fourier-Transform. Proceedings of the Ieee, 66(1): 51-83.

Hatch, C.E., Fisher, A.T., Revenaugh, J.S., Constantz, J. and Ruehl, C., 2006. Quantifying surface water-groundwater interactions using time series analysis of streambed thermal records: Method development. Water Resources Research, 42(10).

Healy, R.W., 1990. Simulation of solute transport in variably saturated porous media with supplemental information on modifications to the US Geological Survey's computer program VS2D. 90-4025, U.S. Geological Survey.

Healy, R.W. and Ronan, A.D., 1996. Documentation of computer program VS2Dh for simulation of energy transport in variably saturated porous media; modification of the US Geological Survey's computer program VS2DT. 96-4230, U.S. Geological Survey.

Hsieh, P.A., Wingle, W.L. and Healy, R.W., 2000. VS2DI-A graphical software package for simulating fluid flow and solute or energy transport in variably saturated porous media, U.S. Geological Survey.

Huggenberger, P., Hoehn, E., Beschta, R. and Woessner, W., 1998. Abiotic aspects of channels and floodplains in riparian ecology. Freshwater Biology, 40(3): 407-425.

Kanasewich, E.R., 1981. Time Sequence Analysis in Geophysics. University of Alberta Press.

Keery, J., Binley, A., Crook, N. and Smith, J.W.N., 2007. Temporal and spatial variability of groundwater-surface water fluxes: Development and application of an analytical method using temperature time series. Journal of Hydrology, 336(1-2): 1-16.

Lachenbr.Ah, 1971. VERTICAL GRADIENTS OF HEAT PRODUCTION IN CONTINENTAL CRUST .1. THEORETICAL DETECTABILITY FROM NEAR-SURFACE MEASUREMENTS. Journal of Geophysical Research, 76(17): 3842-&.

Lappala, E.G., Healy, R.W. and Weeks, E.P., 1987. Documentation of computer program VS2D to solve the equations of fluid flow in variably saturated porous media. 83-4099, U.S. Geological Survey.

Loheide, S.P. and Gorelick, S.M., 2006. Quantifying stream-aquifer interactions through the analysis of remotely sensed thermographic profiles and in situ temperature histories. Environmental Science & Technology, 40(10): 3336-3341.

Merritt, M.L., 2004. Estimating hydraulic properties of the Floridan Aquifer System by Analysis of earth-tide, ocean-tide, and barometric effects, Collier and Hendry Counties, Florida, U.S. Geological Survey, Tallahassee (Florida).

Metzger, T., Didierjean, S. and Maillet, D., 2004. Optimal experimental estimation of thermal dispersion coefficients in porous media. International Journal of Heat and Mass Transfer, 47(14-16): 3341-3353.

Muskat, M., 1937. The flow of fluids through porous media. Journal of Applied Physics, 8(4): 274-282.

Nakayama, A. and Kuwahara, F., 2005. Algebraic model for thermal dispersion heat flux within porous media. Aiche Journal, 51(10): 2859-2864.

Neuman, S.P., 1990. Universal Scaling of Hydraulic Conductivities and Dispersivities in Geologic Media. Water Resources Research, 26(8): 1749-1758.

NIST, 2005. Thermophysical Properties of Water. National Institute of Standards and Technology (US Government), http://webbook.nist.gov.

Oppenheim, A.V. and Schafer, R.W., 1989. Discrete-time signal processing. Prentice-Hall, Inc. Upper Saddle River, NJ, USA.

Palumbo, A., 1998. Atmospheric tides. Journal of Atmospheric and Solar-Terrestrial Physics, 60(3): 279-287.

Peterson, E.W. and Sickbert, T.B., 2006. Stream water bypass through a meander neck, laterally extending the hyporheic zone. Hydrogeology Journal, 14(8): 1443-1451.

Pulido-Velazquez, M.A., Sahuquillo-Herraiz, A., Ochoa-Rivera, J.C. and Pulido-Velazquez, D., 2005. Modeling of stream-aquifer interaction: the embedded multireservoir model. Journal of Hydrology, 313(3-4): 166-181.

Ronan, A.D., Prudic, D.E., Thodal, C.E. and Constantz, J., 1998. Field study and simulation of diurnal temperature effects on infiltration and variably saturated flow beneath an ephemeral stream. Water Resources Research, 34(9): 2137-2153.

Ryan, R.J. and Boufadel, M.C., 2006. Influence of streambed hydraulic conductivity on solute exchange with the hyporheic zone. Environmental Geology, 51(2): 203-210.

Sass, J.H., Lachenbr.Ah, Munroe, R.J., Greene, G.W. and Moses, T.H., 1971. Heat Flow in Western United-States. Journal of Geophysical Research, 76(26): 6376-&.

Schön, J.H., 1996. Physical Properties of Rocks: Fundamentals and Principles of Petrophysics. Pergamon.

Silliman, S.E. and Booth, D.F., 1993. Analysis of Time-Series Measurements of Sediment Temperature for Identification of Gaining Vs Losing Portions of Juday-Creek, Indiana. Journal of Hydrology, 146(1-4): 131-148.

Silliman, S.E., Ramirez, J. and McCabe, R.L., 1995. Quantifying Downflow through Creek Sediments Using Temperature Time-Series - One-Dimensional Solution Incorporating Measured Surface-Temperature. Journal of Hydrology, 167(1-4): 99-119.

Sinclair, P., Barrett, C. and Williams, R.M., 2006. Impact of groundwater extraction on Maules Creek – Upper Namoi Valley, NSW, Australia. Department of Infrastructure and Natural Resources NSW

Smith, J.O., 2007. Introduction to Digital Filters with Audio Applications, http://ccrma.stanford.edu/~jos/filters/.

Song, J.X., Chen, X.H., Cheng, C., Summerside, S. and Wen, F.J., 2007. Effects of hyporheic processes on streambed vertical hydraulic conductivity in three rivers of Nebraska. Geophysical Research Letters, 34(7).

Sophocleous, M., 2002. Interactions between groundwater and surface water: the state of the science. Hydrogeology Journal, 10(1): 52-67.

Stallman, R.W., 1965. Steady 1-Dimensional Fluid Flow in a Semi-Infinite Porous Medium with Sinusoidal Surface Temperature. Journal of Geophysical Research, 70(12): 2821-&.

Stearns, S.D. and David, R.A., 1996. Signal processing algorithms in MATLAB. Prentice-Hall, Inc. Upper Saddle River, NJ, USA.

Stonestrom, D.A. and Constantz, J., 2003. Heat as a tool for studying the movement of ground water near streams. U.S. Geological Survey, Reston (Virginia)

Su, G.W., Jasperse, J., Seymour, D. and Constantz, J., 2004. Estimation of hydraulic conductivity in an alluvial system using temperatures. Ground Water, 42(6-7): 890-901.

Suzuki, S., 1960. Percolation Measurements Based on Heat Flow through Soil with Special Reference to Paddy Fields. Journal of Geophysical Research, 65(9): 2883-2885.

Testu, A. et al., 2007. Thermal dispersion for water or air flow through a bed of glass beads. International Journal of Heat and Mass Transfer, 50(7-8): 1469-1484.

Van Camp, M. and Vauterin, P., 2005. Tsoft: graphical and interactive software for the analysis of time series and Earth tides. Computers & Geosciences, 31(5): 631-640.

Winter, T.C. and Us, G.S., 1998. Ground Water and Surface Water: A Single Resource. Geological Survey (USGS).

Woessner, W.W., 2000. Stream and fluvial plain ground water interactions: Rescaling hydrogeologic thought. Ground Water, 38(3): 423-429.

Woodside, W. and Messmer, J.H., 1961. Thermal Conductivity of Porous Media .1. Unconsolidated Sands. Journal of Applied Physics, 32(9): 1688-&.

WPI, 2008. Air Property Calculator. Worcester Polytechnic Institute, http://users.wpi.edu/~ierardi/FireTools/air_prop.html.

Yeh, Y.J., Lee, C.H. and Chen, S.T., 2000. A tracer method to determine hydraulic conductivity and effective porosity of saturated clays under low gradients. Ground Water, 38(4): 522-529.

10. Appendix

Data processing with Matlab

A. Band-pass Filtration of Temperatures

```
% excel source file
sheet = 'HC';
% excel source tab
record = 'HC-filt';
% data range
range1 = 2;
range2 = 6140;
% up-sampling factor
upsample = 5;
% read all five temperature time series plus time values
b = transpose(xlsread(excel, sheet, ['B' int2str(range1) ':B' int2str(range2)]));
c = transpose(xlsread(excel, sheet, ['C' int2str(range1) ':C' int2str(range2)]));
d = transpose(xlsread(excel, sheet, ['D' int2str(range1) ':D' int2str(range2)]));
e = transpose(xlsread(excel, sheet, ['E' int2str(range1) ':E' int2str(range2)]));
f = transpose(xlsread(excel, sheet, ['F' int2str(range1) ':F' int2str(range2)]));
g = transpose(xlsread(excel, sheet, ['G' int2str(range1) ':G' int2str(range2)]));

% specify filter
N     = 576;        % Order
Fc1   = 0.01875;    % First Cutoff Frequency
Fc2   = 0.02291666; % Second Cutoff Frequency
flag  = 'scale';    % Sampling Flag
Alpha = 0.75;       % Window Parameter
% Create the window vector for the design algorithm.
win = tukeywin(N+1, Alpha);
% Calculate the coefficients using the FIR1 function.
coe  = fir1(N, [Fc1 Fc2], 'bandpass', win, flag);

% perform zero-phase filtration
c1 = filtfilt(coe,1,c);
d1 = filtfilt(coe,1,d);
e1 = filtfilt(coe,1,e);
f1 = filtfilt(coe,1,f);
g1 = filtfilt(coe,1,g);

% up-sample data
c1 = interp(c1, upsample);
d1 = interp(d1, upsample);
e1 = interp(e1, upsample);
f1 = interp(f1, upsample);
g1 = interp(g1, upsample);
i1 = resample(i, 5, 1);

% plot results
plot(c1, '-r');
hold on;
plot(d1, '-m');
plot(e1, '-y');
plot(f1, '-b');
plot(g1, '-k');
plot(i1, ':k');
```

```
hold off;

% up-sample time linearly
time = [0:(15/upsample)*60:length(c)*900-(15/upsample)*60];
h1 = interp1([0:900:(length(b)-1)*900], h, time);
% adjust absolute date values
dates = [b(1):(b(length(b))-b(1))/(length(c1)-1):b(length(b))]

% write all data to excel file
xlswrite(excel, [transpose(time) transpose(dates) transpose(c1) transpose(d1) transpose(e1) trans-
        pose(f1) transpose(g1) transpose(h1) transpose(i1)], record, 'A2')
```

B. Extraction of Amplitude Ratio and Phase Shift

```
clear;
% specify excel file
excel = 'data/HC.xls'
% specify sheet to read from
sheet = 'HC';
% specify sheet to write to
record = 'HC-XX';
% specify data range
range1 = 1600; range2 = 29000;

% read absolute dates
uu = transpose(xlsread(excel, sheet, ['B' int2str(range1) ':B' int2str(range2)]));
% read absolute time values (seconds)
xx = transpose(xlsread(excel, sheet, ['A' int2str(range1) ':A' int2str(range2)]));
% read original seepages (if available)
ww = transpose(xlsread(excel, sheet, ['H' int2str(range1) ':H' int2str(range2)]));
% read gradient data (if available)
gg = transpose(xlsread(excel, sheet, ['I' int2str(range1) ':I' int2str(range2)]));

% read first filtered temperature time series
yy = transpose(xlsread(excel, sheet, ['F' int2str(range1) ':F' int2str(range2)]));
% read second filtered sinosoidal temperature series
zz = transpose(xlsread(excel, sheet, ['G' int2str(range1) ':G' int2str(range2)]));

% set first values of various variables required for looping
loop = 0; count1 = 0; count2 = 0; w1 = 0; w2 = 0; peak1 = 0; startd = NaN; stopd = NaN; g1 = 0; g2 =
        0;
Ar1 = NaN; Ar2 = NaN; Ps1 = NaN; Ps2 = NaN; Vavg = NaN; Atime = NaN; Ar1s = NaN; Ar2s = NaN;
        Aratio = NaN; Pshift = NaN; Vavg = NaN; Grd = NaN;

% calculate derivation of starting values
op1 = (yy(2) - yy(1)) / (xx(2) - xx(1));
sdev = op1;
op2 = (zz(2) - zz(1)) / (xx(2) - xx(1));

% run through all values in a loop
for n = 2:length(yy)
   % compute derivation of first series
   dev1 = (yy(n) - yy(n-1)) / (xx(n) - xx(n-1));
   % sum original seepage values between peaks
   w1 = w1 + ww(n-1);
   g1 = g1 + gg(n-1);
   count1 = count1 + 1;
```

```
% if slope of derivation 1 changes to below zero zero -> upper peak
if ((op1 > 0) & (dev1 <= 0))
   % save values of amplitude and phase time of peak
   Ar1 = [Ar1 yy(n-1)];
   Ar1s(n) = yy(n-1);
   Ps1 = [Ps1 xx(n-1)];
   Atime = [Atime xx(n-1)];
   startd = [startd uu(n-1)];
   peak1 = 1;
   w1 = ww(n-1);
   g1 = gg(n-1);
   count1 = 1;
 % if slope of derivation 1 changes to below zero zero -> lower peak
elseif ((op1 < 0) & (dev1 >= 0))
   % save values of amplitude and phase time of peak
   Ar1 = [Ar1 yy(n-1)];
   Ar1s(n) = yy(n-1);
   Ps1 = [Ps1 xx(n-1)];
   Atime = [Atime xx(n-1)];
   startd = [startd uu(n-1)];
   peak1 = 1;
   w2 = ww(n-1);
   g2 = gg(n-1);
   count2 = 1;
 else
   Ar1s(n) = NaN;
 end
 % set to last values
 op1 = dev1;
 % compute derivation of second series
 dev2 = (zz(n) - zz(n-1)) / (xx(n) - xx(n-1));
 % sum original seepage value
 w2 = w2 + ww(n-1);
 g2 = g2 + gg(n-1);
 count2 = count2 + 1;
 % after first peak was detected always enter here
 if (loop == 1)
    % if slope of derivation 2 changes to below zero -> upper peak
    if ((op2 > 0) & (dev2 <= 0))
       Ar2 = [Ar2 zz(n-1)];
       Ar2s(n) = zz(n-1);
       Ps2 = [Ps2 xx(n-1)];
       stopd = [stopd uu(n-1)];
       Vavg = [Vavg (w1/count1)*24*3600];
       Grd = [Grd (g1/count1)];
    elseif ((op2 < 0) & (dev2 >= 0))
       % calculate values for amplitude and phase shift ratio
       Ar2 = [Ar2 zz(n-1)];
       Ar2s(n) = zz(n-1);
       Ps2 = [Ps2 xx(n-1)];
       stopd = [stopd uu(n-1)];
       Vavg = [Vavg (w2/count2)*24*3600];
       Grd = [Grd (g2/count2)];
    else
       Ar2s(n) = NaN;
    end
 else
   Ar2s(n) = NaN;
end
```

```
   op2 = dev2;
   if ((sdev/dev2 > 0) && (peak1 > 0)); loop = 1; end;
end

% plot both time series
plot(xx, yy, '-b')
hold on;
plot(xx, zz, '-r');
plot(xx, Ar1s, 'xk');
plot(xx, Ar2s, 'xk');
hold off;

% shorten data set in case of difference in peak numbers
if (length(Ar1) > length(Ar2))
   Ar1 = Ar1(1:length(Ar2));
else
   Ar2 = Ar2(1:length(Ar1));
end
Ps1 = Ps1(1:length(Aratio));
Ps2 = Ps2(1:length(Aratio));

% compute amplitude ratio values
Aratio = Ar2 ./ Ar1;
% compute phase shift values
Pshift = Ps2 - Ps1;
% record absolut peak times
startd = startd(1:length(Aratio));
stopd = stopd(1:length(Aratio));
Atime = Atime(1:length(Aratio));
% compute average original velocities between peaks (if applicable)
Vavg = Vavg(1:length(Aratio));

% write data to excel file
xlswrite(excel, [transpose(startd) transpose(stopd) transpose(Vavg) transpose(Grd) transpose(Aratio)
           transpose(Pshift)], record, 'A2');
```

C. Iterate Seepage Values

```
clear;
% specify excel file
excel = 'data/HC.xls'
% specify sheet to read from and write to
sheet = 'HC-XX';
% specify range
range1 = 2;
range2 = 114;
% specify probe spacing (m)
dz = 0.15;

% amplitude ratio values (-)
Aratio = transpose(xlsread(excel, sheet, ['E' int2str(range1) ':E' int2str(range2)]));
% read phase shift values (s)
Pshift = transpose(xlsread(excel, sheet, ['F' int2str(range1) ':F' int2str(range2)]));
% read original seepage data (if applicable)
Vavg = transpose(xlsread(excel, sheet, ['C' int2str(range1) ':C' int2str(range2)]));
% read gradient data (if applicable)
Grd = transpose(xlsread(excel, sheet, ['D' int2str(range1) ':D' int2str(range2)]));
```

```
% specify physical parameters
P = 24*3600;
por = 0.39;
beta = 0.015;
lamf = 0.6;
lams = 1.8;
lam = (lamf^por) * (lams^(1-por));
rohf = 998;
cf = 4183;
rohs = 2650;
cs = 750;
rohc = por * rohf * cf + (1 - por) * rohs * cs;
gammab = rohc / (rohf * cf);

% amplitude ratio function
func1 = inline('v +(2*(lam/rohc + beta*abs(v*gammab))/dz)*log(Ar) +sqrt((sqrt(v^4+(8*pi*(lam/rohc +
        beta*abs(v*gammab))/P)^2) + v^2)/2)', 'v', 'Ar', 'dz', 'P', 'lam', 'rohc', 'beta', 'gammab');
% phase shift function
func2 = inline('-v +sqrt(sqrt(v^4+(8*pi*(lam/rohc + beta*abs(v*gammab))/P)^2)-2*((Ps*4*pi*(lam/rohc +
        beta*abs(v*gammab)))/(P*dz))^2)', 'v', 'Ps', 'dz', 'P', 'lam', 'rohc', 'beta', 'gammab');

% loop through all values
for n = 1:length(Aratio)
  Ar = Aratio(n);
  % calculate only if amplitude ratio is valid
  if (Ar > 0) && (Ar <= 1)
    % iterate seepage from amplitude ratio
    v1 = fzero(func1, -0.1, optimset('TolX', 5e-18, 'Display', 'off'), Ar, dz, P, lam, rohc, beta, gammab);
    v1 = v1 * gammab;
    % hydraulic conductivity estimation (if applicable)
    Conductivity1(n) = abs(v1 / Grd(n));
    % correct for units m/s -> m/d
    Velocity1(n) = v1 * 24 * 3600;
  else
    Velocity1(n) = NaN;
  end

  Ps = Pshift(n);
  % calculate only if phase shift is valid
  if (Ps > 0)
    % iterate velocity from phase shift
    v2 = fzero(func2, -0.1, optimset('TolX', 5e-18, 'Display', 'off'), Ps, dz, P, lam, rohc, beta, gammab);
    % take only real value in case of odd solution
    v2 = real(v2) * gammab;
    % hydraulic conductivity estimation (if applicable)
    Conductivity2(n) = abs(v2 / Grd(n));
    % correct signum for second solution derived from first solution!
    if (v1 < 0); v2 = -1 * v2; end;
    % correct for units m/s -> m/d
    Velocity2(n) = v2 * 24 * 3600;
  else
    Velocity2(n) = NaN;
  end
  % correct original average seepage values (if applicable)
  if (Velocity1(n) < 0) Vavg(n) = -1 * Vavg(n); end;
  % kill values smaller than visible in case of failed iteration
  if (abs(Velocity2(n)) < 0.001) Velocity2(n) = NaN; end;
end
```

```
% plot results
subplot(3, 1, 1);
plotyy(Aratio, ':xr', Pshift, ':xb');
hold off;

subplot(3, 1, [2 3]);
splot = plot(Velocity1, ':xr'); grid on;
hold on;
splot = plot(Velocity2, ':xb');
plot = plot(Vavg, '-k');
hold off
legend('vAr', 'vPs', 'vOrig', 'Location', 'EastOutside')

% write values to excel sheet
xlswrite(excel, [transpose(Velocity1) transpose(Velocity2) transpose(Conductivity1) trans-
        pose(Conductivity2)], sheet, 'G2');
xlswrite(excel, [Vavg], sheet, 'C2');
```

D. Forward Modelling Function

```
% function calculating depth response to surface water temperatures
function F = temp_forward_model(param, xdata)

% set values for iteration of equations
% global variable: temperature probe spacing [m]
global dz;
por = 0.39; %0.31; %0.34;
beta = param(2);
lamf = 0.6;
lams = 1.8;
lam =  (lamf^por) * (lams^(1-por));
rohf = 998;
cf = 4183;
rohs = 2650;
cs = 750;
rohc = por * rohf * cf + (1 - por) * rohs * cs;
gammab = rohc / (rohf * cf);

x = 0; y = 0; ft = 0; t2 = 0; dT2 = 0;
% surface water temperatures
x = xdata;
% global variable: ambient temperature (°C)
global Tamb;
% print intermediate output
fprintf('Tamb: %i, Seepage: %i, Dispersivity: %i \n', Tamb, param(1), param(2));
% set sampling time (s)
timestep = 900;
% prepare values
vf = param(1) / (24*3600);
x2 = [Tamb x];
x2 = x2(1:length(x));
% compute delta T
dT = x - x2;
% compute heat conductivity including dispersion
ke = lam/rohc + beta*abs(vf * gammab);
t1 = [0:timestep:length(x)*timestep];
```

```
Z = vf / gammab;
D = ke;
ft = zeros(1, length(x));
% loop through to sum values
for i = 1:length(x)
    time = i*timestep;
    t2 = t1(1:i);
    dT2 = dT(1:i);
    t = time - t2;
    ft(i) = Tamb + sum((dT2 ./ 2) .* (erfc((dz - t * Z) ./ (2 * sqrt(t * D))) + exp((Z*dz)/D) .* erfc((dz + t * Z)
            ./ (2 * sqrt(t * D)))));
end
F = ft;
```

E. Multi-parameter Fitting

```
clear;
% specify excel file
excel = 'data/HC.xls';
% specify sheet to read from
sheet = 'EC';
% specify sheet to write
record = 'EC-F-XX';
% specify data range
range1 = 2; range2 = 2059;
% global variable: probe spacing (m)
global dz;
dz = 0.3;
% global variable: ambient temperature (m)
global Tamb;
Tamb = ydata(1);
% read upper temperature time series
xdata = transpose(xlsread(excel, sheet, ['D' int2str(range1) ':D' int2str(range2)]));
% read lower temperature time series
ydata = transpose(xlsread(excel, sheet, ['F' int2str(range1) ':F' int2str(range2)]));

% set starting values for fitting [seepage dispersivity]
start = [0.1 0];
% set fitting restrictions
lowerlimit = [-2 0];
upperlimit = [2 0.1*dz];
% compute non-linear fitting
[x, resnorm, residual, exitflag, output] = lsqcurvefit(@temp_forward_model, start, xdata, ydata, lower-
            limit, upperlimit, optimset('LevenbergMarquardt', 'on'));

% output computation progress
disp(output); disp(x);
% calculate forward model for fitted parameters
newdata = temp_forward_model(x, xdata);
% plot data
plot(xdata);
hold on;
plot(ydata);
hold off;
% compute seepage result
seepage = ones(1, length(xdata)) * x(1);
% compute dispersion coefficient result
```

```
disp = ones(1, length(xdata)) * x(2);
% compute mean square error MSE
msee = ones(1, length(xdata)) * sum((ydata - newdata).^2)/length(ydata);
% compute root of mean square error RMSE
rmsee = ones(1, length(xdata)) * sqrt(mse);
% write results to excel file
xlswrite(excel, [transpose(xdata) transpose(ydata) transpose(newdata) transpose(disp) trans-
        pose(seepage) transpose(-seepage) transpose(rmsee) transpose(msee)], record, 'B2');
```

Climate Station Data

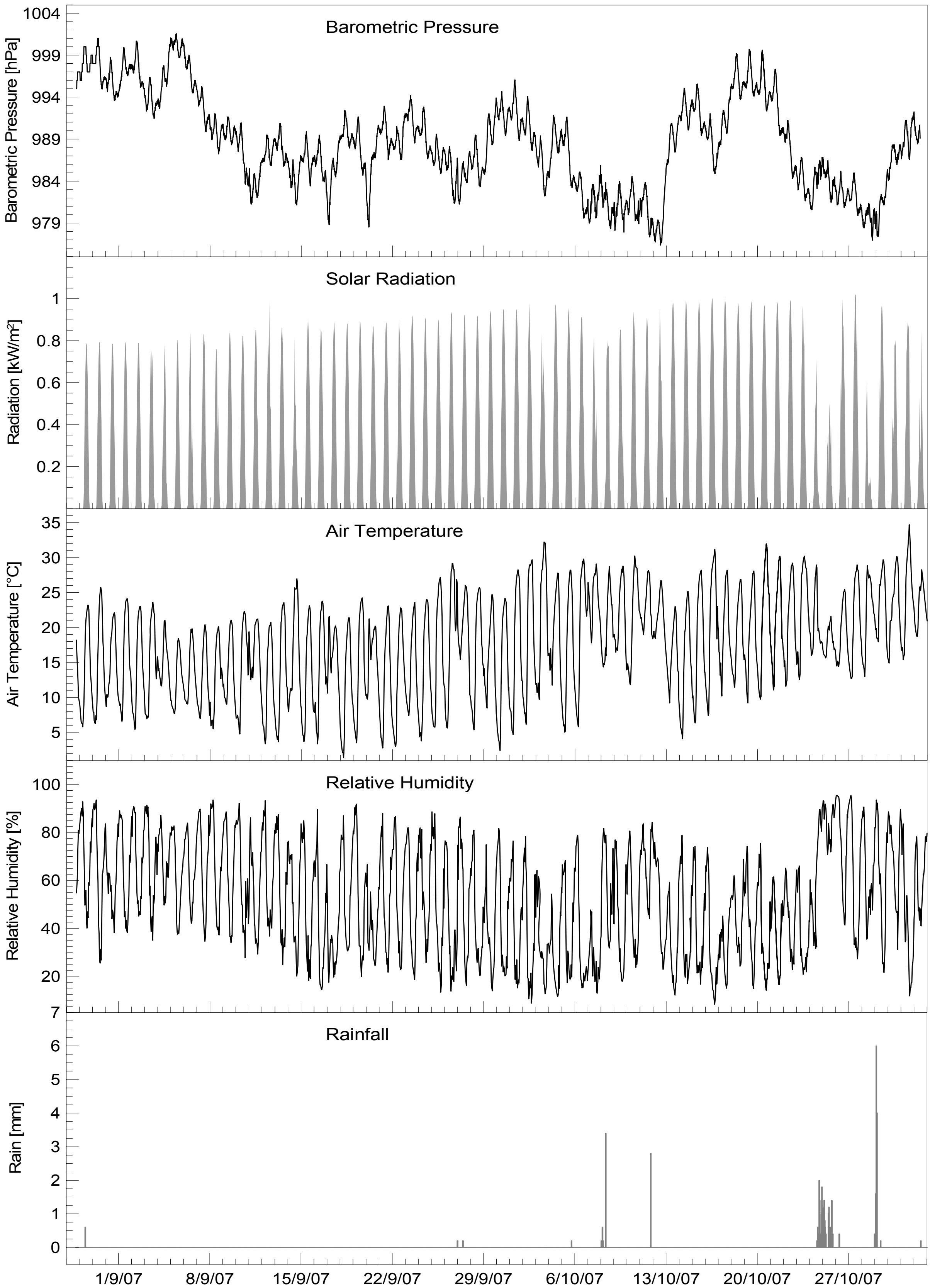

Elfin Crossing Temperatures

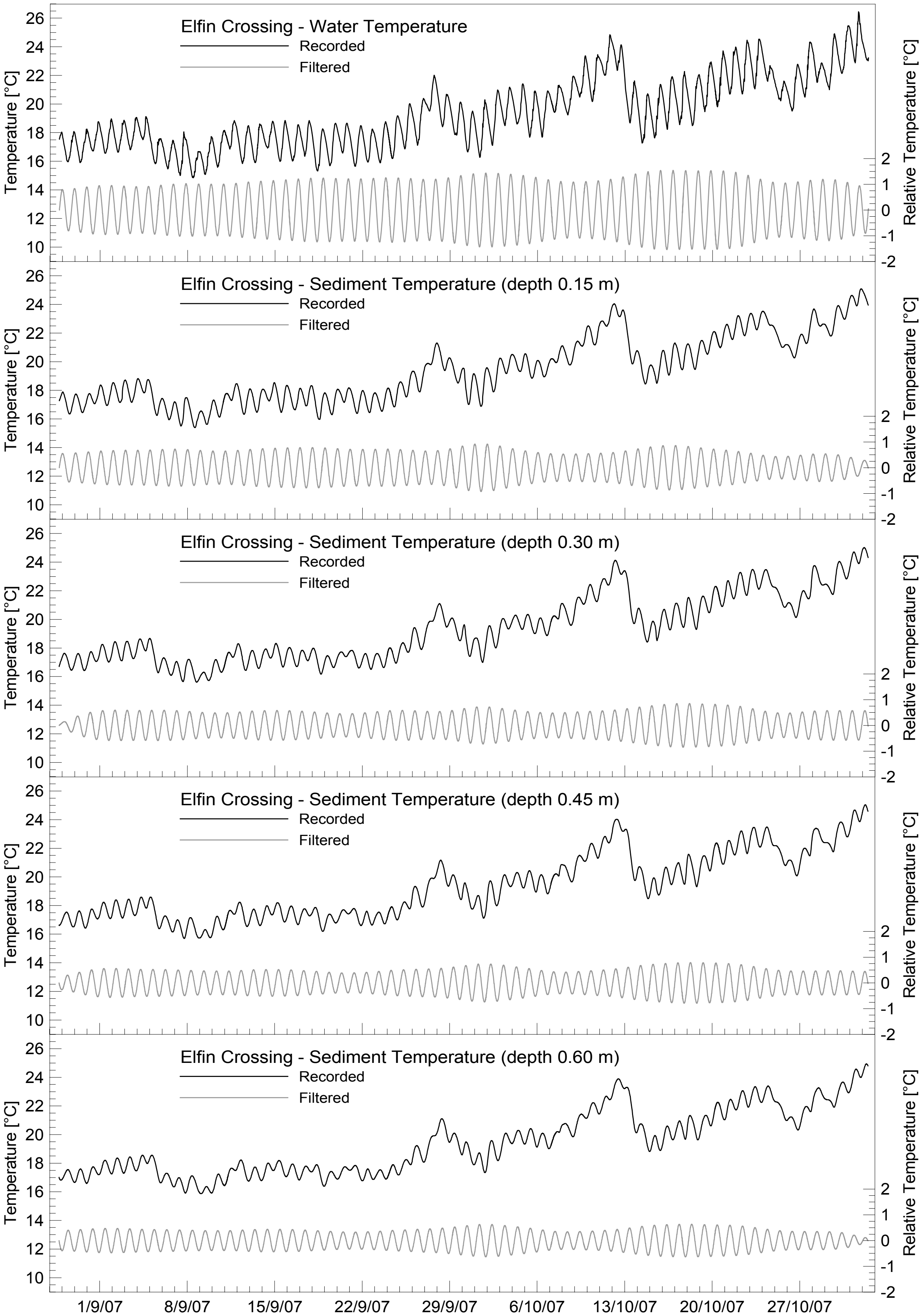

Downstream Elfin Crossing Temperatures

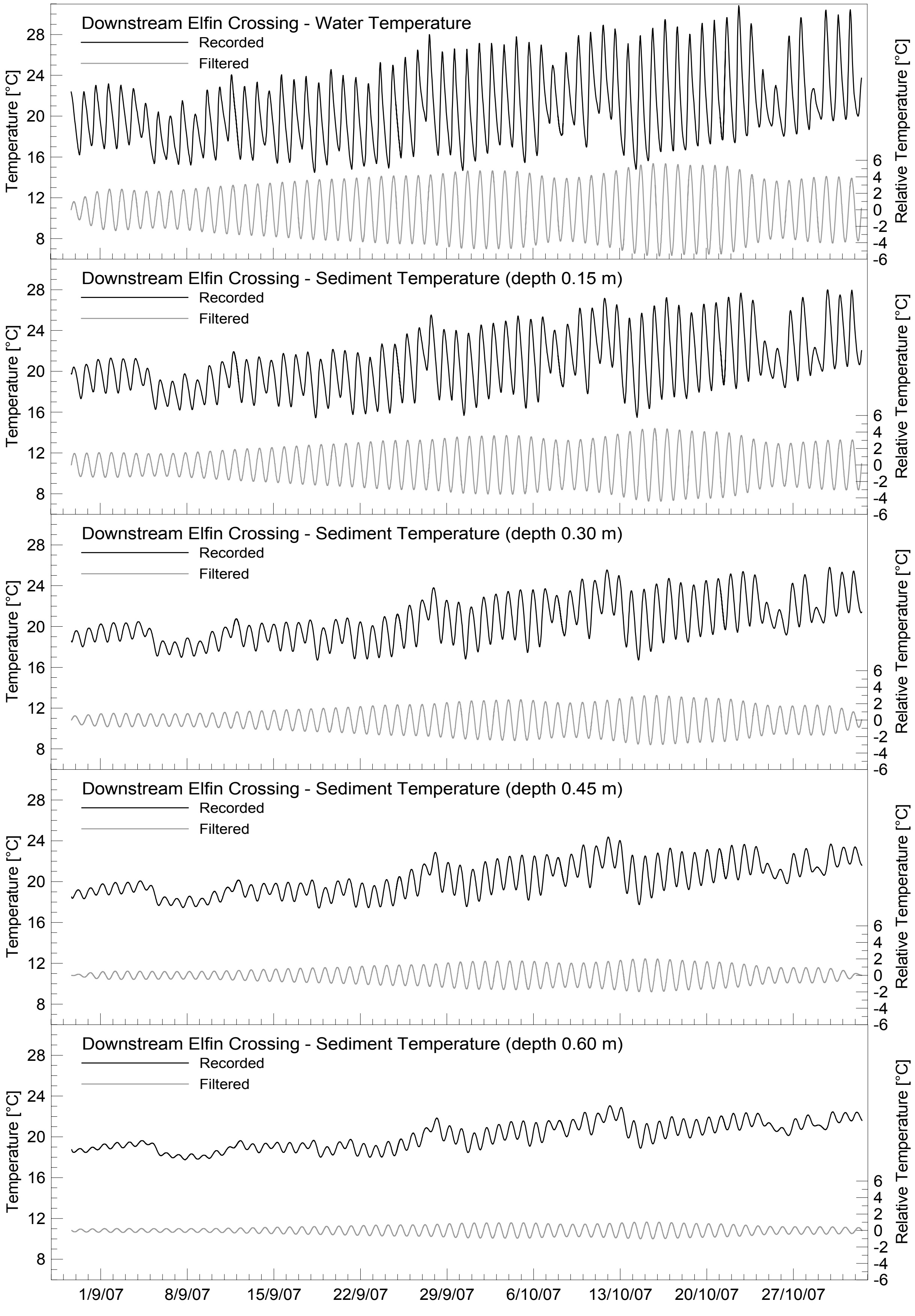

Horsearm Creek Temperatures

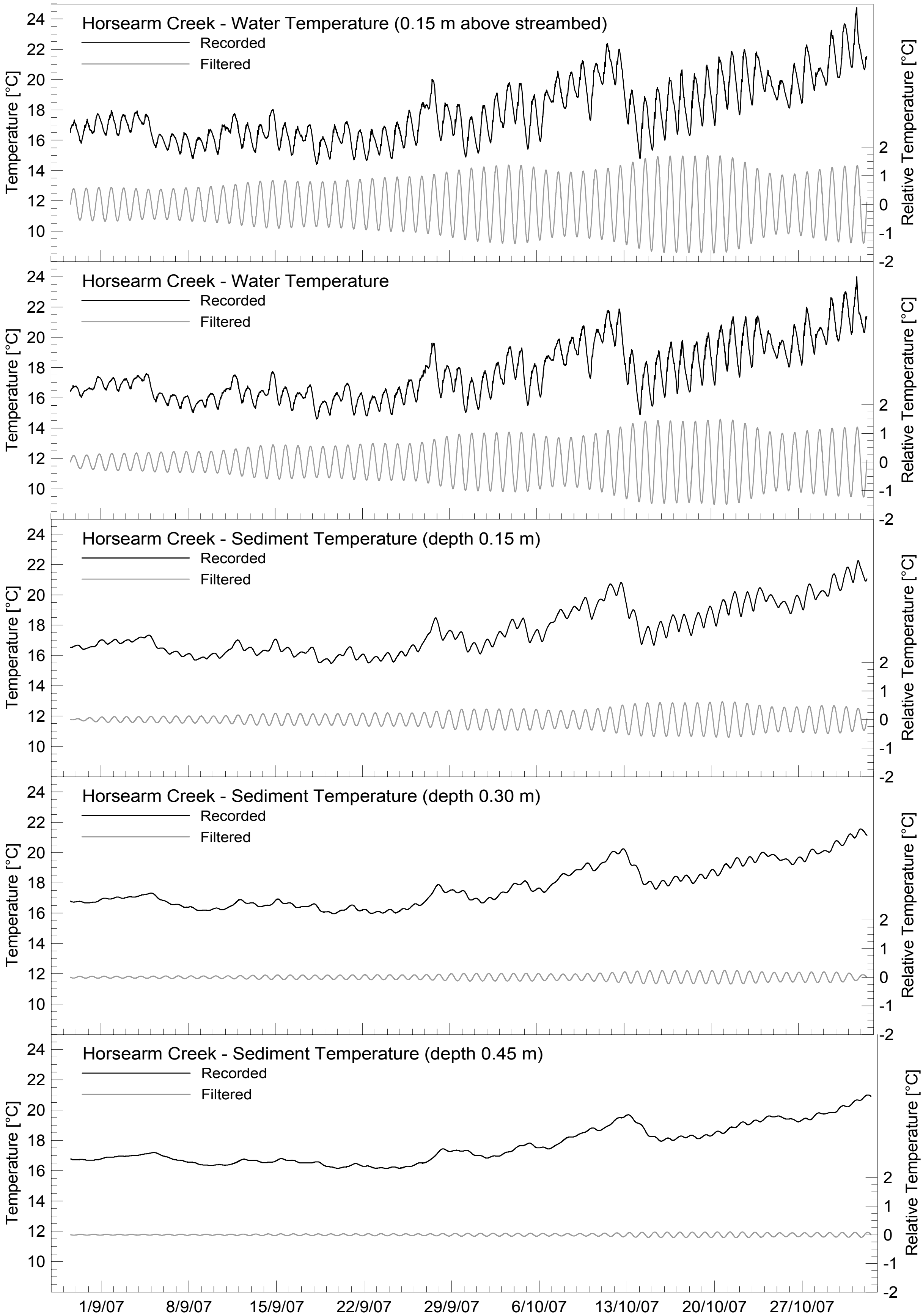

Filter Specifications

A. Tukey Window

Applied to the time domain with the parameters: α = 0.75, 576 Samples

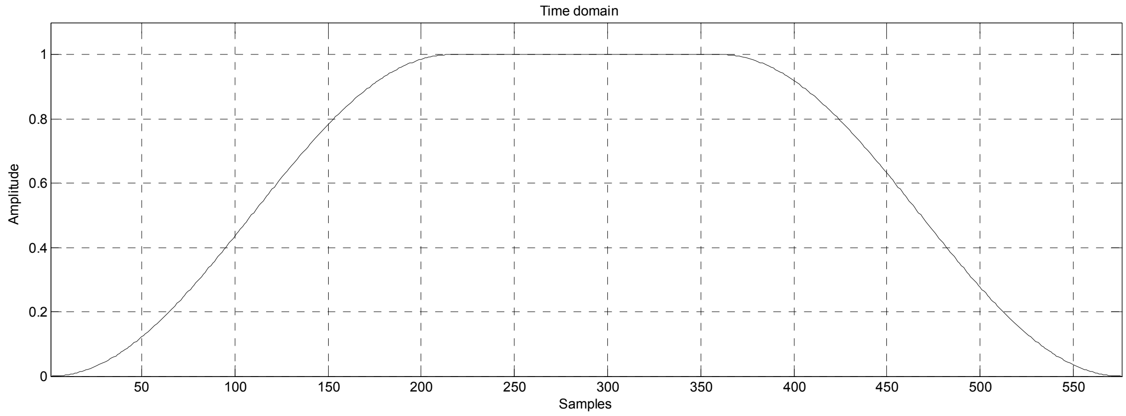

B. Magnitude Frequency Response

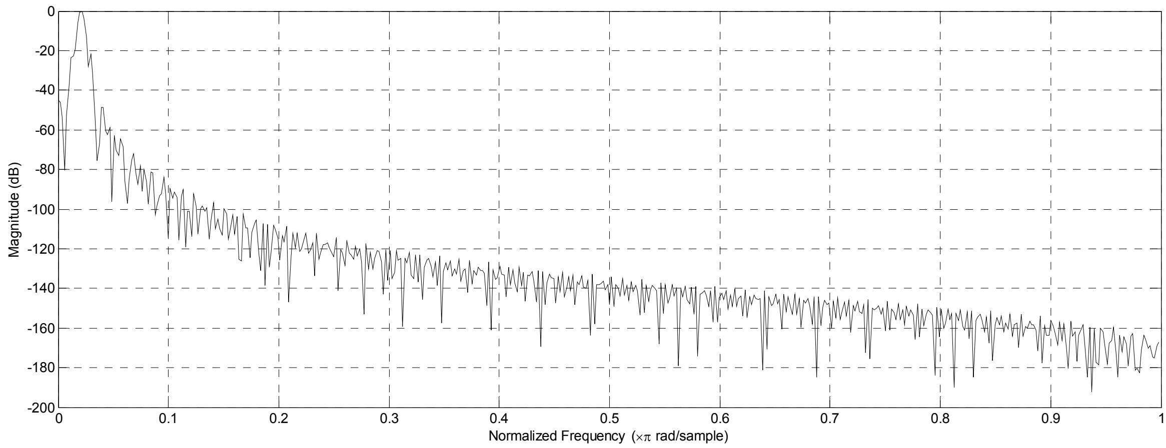

C. Magnitude Phase Response